Table of Contents for Chapter 2

Chapter 2

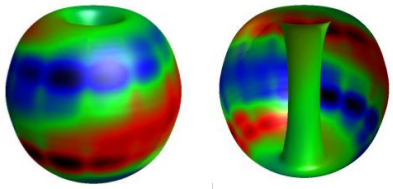

Stability

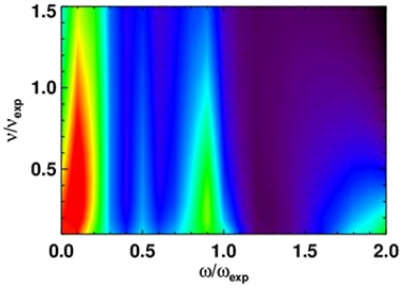

3D Fields

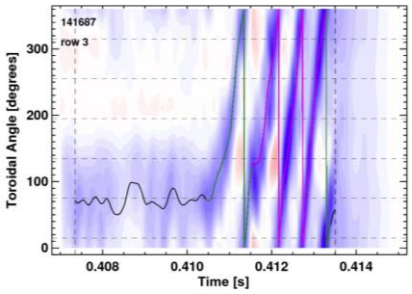

Disruptions

Research Goals and Plans for Macroscopic Stability

2.1 Overview of goals and plans

2.1.1 Overall goal and motivation

The overall goal of macroscopic stability research in NSTX-U is to establish the physics understanding and control capabilities needed to produce sustained stability of high performance ST plasmas in a yet unexplored hotter operational regime at the highest level of current self-sustainment ever routinely produced in such a device. With double the toroidal field, plasma current, and heating power compared to NSTX, the upgraded device will be the most powerful ST in the world, producing the highest stored energy and lowest collisionality ever produced in an ST. Additionally, NSTX-U will provide expanded capability to vary key stability parameters including the plasma rotation and energetic particle density profiles via the unique more tangential injection geometry of the second neutral beam system. This research will provide the predictive physics understanding needed to confidently extrapolate toward the goal of a steady-state Fusion Nuclear Science Facility (ST-FNSF) / Component Test Facility (ST-CTF) [1-3], a pilot plant [4], or DEMO based on the ST [5,6]. As was exploited in NSTX, the unique ST operational space and device geometry of NSTX-U will be leveraged to extend and test physics theories and technological solutions for next-step spherical torus (ST) and tokamak operation, including ITER.

A present urgent need for ITER, as well as for future ST fusion devices planned to operate continuously, is the prediction, avoidance, and mitigation (PAM) of plasma disruptions. Macroscopic stability research on NSTX from its inception has targeted the stabilization of beta-limiting, disruptive instabilities that stop the plasma, or otherwise prevent it from operating at high fusion performance. Passive [7-9] and active [9-11] stabilization studies of global mode stability, and advanced understanding of 3D plasma response [12], including magnetic island dynamics such as neoclassical tearing modes [13], on NSTX provide a firm foundation for the advanced disruption prediction and avoidance research on NSTX-U (Sections 2.2.1, 2.2.3, and 9.2.3). Macrostability research will strongly contribute to a multi-layered control approach toward an ambitious goal of nearly 100% disruption avoidance. The research for NSTX-U will expand to include disruption mitigation as well (Section 2.2.3). NSTX-U will also expand the capability to alter profiles that affect stability. For the better part of a decade, research on NSTX has utilized non-resonant magnetic braking via neoclassical toroidal viscosity (NTV) – an inherent 3D field effect – to finely control the level and profile of plasma rotation to low levels without causing mode locking. Several unanswered questions remain regarding the understanding of this physics and scaling to next-step devices (Section 2.2.2). A significant and unique advancement in the use of NTV will be as an actuator for real-time feedback control of the plasma rotation profile – a unique capability for tokamaks. This research will strongly interconnect with other topical science areas – in particular with Advanced Scenario and Control research (Chapter 9), but also with Transport and Turbulence, Boundary Physics, and Energetic Particle research (Chapters 3, 4, and 6).

2.1.2 Bridging knowledge gaps for ST fusion devices and to support ITER

NSTX-U is designed to address critical stability physics understanding for future STs, and for tokamaks/ITER as stated in Section 2.1.1. Due to its critical need, this physics has been considered in recent DOE reports defining such needs. For example, the report “Research Needs for Magnetic Fusion Energy Sciences” (ReNeW - 2009) [14] defines the key scientific and technical knowledge gaps in magnetic fusion research needed to bridge present systems to devices producing significant fusion power for long (many minutes to weeks) duration. NSTX-U macrostability research will address elements of three of the five ReNeW Themes:

- Theme 1: Burning Plasmas in ITER
- Theme 2: Creating Predictable, High-Performance, Steady-State Plasmas
- Theme 5: Optimizing the Magnetic Configuration

Elements of Themes 2 and 5 will be addressed directly, while elements of Theme 1, for example, "Thrust 2: Control transient events in burning plasmas", will be addressed indirectly. The centerpiece thrust for the spherical tokamak from ReNeW is "Thrust 16: Develop the spherical torus to advance fusion nuclear science". This thrust contains 7 elements, 5 of which address physics needs of next-step ST experiments. Three of these 5 elements are addressed in the macrostability research described in this section, summarized here in sub-bullets:

- ReNeW Thrust 16 Element: *Utilize upgraded facilities to increase plasma temperature and magnetic field to test the understanding of ST confinement and stability at fusion-relevant parameters*
    - Lower collisionality operation of NSTX-U at higher temperature will provide a unique laboratory for the ST to investigate the physics of kinetic resistive wall mode stability at lower ν. It will be determined whether the observed and measured *increase* of mode stability at the highest levels of β_N/l_i in NSTX continues as ν is further reduced, and whether this trend is due to kinetic RWM stability physics.
    - NSTX-U researchers will determine the important dependence of NTV at reduced values of ν^* that is theoretically expected to show an increase in plasma rotation drag, and compare physical models of NTV including fluid models with kinetic effects and particle-in-cell models to determine the most important physics aspects
    - The role of energetic particles on ST plasma macrostability has only begun to be investigated. NSTX-U will provide a greater capability to vary the energetic particle profile via a greater range of B_T, I_p, and NBI injection angles.

- ReNeW Thrust 16 Element: *Implement and understand active and passive control techniques to enable long-pulse disruption-free operation in plasmas with very broad current profiles.*
    - The physics understanding of passive control of low frequency modes will be significantly enhanced by the unique NSTX-U capability of utilizing both NBI and 3D-field (via NTV) actuators to change mode stability by controlling the plasma rotation and equilibrium profiles, including the effect of kinetic RWM stabilizing resonances, and to study and attempt to avoid NTM mode locking conditions.
    - Active control of low frequency modes with toroidal mode number, n = 1 and 2 will be studied in NSTX-U using a combination of upgraded control hardware (available on Day 1), dual-component magnetic field perturbation measurements, and expansion of the present NSTX model-based RWM state space controller (RWMSC) proposed for use in ITER.

- The advantages gained by expanded multi-mode controller capability of the RWMSC will be determined, including enhanced ability to reduce error fields.
- The theoretically computed increase in global eigenmode amplitude in the divertor region at high β_N will be investigated utilizing an expanded RWM sensor set. The prominence of this mode in the full computed multi-mode spectrum and the impact on active mode control will be determined. The impact of snowflake divertor operation on this mode will be assessed.
- Present models will be tested and continued to be developed, and real-time physics criteria will be implemented for use in the NSTX-U disruption avoidance system including simple models of kinetic RWM stability, and the RWM state space controller observer.
- Active, low frequency MHD spectroscopy will be analyzed and developed for real time use to avoid disruptions by altering NBI power and/or rotation/equilibrium profiles, and the importance of multiple modes will be determined.
- Dynamic error field correction will be possible for simultaneous correction of n up to 3 with the present midplane coils.
- The addition of an upgraded non-axisymmetric control coil set (NCC) will significantly expand stability physics research capabilities for dynamic error field correction (n up to 6), RWM control (n up to 4), and NTV physics studies and will be used in rotation profile control, and ELM mitigation/stabilization.

- ReNew Thrust Element: *Employ energetic particle beams, plasma waves, particle control, and core fueling techniques to maintain the current and control the plasma profiles.*
  - The significant impact of fully non-inductive current sustainment on macrostability physics will be determined. This pioneering milestone for NSTX-U is expected to have multi-faceted ramifications on both tearing and ideal instabilities.
  - Improvements to plasma stability enabled by rotation profile control and the RWMSC on plasmas with very low (ITER-relevant) plasma rotation speeds will be determined.
  - NSTX-U researchers will develop reduced NTV models incorporating the most important physical effects possible for real-time use supporting the rotation profile control system.
  - The utility of NBI, and ability and physics of NTV in controlling rotation in plasmas with very low rotation speed will be determined - expanding past NSTX operation in the NTV superbanana plateau regime.

The analysis and use of three-dimensional field (3D) effects in systems that primarily have toroidal symmetry (two-dimensional fields) is considered important, and in many cases essential in present macrostability research. Therefore, research on 3D effects pervades the full NSTX-U macrostability program.

The proposed NSTX-U 5 Year Plan research on macroscopic stability is also highly-aligned with the Department of Energy's vision of US magnetic fusion research. The associate director of DOE's Fusion Energy Sciences Office of Science, Dr. Edmund Synakoswki has defined a program vision incorporating three major components: burning plasma dynamics, long-pulse plasma control science, and fusion materials science. The second element is the major focus of NSTX-U macroscopic stability research for 2014-2018. The research is particularly unique and pioneering in that it plans to move tokamak stability research solidly into a new realm of controlling fully non-inductive plasmas at high beta, with a unique combination of control actuators.

The proposed research is also directly coupled to ITER through the ITPA. Past NSTX research has been communicated bi-annually at each ITPA MHD Stability group meeting for many years. The NSTX-U macrostability group leads the MDC-2 joint experiment / analysis on RWM physics, and co-leads the Working Group 7 effort on aspects of active mode control. The NSTX-U group has also led two elements of the recent ITPA Integrated Plasma Control Working Group study, led by Dr. Joseph Snipes of ITER. The group also contributed with direct calculations for ITER on RWM and error field control associated with this effort. Even through the experimental outage period, the stability research group maintains contributions to five MDCs and two working groups. NSTX-U stability research plans to expand this effort in the coming five year period, especially through the stronger cross-coupling between the NSTX-U macrostability and the advanced scenarios and control topical science groups.

In the following section (2.1.3), an overview is provided of the research goals and plans in macroscopic stability summarized above, now logically subdivided into three separate, but strongly related thrusts. Interconnections between the thrusts are then briefly highlighted. Several experiments proposed for the last NSTX run campaign are appropriate to initiate macrostability research on NSTX-U, and will provide a seamless start to continued experimental research once the upgrade is completed. Finally, the motivation and design of a significant upgrade which will greatly benefit macroscopic stability research – the proposed non-axisymmetric control coil (NCC) - is briefly motivated and discussed in Section 2.1.4, with further detail on the significant physics design analysis performed to date for this system. This upgrade will serve research in several other topical science groups as well, including boundary physics, energetic particle physics, and advanced scenarios and control. Specific uses of the NCC in various physics studies are covered in this chapter, and also in other research thrusts chapters.

2.1.3 Thrusts and goals by topical area

2.1.3.1 Sustainment of macroscopic stability

Macroscopic MHD instabilities (such as the kink/ballooning mode, resistive wall mode (RWM), and tearing modes that lock) are critically important to avoid or control as they lead to plasma disruption, terminating the discharge and leading to large, potentially damaging electromagnetic forces and heat loads on the structure of fusion producing devices.

While many targeted performance parameters have been reached in world tokamaks, such high performance plasmas will need to be sustained for far longer pulse lengths in machines such as FNSF, ITER, and DEMO than have been produced to date. Research has therefore changed focus to examine sustained global mode stability over long pulses and to examine profile evolution for routine long pulse operation at high beta and at high non-inductive current fraction. Common to the following studies is the unique physics understanding and control ramifications that come from such operation, and the understanding and prediction of the effect of excursions from this condition due to transient behavior. It is especially important to realize that plasma operation near but below marginal stability points (set for example by plasma beta, internal inductance, rotation) is insufficient to ensure disruption-free, continuous operation in either ITER inductive or advanced scenarios due to these transients in plasma profiles. Such transients can rapidly change a stable operational point to an unstable plasma state. Therefore, understanding plasma stability gradients vs. key profiles affecting stability is essential for all operational states in ITER or an FNSF.

NSTX-U will provide key capabilities for critical physics understanding based on present research in plasma operation regimes applicable to ITER and future magnetic fusion devices. The NSTX-U plan is unique in its goal to operate 100% non-inductively driven plasmas routinely. This major operational regime for NSTX-U, which may require greater control, provides a unique lab to test advanced stability physics. Additionally, NSTX-U will operate in the unique high beta ST operational space, which will allow performance of advanced stability control in an operating space where disruptivity is *not* most probable at the highest β_N, or β_N/l_i. The research is enabled by independent control of the present midplane RWM coils – a new capability that NSTX-U brings, along with the continued physics development of the present model-based RWM state-space controller for both slow and fast correction of 3D field perturbations with toroidal mode number, n up to 3. The research capability will be significantly expanded in the last two years of the five year period by the planned NCC system (details given

in Section 2.2.1.5 and throughout the chapter), allowing n up to 6, and a broader poloidal spectrum and variability of field helicity. These considerations motivate the following thrust:

Thrust MS-1: Understand and advance passive and active feedback control to sustain macroscopic stability

With significantly expanded profile control capabilities (e.g. q, plasma rotation), NSTX-U will allow greater ability to vary these important profiles for investigations of how to prevent plasma disruptions excited by profile excursions. Additionally, profiles theoretically expected to improve stability will be attempted to be sustained at high performance, including fully non-inductive operation. Real-time models to determine favorable profiles for stability will be developed from experimental testing of full theoretical models. Research will focus on the effect of reduced plasma collisionality and energetic particles on the kinetic stabilization of disruptive instabilities, and sustaining stability. Shape and aspect ratio changes, the effect of advanced divertor configurations, and 3D multi-mode spectrum will be assessed. ITER-relevant low plasma rotation regimes will be evaluated. Disruption prevention research will be conducted as a combination of advanced active mode control techniques and active profile control. For example, instability onset leading to global modes growing on a relatively fast timescales (milliseconds) will be actively controlled by an expanded model-based RWM state space controller, while concurrent control of q and plasma rotation profile working on slower timescales (~100ms) will steer the plasma toward stability. Instabilities occurring before plasmas attain full current, and the ability to control largely internal modes will be addressed.

2.1.3.2 Utilization of non-axisymmetric (3D) magnetic fields

A small non-axisymmetric (3D) field almost always exists in tokamaks, due to imperfect primary magnets and surrounding conductors and machine components. Tokamaks are highly sensitive to 3D fields, which can cause unnecessary transport and instability and even lead to a disruption if not properly compensated [12,15-17]. On the other hand, 3D fields can be greatly beneficial if properly controlled, by using non-ambipolar transport [18] that can modify equilibrium and plasma rotation profiles and therefore macroscopic stability, as well known by edge localized mode (ELM) control using resonant magnetic fields [19,20] and resistive wall mode (RWM) [8,10], and tearing mode (TM) and/or neoclassical tearing mode (NTM) [13,21,22] control using non-resonant magnetic fields. Therefore, it will be critical to achieve the controllability as well as

the predictability of these 3D field applications, in order to improve plasma stability and performance in next-step devices such as FNSF, ST Pilot, and ITER.

There has been substantial progress in understanding 3D field effects. Research on n = 1 resonant error field correction in NSTX using the ideal perturbed equilibrium code (IPEC) (Section 2.4.3) highlighted the importance of ideal plasma response [12,23,24] and the developed method has been actively applied to ITER [25] along with a paradigm change in error field correction. Also, n = 3 non-resonant error field correction has been routinely used to maximize the toroidal angular momentum based upon successful validation across experiments and neoclassical toroidal viscosity (NTV) calculations [18,26]. Based on the improved knowledge on 3D field effects in general, resonant and non-resonant error field effects will be studied together [27-29] in order to provide comprehensive error field correction schemes for the next-step devices. The rotating island dynamics such as neoclassical tearing modes and the interplay with error fields, which are fundamentally 3D effects, will require further extensive research in non-ideal and non-linear regimes [15,30-35]. The strong shaping and high-β in NSTX-U, and with the addition of the NCC, will provide a unique test environment of the island 3D dynamics.

The NTV transport and its magnetic braking on toroidal rotation are well-known effects produced by 3D fields, and the braking can be a useful tool to control the toroidal rotation and thereby suppress various instabilities in NSTX-U. The magnitude of NTV is theoretically expected to change significantly at lower plasma collisionality, so requires further research in this regime. Several NTV physics elements have been theoretically investigated [18,36-51], numerically computed [52-54], and examined in experiments in various devices including NSTX [7,9,55,56], DIII-D [57,58], and KSTAR [59,60]. However, a number of aspects in NTV physics are still not fully resolved and need further study in order to confidently extrapolate understanding to next-step devices. Another outstanding issue regarding 3D fields is their role in local modification of transport and stability, either by non-ambipolar transport such as NTV or by stochastic transport with magnetic islands, which is believed to be the main physics mechanism behind ELM control by resonant magnetic perturbations.

NSTX-U will provide strong capabilities for this research, including unique control of toroidal rotation using both NBI and non-resonant 3D fields, and providing various possibilities of toroidal momentum and rotation profile control in unexplored parametric regimes for NTMs and RWMs. Furthermore, the NCC will give significantly greater flexibility in 3D field studies. The poloidal field spectrum will also be as rich as the ITER RMP coils when the NCC is combined with the present midplane coils. These considerations motivate the following thrust:

Thrust MS-2: Understand 3D field effects and provide the physics basis for optimizing stability through equilibrium profile control by 3D fields

Expanded 3D field application capabilities will be utilized to study 3D field effects on resonant error field correction, and to develop the physics basis for control of toroidal rotation through non-resonant magnetic braking while simultaneously applying RWM control and dynamic error field correction. Non-ideal and non-linear island dynamics including neoclassical tearing modes, and the interplay with resonant and non-resonant error fields, will be studied together with strong shaping, high-β, and low collisionality. The NTV physics yielding magnetic alteration of the rotation profile will be systematically studied as a function of plasma collisionality as density control tools are improved during the 5 year plan period. This physics research will be greatly enhanced by the proposed NCC coils. The toroidal rotation profile will also be more widely varied using the 2nd off-axis NBI system. The combination of the new NBI, upgraded independent control of the present midplane coils, and proposed NCC will be utilized to vary and understand toroidal momentum transport for a range of magnetic field spectra and plasma collisionality conditions to develop the physics basis for magnetic rotation profile control to improve and optimize plasma performance.

2.1.3.3 Disruption physics, prediction, avoidance, and mitigation

A key issue for ITER, and the tokamak/ST line of fusion devices in general, is the avoidance and mitigation of disruptions. As a general goal, disruptions must be avoided. The research program in Thrusts 1 and 2 of this chapter, as well as in Thrusts 2 and 3 of the Advanced Scenarios and Control chapter (Chapter 9), develops the physics understanding and many of the necessary tools for disruption avoidance. These tools by themselves, however, are not sufficient to meet the stringent requirements for reliable tokamak/ST operations. The present thrust describes four additional research tasks for disruption prediction, avoidance, mitigation, and characterization.

The first two elements, described in Sections 2.2.3.1-2.2.3.2, describe the development of techniques for integrated disruption prediction and avoidance. Methods developed in these sections combine various actuators and measurements, in order develop more integrated control of global stability. For instance, resonant field amplification methods will be developed to assess global stability, and will be coupled to the β_N and/or rotation control algorithms with the goal of keeping the plasma in a stable regime. Similarly, the difference between the state-space RWM control observer and measurements will be used to provide an indicator of the onset of disruptions, separate from its use for direct mode control.

The third element, described in Section 2.2.3.3, addresses the topic traditionally known as disruption "mitigation". This topic is also of great importance to ITER, where methods to terminate a discharge without excessive thermal or mechanical loading of the device are required. This research will focus on two technologies for rapidly terminating a tokamak discharge. Massive gas injection (MGI) will be explored: the poloidal angle dependence of mitigation efficacy will be examined, and modeling of the gas penetration with the DEGAS-2 code (Section 2.4.11) will be done. Secondly, a novel electromagnetic particle injector (EPI) will be developed. This technology has the potential to very rapidly deliver large amounts of the material to the plasma, and will be tested on NSTX-U. Note that this topic is complementary to that discussed in ASC Thrust 3, focusing on rapid discharge terminations using traditional inductive ramp-down techniques. NSTX-U is also capable of studying runaway current suppression as described in Section 2.2.3.3.3.

The final element, described in Section 2.2.3.4, focuses on the physics of disruptions themselves. Key topics to be addressed here are the physics of, and heat loading from the thermal quench of a disruption, and generation of halo currents.

Thrust MS-3: Study and develop techniques for disruption prediction, avoidance, and mitigation, and understand disruption dynamics and in high-performance ST plasmas

> *The physics understanding gained in the balance of the macroscopic stability research will be applied to improve disruption prediction and avoidance. Kinetic stability physics models, low frequency resonant field amplification, RWM state-space control models, and expanded sensor input will be used to improve disruption prediction. Real-time implementation of these physical models and measurements will be used for disruption avoidance. The plasma dynamics resulting from the interplay of different stability controllers will be measured and simulated. For instance, resonant field amplification methods will be developed to assess global stability, and may be coupled to the β_N or rotation control algorithms to ensure that the plasma remains in a stable regime. The characteristics and dynamics of NSTX-U disruptions will be measured and modeled – in particular heat loading, the thermal quench, and the generation of halo currents – all to improve the understanding of the impact of disruptions in STs and tokamaks. Techniques for disruption mitigation will be developed and explored. Massive gas injection (MGI) will be explored: the poloidal angle dependence of mitigation efficacy will be examined, and modeling of the gas penetration will be done. A novel electromagnetic particle injector (EPI) will be developed and tested. This technology has the potential to very rapidly deliver large amounts of the material to the plasma.*

2.1.3.4 Thrust and topical science group interconnections

The macroscopic stability research described in this chapter has many interconnections between the stated three thrusts, and also to many of the other topical science group (TSG) research topics in NSTX-U. A summary of several significant elements are:

- Thrust 1 elements that aim to understand the physics of macroscopic mode stability, and the related advanced mode control capabilities, directly serve the disruption prediction and avoidance control elements in Thrust 3
- Thrust 2 elements that aim to control dynamic error fields and understand tearing mode locking directly support disruption avoidance elements of Thrust 3. NTV physics aspects and reduced physics models for real-time use directly support plasma rotation control elements of the Advanced Scenario and Control (ASC) TSG.
- Thrust 3 elements serve the entire NSTX-U Team in producing greater reliability (and eventually, routine capability) of reducing disruptions in the device. These critical capabilities will also have a direct connection to certain tasks as needed, for example, to attempt sustaining Enhanced Pedestal H-mode operation.
- Direct interaction between the Macrostability (MS) and ASC TSGs will occur in all Thrusts, with complementary tasks associated with physical models for plasma rotation control and physical mode stability models used to trigger the disruption warning system.
- Significant interaction between the MS and Boundary TSGs will occur in determining ths impact of snowflake divertor operation on global mode stability, and understanding the physical effects of 3D fields on ELMs.
- The physical effects of energetic particles on macroscopic instabilities found in NSTX will continue to be studied in Thrust 1, coupled to the Energetic Particle TSG.
- The NTV physics and the effects of 3D fields on transport in Thrust 2 interconnects with momentum transport work conducted by the Transport and Turbulence TSG.

2.1.4 Non-axisymmetic control coil (NCC) motivation

The powerful utility of 3D fields has been rapidly appreciated in the tokamak research community, as 3D fields can provide selective channels of transport and thereby allow stability control. The NTV momentum transport by 3D magnetic braking can be well utilized to control and optimize toroidal rotation, and stabilize macroscopic instabilities such as the RWM and NTM, microscopic instabilities such as ITG, TEM, and ETG, and fast ion instabilities such as TAE and GAE by altering the energetic particle population. Also 3D fields can provide particle transport to alter the pedestal and thus modify ELMs, as well known by RMP ELM control.

However, such plasma instabilities are not simple functions of rotation, and NTV itself depends on rotation. RMP ELM control is also not yet well understood and predictable, as essentially all different devices, with different 3D coils, have yielded somewhat different results. In NSTX, 3D fields generated by the existing midplane coils can trigger ELMs, an opposite and nearly unique result compared to other devices. Further extensive studies of 3D fields are therefore necessary, and NSTX-U will provide a unique and important contribution to 3D field physics understanding utilizing its strong 2D shaping and operation in an advanced high-β regime. The results will be greatly enhanced by additional 3D coils added to give greater flexibility in the applied 3D field spectrum that can be coupled to the strong 2D shaping. This motivates the addition of a new non-axisymmetric control coil (NCC).

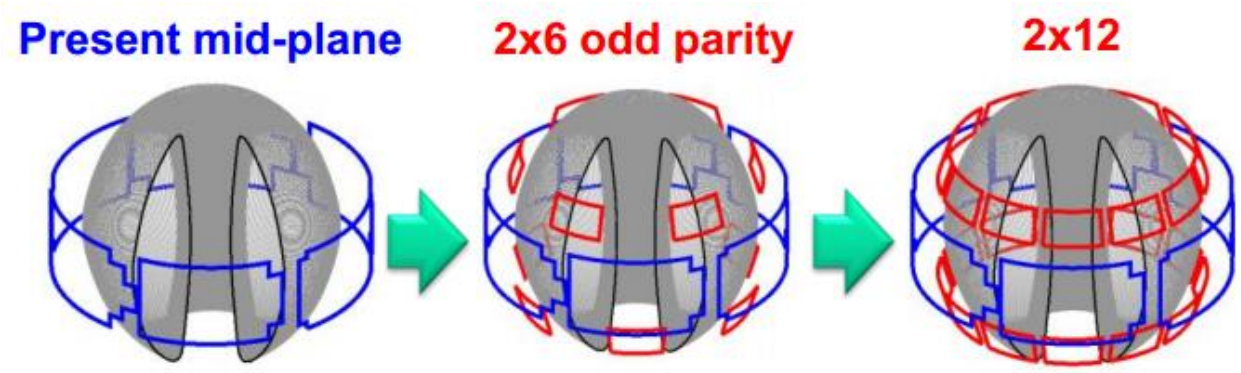

Figure 2.1.4-1. Non-axisymmetric control coil (NCC) (red) proposed for NSTX-U, in a staged installation with partial NCC (2x6-Odd) and full NCC (2x12). The coils shown in blue are the present midplane RWM coils.

The NCC will provide a significant expansion of physics research not only in the Macrostability TSG, by in several physics areas spanning the majority of the NSTX-U topical science areas. The NCC has been proposed as a set of off-midplane coils implemented in a staged approach, with one example illustrated in Figure 2.1.4.1. The NCC, combined with the present midplane coils, can produce a highly flexible 3D field spectrum, comparable to the proposed ITER RMP coils, and. The NCC can significantly increase the RWM β-limit by active control, allows a significant increase in stability physics and disruption control studies (MS, Section 2.2.1), and can increase dominance of non-resonant over resonant field components (MS, Section 2.2.2.1) and NTV variability in the core (MS, Section 2.2.2.5) by an order of magnitude. The NCC will be able to provide edge-resonant field enough to create a stochastic layer, with greater extent than needed for ELM control based on empirical RMP criteria, while decreasing the non-resonant field by an order of magnitude (MS,BP, Section 2.3), and to substantially modify 3D stability and actively control or pace ELMs (BP, Section 4.2.1.3). Also, the improved rotation and rotation-shear control will be very important to perform advanced studies for micro-instabilities such as ITG/TEM/ETG (T&T, Section 3.3.3.1), and momentum transport studies in general (T&T, Section 3.3.3.2). The change of fast-ion transport and stability by 3D fields can be further investigated using the NCC, as such studies started in NSTX using the midplane coils

(EP, Section 6.3.3.1). As is apparent from these applications, the NCC will be a critical tool for NSTX-U research and will largely advance understanding of 3D field physics for tokamaks in general. More details for each subject can be found in the other TSG chapters as indicated above. The main physics design activities of the NCC including quantitative assessment of error field correction, NTV, RMP, and RWM control will be separately described in Section 2.3.

2.2 Research Plans

This section describes the research to be conducted in the macroscopic stability topical science area for the five year period.

Each subsection follows a similar format: First, a description of the research is given, with appropriate motivating work shown which also establishes context, and second, a "Summary of research plans by year" is provided. Note that in these summary subsections, years 1-5 refer to the years of the NSTX-U 5 year plan, with the first year of device operation starting in year 2.

On Day 0 of NSTX-U operation, the device will have significantly upgraded capabilities compared to NSTX, and will also benefit from capabilities that were unable to be utilized in the abbreviated 2010 run. In addition, several significant new control and diagnostic hardware capabilities (described in several sections of this document) will be added during the 5 year period described. Capabilities of special note include a new MGI disruption mitigation system, a partial implementation of a new set of non-axisymmetric field coils, and an extended sensor set for improved low frequency (NTM and RWM) mode characterization. Macrostability research will also help produce, and greatly leverage techniques to control plasma rotation, q, pressure, and $n > 0$ modes. The largest hardware component supporting macrostability research during the 5 year period will be the partial NCC, which is planned to be implemented during an outage between the third and fourth years in the baseline funding scenario.

The timing of research deliverables listed below best utilizes the new capabilities as presently planned. Modification of the availability of these capabilities will logically lead to modification of the deliverables timeline, with completion of tasks shifting to match changes to the hardware and control capability timelines.

2.2.1 Thrust MS-1 – Understand and advance passive and active feedback control to sustain macroscopic stability at low collisionality

2.2.1.1 Macroscopic mode stability at lower collisionality

NSTX-U will provide several important upgraded capabilities to study key dependencies of global mode stability on plasma characteristics. The second neutral beam line with double the available power and will provide the ability to alter the power and momentum deposition profile. This will allow changes to the most basic equilibrium profiles: pressure and q, but it will also, in combination with neoclassical toroidal viscosity (NTV) generated by applied 3D fields, allow significant variation of the plasma rotation profile, which effects both tearing and kink/ballooning/RWM instabilities. Added to these basic variations is another key parameter, the plasma collisionality, ν. Stability is indirectly affected by ν as it changes the steady state rotation profile. But NSTX data has shown that a more direct effect occurs from the influence of ν on kinetic stabilization of global modes. Therefore, it is crucial to create and study the self-consistent, quasi-steady-state equilibrium variations at values of ν not yet attained in the ST. Energetic particle profile and velocity space distribution also influences mode stability, and NSTX-U upgrades will allow variations of this profile as well.

2.2.1.1.1 Assess beta and q limits in NSTX-U shape and off-axis NBI

The upgraded center column of NSTX-U will be approximately double the diameter of the NSTX predecessor. This will increase the plasma aspect ratio and will change the boundary shape. In addition, it is planned that the snowflake divertor [61] configuration will be used in a larger number of plasmas in NSTX-U to handle the high first wall heat loads at high P_{aux}. Such changes to the boundary are expected to affect the ideal stability of the plasma, which will be investigated experimentally. This investigation has already begun, as experimental scenario development in NSTX has already accessed aspect ratios (up to 1.73) and boundary shaping (elongation greater than 2.9) planned for NSTX-U [62] (Figure 2.2.1.1.1-1). The new off-axis neutral beam line will also produce changes to plasma pressure and current profiles that will affect stability. Therefore, a new space of beta and q-profile will be explored to determine the limits on plasma stability. Such studies of the ideal stability are needed as input to studies of the actual marginal stability boundaries that include kinetic stabilization effects.

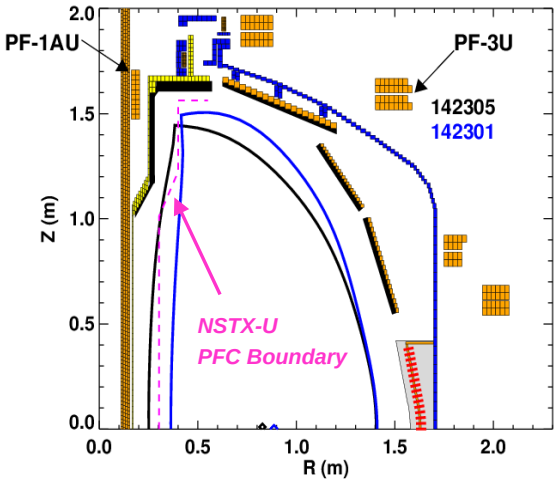

Figure 2.2.1.1.1-1: NSTX plasmas have matched the aspect ratio and elongation planned for NSTX-U.

The three new NBI sources in NSTX-U will inject farther outboard of the magnetic axis at the plasma midplane. This capability can be used to drive off-axis current and therefore raise the core q-profile, which will have a major effect on the macroscopic stability of the plasma, including neoclassical tearing modes (NTMs). Note that NTM physics is discussed mainly in Section 2.2.2.1 of this chapter. Additionally, off-axis NB injection can potentially broaden the plasma rotation profile. This too would have a major impact on stability, particularly RWM stability, and will be fully investigated and compared to theoretical predictions.

2.2.1.1.2 Define favorable combined rotation / kinetic profiles for plasma stability

Time-evolved NSTX-U equilibrium simulations have been created, and these equilibria will be used to best prepare for NSTX-U macroscopic stability experiments. TRANSP calculations are available which provide the full kinetic and energetic particle population information for use by the MISK code (Section 2.4.4) to determine kinetic RWM stability boundaries. These computations will be performed in the years prior to NSTX-U first plasma. In addition to the boundary variations discussed in the prior section, the equilibrium, rotation, and energetic particle profile variations will be considered in this analysis to determine how the kinetic resonances will change in NSTX-U, and therefore how global mode stability will change.

2.2.1.1.3 Test kinetic RWM stability theory in lower collisionality plasmas

Past NSTX research has established a new understanding of resistive wall mode stability by making quantitative correlation between experiments reaching the mode marginal stability point and kinetic RWM stabilization theory [8,9]. This model has important implications for next-step devices operating at reduced collisionality. Early RWM stabilization models relied solely on plasma collisionality as a stabilizing energy dissipation mechanism, yielding reduced stability at reduced collisionality. The present kinetic RWM stabilization theory changes this significantly, yielding a more complex stability picture. As before, stabilizing effects of collisional dissipation are reduced at lower ν, but new stabilizing resonant kinetic effects can be enhanced [63]. Generally, stronger resistive wall mode (RWM) stabilization occurs near broad dissipative kinetic resonances (which depend on the plasma rotation profile) and this stabilization increases with decreasing collisionality, but in stark contrast has almost no dependence on collisionality when the plasma is off-resonance (see Figure 2.2.1.1.3-1). In this figure, ν_{exp} and ω_ϕ^{exp} represent NSTX experimental values in high beta plasmas, and kinetic RWM stability calculations producing the mode growth rate are made using the MISK code [63]. Experiments that utilized n = 1 active MHD spectroscopy [64] diagnosis, which uses n = 1 resonant field amplification to measure

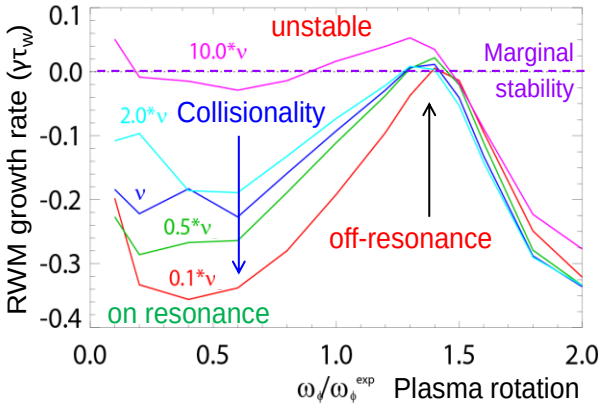

Figure 2.2.1.1.3-1: MISK computed kinetic RWM n = 1 stability vs. collisionality and plasma rotation.

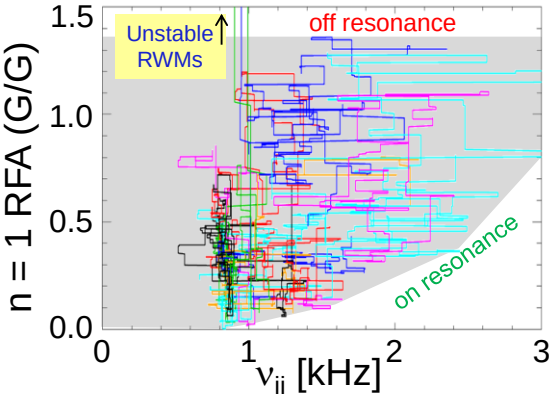

Figure 2.2.1.1.3-2: n = 1 RFA amplitude vs. ν_{ii}, showing a relatively large change at low RFA ("on resonance") vs. almost no change at high RFA.

RWM stability [65], indicate the expected gradient in RWM stability for plasmas with high $5.5 < \beta_N/l_i < 13.5$ (most are above the n = 1 ideal no-wall stability limit) (Figure 2.2.1.1.3-2). The figure shows the trajectory of the RFA amplitude over the entire discharge for 20 shots, over which the ion collisionality, ν_{ii}, is varied by a factor of 3.75. The theoretically expected gradients in kinetic RWM stability are generally reproduced by the upper/lower boundaries of n = 1 RFA amplitude. At high n = 1 RFA amplitude (the upper boundary), the plasma is off-resonance, and there is almost no change in RWM stability (indicated by the n = 1 RFA amplitude) vs. ν_{ii}. At low n = 1 RFA amplitude (the lower boundary), the plasma has greater stabilization by kinetic resonances, and there is a clear increase in RWM stability (decrease in n = 1 RFA amplitude) as ν_{ii} is decreased. Here, ν_{ii} is averaged over $0.55 < \psi_N < 0.75$ of the profile, inside of the pedestal, and ψ_N is the normalized poloidal flux, $(\psi - \psi_0)/(\psi_a - \psi_0)$, where subscript "a" represents the plasma edge, and "0" represents the magnetic axis.

In NSTX-U, it is planned to extend these experimental measurements of mode stability and expectations of kinetic RWM stability theory in experiments ranging to the lowest possible ion collisionality in the device, and also in plasmas having the extra constraint of full non-inductive current drive, which are expected from TRANSP simulations to be constrained to plasma collisionality reduction of a factor of four. Variations of the proximity to stabilizing kinetic resonances (e.g. ion precession drift resonance) will be primarily attained by variation of the plasma rotation profile, by a combination of varying NBI sources at different tangency radii and NTV variation to precisely and reliably produce different rotation speeds and profiles. In early years, the rotation will be changed with open-loop rotation control. Once the rotation feedback system becomes available in later years, closed-loop feedback will be used, using independent and combined variations of NBI and NTV actuators.

Energetic particle effects have also been shown to significantly influence RWM stability. Stabilizing effects of the energetic particle population have been computed, using the MISK code, to play a significant role in the RWM stability of NSTX plasmas [66]. This continues to be an active area of research, as the present EP stability model needs to be tested over a wider range of plasma operation. Extrapolation to ITER Advanced Scenario plasmas shows that the stabilizing effect of alpha particles will be required at expected plasma rotation levels. The greater variations made available by the NSTX-U upgraded NBI system with three additional neutral beam heating sources all aimed at different, and larger tangency radii (farther from the magnetic axis) than the present first three NBI sources, and the larger variation of plasma parameters in NSTX-U will allow greater variation of the EP population, and non-resonant NTV plasma rotation control allows access to very low plasma rotation (applicable to ITER) without mode locking.

2.2.1.1.4 Establish and test approach to marginal stability based on kinetic RWM stability

Previous NSTX research has established the present understanding that a single point rotation measurement is not sufficient as an indicator of RWM stability. Full kinetic RWM calculations with the MISK code [67] capture the necessary physics needed to determine marginal stability. A key goal of the NSTX-U stability research plan is to establish and test the approach to marginal stability both with the more involved kinetic model calculation, and to develop a simpler model that may be used in real-time calculations as input to the NSTX-U disruption warning system.

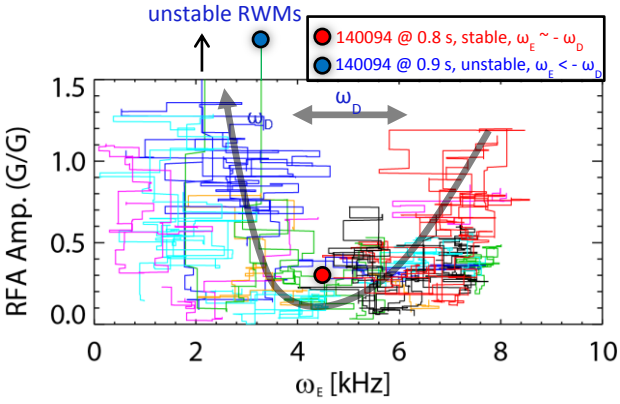

Figure 2.2.1.1.4-1: RFA amplitude vs. an average E×B frequency, ω_E.

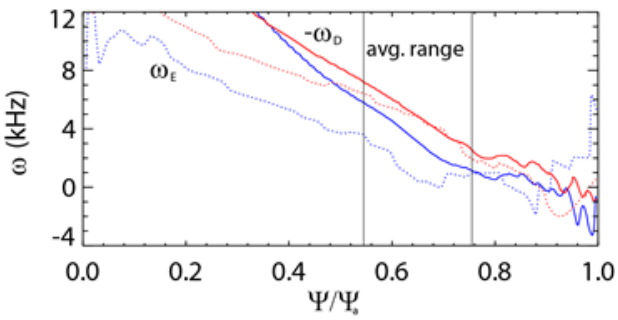

Figure 2.2.1.1.4-2: E×B frequency, ω_E, profiles (dashed) and -ω_D profiles (for ε/T = 2.5 and zero pitch angle), vs. ψ/ψ_a, for NSTX discharge 140094 at 0.8 s (red) and 0.9 s (blue).

An intermediary step in the full MISK calculation that can provide physical insight, and perhaps a calculation than could be approximated in real-time, is to examine the effect of plasma rotation in the context of kinetic resonances between the mode and the particles by examining the E×B

frequency, ω_E, and comparing to the ion precession drift frequency, ω_D. Figure 2.2.1.1.4-1 shows RFA amplitude generated by active MHD spectroscopy measurements plotted against an average ω_E, taken over $0.55 < \psi/\psi_a < 0.75$ of the profile. In Figure 2.2.1.1.4-2 one can see that $-\omega_D$ for hot thermal ions in this ψ range averages roughly 4.5 kHz for discharge 140094 at time 0.8 s (also shown is t = 0.9 s, the time just before this discharge goes unstable). Note that $\omega_E \sim -\omega_D$ at the stable time, and $\omega_E < -\omega_D$ at the unstable time, corresponding to the middle and left sides of Figure 2.2.1.1.4-1, respectively. This can explain the low RFA amplitude in this ω_E range in Figure 2.2.1.1.4-1, with low rotation instability below this, and intermediate rotation marginal stability above. Presumably the RFA would return to lower values at higher ω_E as the mode begins to resonate with the bounce frequency, but this higher level of rotation was not explored in this particular experiment. Similar experiments with MHD spectroscopy in stable plasmas in DIII-D yielded conclusions similarly supportive of kinetic stability theory [68].

This recent NSTX analysis indicates that a simple criterion such as $-\omega_E/\omega_D < K$, where K is a constant, might be used to set a marginal stability condition for NSTX-U in real-time. As this condition is a local condition, further analysis of the present database, and further experiments in the early years of NSTX-U operation will be used to determine how best to implement a criterion such as this for real-time disruption avoidance in later years of the five year research period.

2.2.1.1.5 Investigate early MHD modes

Early MHD modes locking to the wall were a source of low density disruptivity in NSTX. These modes were typically associated with the rational surfaces entering the plasma. Modes at q = 2, 3, and 4 have been observed to lock, with a large degree of variability in the rotation damping dynamics. In NSTX, empirical changes to the fuelling were used to prevent modes from locking. Changes in global parameters due to fuelling changes were quite subtle, but changes to rotation dynamics were profound. A better understanding of mode amplitude and torque dynamics is needed. For example, are there small changes in resistive current evolution, or modification of the early energetic particle modes (EPMs), and is there a measurable quantity to put under feedback control? These questions will be studied in NSTX-U to help improve reliable plasma start-up.

2.2.1.1.6 Summary of research plans by year

Year 1 (2014):

- Begin assessment of theoretically favorable stability conditions, through a combination of existing NSTX data, supplemented by dedicated experiments on DIII-D utilizing low frequency MHD spectroscopy to directly measure stability and creating unstable plasmas, for enhanced kinetic stabilization of global MHD modes. The study will include rotation

profile proximity to stabilizing resonances and energetic particle population variation, for initial experimental scoping studies of the NSTX-U operational space.

- Evaluate simple physics criteria (suitable for real-time use) for the approach to global mode marginal stability based on ideal (e.g. pressure peaking, β_N/l_i) and kinetic stability physics using initial high performance NSTX-U plasmas, emphasizing rotation profile and speed.

Year 2:

- Conduct initial assessment of stability limits on normalized β and q limits at the increased aspect ratio of NSTX-U, with new shaping control and off-axis NBI. Compare to ideal stability limits.
- Utilize off-axis NBI to produce initial investigation determining the effect of pressure, q, and v_ϕ profile variations on RWM and NTM stability.
- Begin investigation of the dependence of global mode stability on reduced collisionality through a combination of dedicated experiments utilizing low frequency MHD spectroscopy to directly measure stability and creating unstable plasmas, and investigating mode-induced disruptions by examining the database in general. Compare experimental results to kinetic stabilization theory. Open-loop rotation control will be the default for these studies, with initial closed-loop control used if available. NBI variations will be conducted with pre-programmed heating, and with β_N feedback.
- Adjust present simplified physics models of RWM marginal stability based on initial high beta, reduced collisionality operation of NSTX-U, appropriate for real-time calculations.

Year 3:

- Theoretically determine improvements to global mode, RWM, and NTM stability expected by the addition of the partial NCC based on improved understanding gained in the first 2 year operation of NSTX-U.
- Test kinetic RWM stability theory expectations, including updated variations of reduced plasma collisionality, based on the more general database of NSTX-U plasmas created during initial device operation.
- Assess modifications of global mode and NTM stability due to expected alteration of q_{min} based on initial device operation, with projections for closed-loop q_{min} control.

Year 4:

- Utilize rotation control to improve RWM/NTM stability: (i) perform closed-loop rotation control studies to alter rotation shear for improved NTM control, and (i) change proximity to stabilizing kinetic resonances for RWM control.

- Validate kinetic RWM stabilization physics at reduced ν^* and varied fast ion populations with closed-loop control of q_{min} in plasmas with non-inductive current fraction approaching, or at 100%.
- Perform initial studies of mode stabilization utilizing improved open-loop plasma rotation profile control afforded by the partial NCC added to the present midplane coil set.
- Initially assess improvements to real-time evaluation of kinetic stabilization model by the addition of initial real-time Thomson scattering results.

Year 5:

- Test kinetic RWM and NTM stabilization models in the lowest ν^* regimes.
- Combine plasma rotation and, q-profile, and, β to demonstrate improved RWM/TM/internal MHD mode stability in 100% non-inductive plasmas, demonstrating very low plasma disruptivity in dedicated experiments.
- Evaluate experimental improvements to real-time kinetic stabilization models through the addition of real-time Thomson scattering.

2.2.1.2 Dual-field component active RWM control and improved mode discrimination at high normalized beta

2.2.1.2.1 Dual-field component active RWM control

Active feedback control of the RWM with the midplane coils was used routinely on NSTX, mostly using poloidal field sensors that discriminated n = 1 mode activity. The control was shown to occur by a combination of limiting mode amplitude and by NTV drag spinning the mode in the presence of the conducting wall at rotation frequency greater than the wall eddy current decay time, leading to strong mode damping [9]. In the last full year of NSTX operation, proportional gain feedback was improved by the addition of radial field sensors and used routinely. Combined radial (24 B_r sensors) and poloidal (23 B_p sensors) field sensor feedback gain and phase were scanned in NSTX experiments to produce significantly reduced n = 1 field and improved stability. The fast (2 - 3 ms) RWM growth was found to be controlled by B_p feedback, while B_r feedback controlled slower n = 1 RFA, which would otherwise cause disruptions once the n = 1 B_r amplitude was sufficiently large (~ 7 – 9 G). Time domain analysis of active control with the VALEN code reproduced the mode dynamics as a function of feedback phase and determined the optimal gain. Modelled feedback evolution agrees with experiment for radial sensor variations examined (Figure 2.2.1.2.1-1), and also shows the optimal gain is still a factor of 2.5 greater than the value used in experiments.

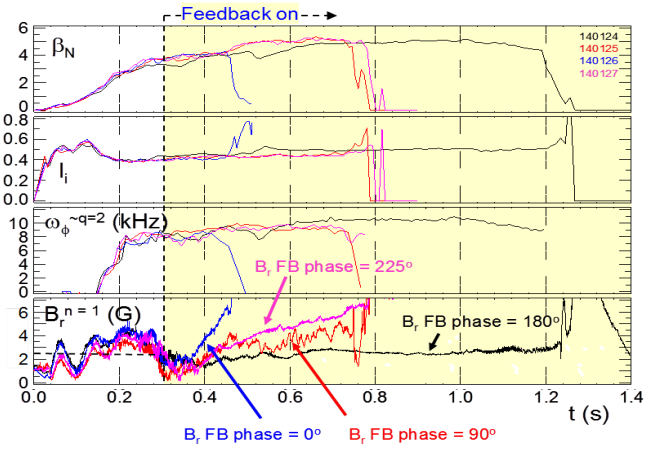

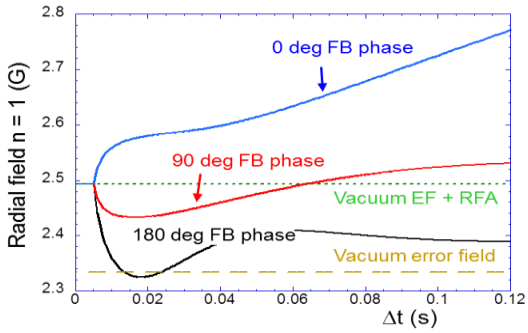

Figure 2.2.1.2.1-1: RWM B_R sensor feeback phase variation with combined radial/poloidal field sensor feedback (a) experiment, (b) theory.

Dual-component active RWM control using proportional gain will be retained on NSTX-U. The system will be improved by adding additional RWM sensors closer to the divertor region. Physics design studies [69] and multi-mode analysis of NSTX (Section 2.2.1.2.2) theoretically show significantly increased mode amplitude in the divertor region at high β_N. This characteristic will be studied using the upgraded sensors, which will be incorporated into the RWM feedback system to further improve mode detection.

2.2.1.2.2 Multi-mode analysis, eigenmode variation at high β_N, and upgraded mode detection

In high β_N plasmas, the influence of multiple RWM eigenfunctions on n = 1 active feedback, including the stable mode spectrum, is a potential cause of β_N fluctuation and loss of control. The multi-mode VALEN code has been applied to NSTX experiments to determine the multi-mode RWM spectrum and characteristics. The perturbed normal field due to induced wall currents shows the influence of the passive conducting plates (Figure 2.2.1.2.2-1a). The computed RWM growth time vs. β_N is in the range observed when such modes are destabilized (Figure 2.2.1.2.2-1b).

The computed spectrum of eigenfunctions comprising the total perturbed field (Figure 2.2.1.2.2-1c) is shown for an unstable mode, and one stabilized by plasma rotation. The RWM multi-mode spectra consist of ideal eigenfunctions computed by the DCON code (Section 2.4.2). These multi-mode components are ordered from lower to higher number, with the lowest number being least stable when each eigenfunction is considered separately in ideal MHD theory. Both spectra show significant amplitude in eigenfunctions up to 10, with the second mode component having the maximum amplitude.

Poloidal cross-sections of the mode components are also shown. Component 1 is ballooning, while component 2, which has dominant amplitude, has maximum perturbation near the lower divertor. There is a significant change in the multi-mode spectrum for the stabilized plasma. In this case, the ballooning component of the perturbation is significantly reduced compared to the component with maximum perturbation in the lower divertor region. The rotationally stabilized multi-mode RWM has a computed rotation frequency of 41 Hz, close to the ~ 30 Hz frequency measured in experiments with both magnetic and kinetic diagnostics (soft X-ray).

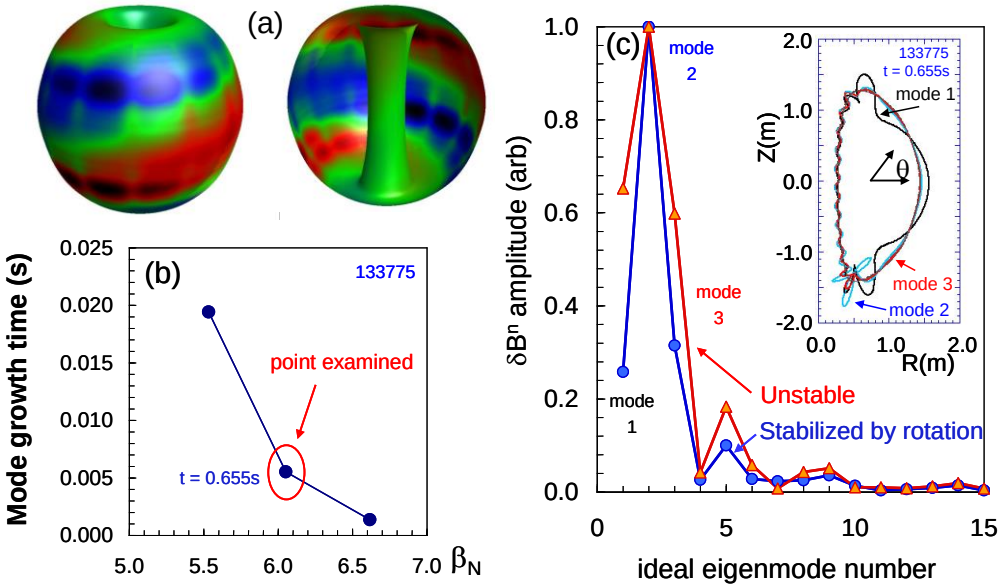

Figure 2.2.1.2.2-1: Multi-mode RWM analysis of high β_N plasmas (a) δB_{normal} from wall currents, (b) growth time vs. β_N, for unstable modes, (c) ideal eigenmode spectrum of multi-mode RWM perturbation showing the spectrum of an unstable mode, and one stabilized by plasma rotation.

Similar calculations for ITER scenario IV plasmas with elevated q_0, β_N = 4, and a modeled blanket conducting structure show multi-mode RWM spectra with up to 6 components of significant amplitude both for unstable n = 1 and n = 2 modes (Figure 2.2.1.2.2-2).

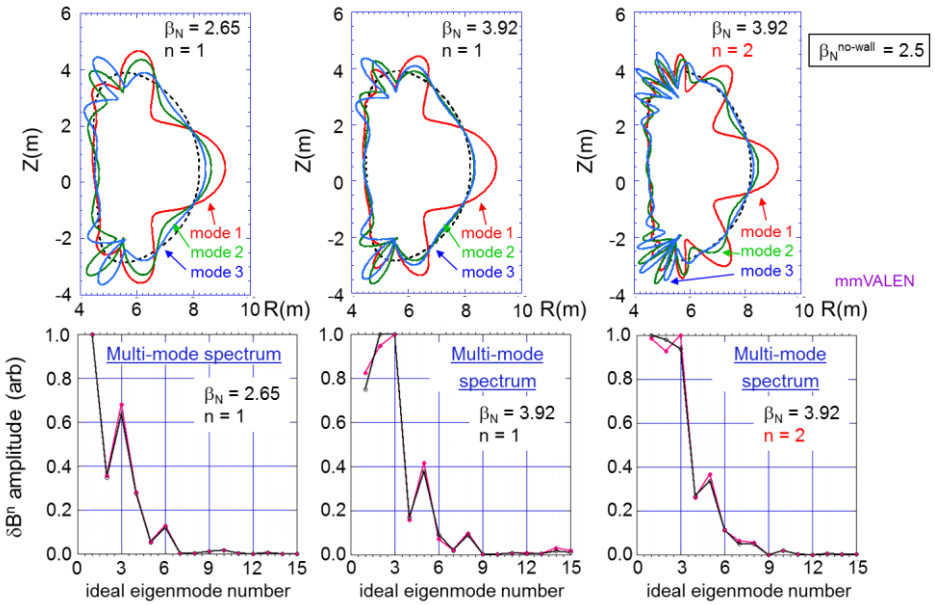

Figure 2.2.1.2.2-2: Multi-mode RWM analysis of ITER advanced scenario discharges, demonstrating a significant eigenmode spectrum in addition to the standard single ideal eigenmode typically assumed in control calculations.

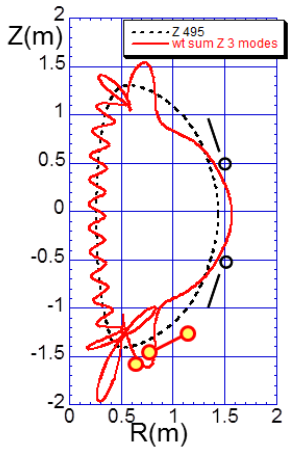

Figure 2.2.1.2.2-3: Weighted sum of three-mode amplitude with present magnetics in black and proposed enhanced magnetics in yellow.

The significant mode amplitude in the divertor region, found both in single and multi-mode studies, motivates the installation of magnetic sensors closer to the divertor region to study the RWM eigenfunction, to compare to expectations of ideal theory, and to directly improve comparisons of the measured mode shape to the real-time RWM state-space controller model (see Section 2.2.1.3.1). Figure 2.2.1.2.2-3 shows the weighted sum of the three modes shown in Figure 2.2.1.2.2-1c as well as the proposed locations of the new sensors, indicating the locations closer to the divertor will improve mode measurement. Figure 2.2.1.2.2-4 shows that a significant change to toroidal phase would be measured by the new sensors due to a significant field line pitch. Note that a relatively long poloidal wavelength still exists (vs. center column region), and the new phase information will help to constrain the RWM state space controller model (Section 2.2.1.3).

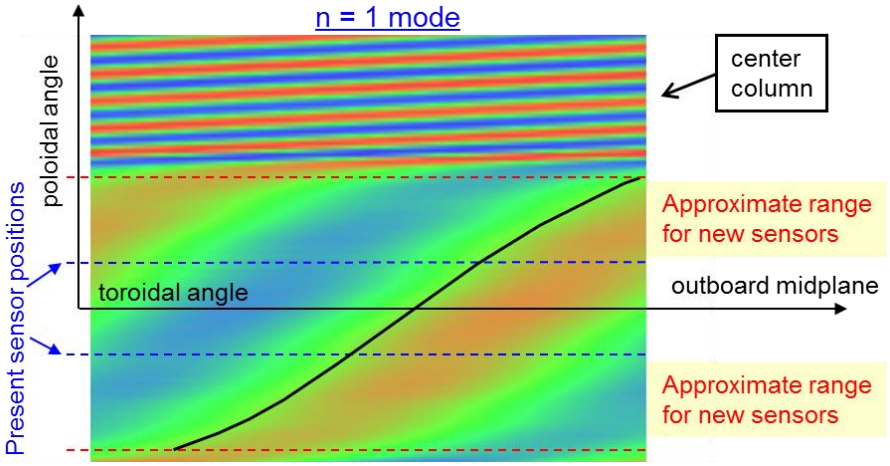

Figure 2.2.1.2.2-4: Mode amplitude vs. toroidal and poloidal angle for an n = 1 mode in NSTX.

Finally, the MARS-K code (Section 2.4.9) will be used to determine the importance of self-consistent alteration of the eigenfunction by kinetic effects and rotation. Additionally, a system of two toroidally displaced, edge and core in-vessel tangential multi-energy soft X-ray arrays (described in detail in Section 10.6.1.3) will be used to measure the mode characteristics.

2.2.1.2.3 Effects of snowflake divertor on RWM stability and eigenfunction

The snowflake divertor configuration is planned to be used extensively in long-pulse, high performance NSTX-U plasmas to handle the high wall heat loads that will be produced by these plasmas. Modifications of the global mode stability due to changes to the edge plasma shaping and eigenfunction modification will be evaluated to determine what ramifications the snowflake will have on stability. In addition, modifications to the RWM control system parameters will be experimentally and theoretically evaluated in the snowflake configuration to determine how the control physics is altered. Changes to the control system will be made to best compensate for any negative ramifications of the configuration.

2.2.1.2.4 Summary of research plans by year

Year 1 (2014):

- Determine theoretically computed optimal feedback parameters for dual component feedback control of projected high beta NSTX-U plasmas.
- Determine multi-mode spectrum for projected high beta NSTX-U plasmas including 3D device geometry.

Year 2:

- Establish dual field component n = 1 active control capability in new NSTX-U operational regime. Compare theoretically expected changes in feedback phase and gain based on NSTX-U plasma shape and aspect ratio to experimental results.
- Examine expanded capabilities allowed by six independent power supplies for the midplane control coils (vs. three in NSTX), including n = 2 pre-programmed error field correction with n = 1 feedback.
- Study and attempt initial control of internal MHD modes that appear at low density during current ramp-up.
- Examine effectiveness of n = 1 active mode control as a function of plasma rotation. Compare theoretically expected changes in optimal n = 1 feedback phase and gain including stabilization effects due to plasma rotation to experimental results.

Year 3:

- Assess global mode stability and control modifications due to more standard use of the snowflake divertor configuration.
- Examine the effect of partial RWM control coil use during n = 1 feedback, examining the impact on the higher-n perturbation spectrum (also supports ITER, JT-60SA).
- Determine effectiveness of n = 1 active control versus operational regime and analyze effectiveness of upgrades including the addition of a poloidally extended sensor set, and multi-mode active control by adding n = 2. Generalize n = 1 control software for $n = 2$ control use and to allow the use of an extended RWM sensor set (available in Year 5).
- Determine theoretically superior partial NCC variations in n = 1 active feedback and update control software to allow actuation of these additional coils for control in Year 4.

Year 4:

- Determine changes to the effectiveness of n = 1 mode control during closed-loop feedback of plasma rotation profile, and q_{min} control in plasmas with non-inductive current fraction approaching, or at 100%.
- Perform initial investigation of dual field component n = 1 active control using the newly-installed partial NCC, including variations feedback phase vs. poloidal angle (varied applied control field helicity with respect to mode helicity).
- Compare n = 2 active feedback control using proportional gain to the NSTX-U model-based RWM state space controller.

Year 5:

- Characterize the poloidal variation of n = 1 – 3 global mode activity using a newly-installed expanded RWM sensor set, including a comparison to the theoretically computed NSTX-U multi-mode spectrum.

- Employ superior multi-mode settings for n = 1 and 2 active control with the partial NCC to demonstrate improved global MHD mode stability in 100% non-inductive plasmas, demonstrating very low plasma disruptivity in dedicated experiments.

2.2.1.3 Model-based RWM state-space controller for active RWM control

A model-based state space controller [70] has been implemented using a state derivative feedback algorithm [71] and incorporating currents due to the unstable RWM eigenfunction and those induced in nearby 3D conducting structure by the applied control field and plasma response. Testing this physics is especially important for ITER [72] and high neutron output devices where greater control coil shielding will be needed. Using a number of states equal or greater than required by Hankel singular value analysis (7 here) provides sufficient 3D conducting structure current detail to match experimental sensors. Open-loop comparisons between sensor measurements and the RWM state space control (RWMSC) model showed agreement with a sufficient number of states and improved agreement when the 3D wall model details (e.g. NBI ports) were added (Figure 2.2.1.3-1). Control was demonstrated to sustain long pulse, high β_N discharges with n = 1 fields applied that normally disrupt the plasma (Figure 2.2.1.3-2). This controller was used for RWM stabilization in long-pulse plasmas (limited by coil heating constraints) reaching β_N = 6.4, and near maximum β_N/l_i = 13.4 (shown in Figure 2.2.1.3-2) [65].

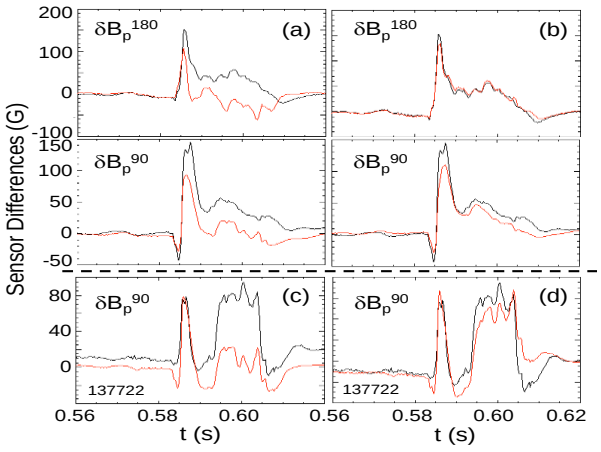

Figure 2.2.1.3-1: Open-loop comparison of RWM sensor subset with RWMSC observer: a) 2 states, b) 7 states, c) without, and d) with the inclusion of the NBI port (7 states).

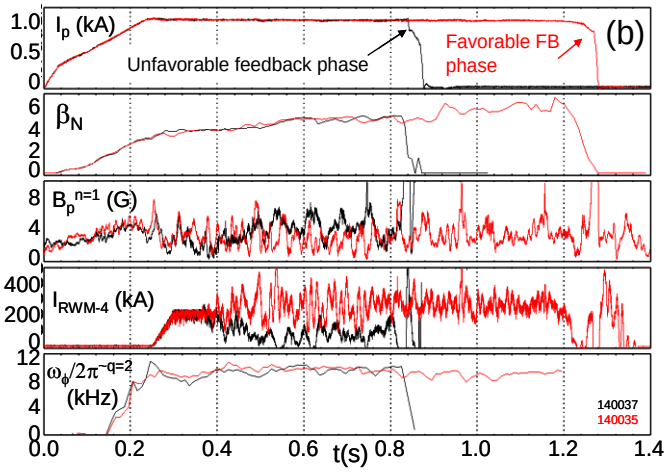

Figure 2.2.1.3-2: Feedback phase variation for RWM state space controller. Favorable feedback phase allowed long pulse plasmas with steady plasma rotation and very high stability parameters $\beta_N > 6.4$, $\beta_N/l_i > 13$.

2.2.1.3.1 Physics model development

The three-dimensional conducting structure (Figure 2.2.1.3.1-1) and plasma response model are defined similarly to detail given in Refs. [10] and [73] and are incorporated in real-time in the RWMSC. NSTX has four rows of 12 copper plates that provide passive stabilization of rotating kink-ballooning modes. Each plate is independently mounted to the stainless steel vacuum vessel with high resistance mounts. The full-order model of this system discretizes magnetic fluxes and currents in the RWM sensors and midplane control coils, and conducting structure along with currents describing the magnetic perturbation of the RWM instability. The geometry of the plasma instability (e.g. see Figures 4 and 6 of Reference [7]) is computed using the DCON code. Magnetic fluxes, Φ, and currents, I, associated with the wall, six control coils, and plasma mode and dissipation (noted by subscripts w, f, p, and d) are determined by equations [24]

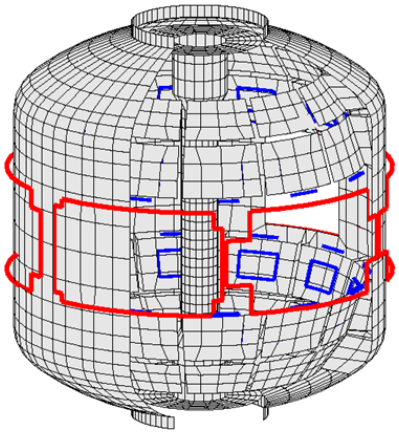

Figure 2.2.1.3.1-1: NSTX 3D conducting structure geometry, including passive stabilizing plates, midplane RWM control coils (red), RWM sensors (blue), and neutral beam (NB) port.

$$\frac{d}{dt}\vec{\Phi}_{w,f,p} + R_{w,f,d}\vec{I}_{w,f,d} = \vec{V}_{w,f,d}$$

with control coil voltage $\vec{V}_f$, and $\vec{V}_w = \vec{V}_d = 0$.

Inductive coupling between elements is defined using computed inductance matrices, L, as

$$\vec{\Phi}_i = L_{iw}\vec{I}_w + L_{if}\vec{I}_f + L_{ip}\vec{I}_d + L_{ip}\vec{I}_p$$

with $i = w,f,p$. The plasma response model alters external field sources through a permeability matrix, P,

$$\vec{\Phi}_p = P(L_{pw}\vec{I}_w + L_{pf}\vec{I}_f + L_{pp}\vec{I}_d) \equiv P\vec{\Phi}_p^{ext}$$

defined for each mode considered as

$$P = -\frac{1}{s^2+\alpha^2}\begin{pmatrix} s & -\alpha \\ \alpha & s \end{pmatrix},$$

where the dimensionless parameters s and α represent the mode instability drive and the differential torque between the plasma and mode [74].

The initial success of the RWMSC on NSTX motivates further expansion of the first implementation and physics model used in the controller. In the initial experiments, the s and α parameters were chosen to represent a mode at marginal stability, but this specification may not

be optimal for control. In NSTX-U, variation of these parameters will be approached in a few ways. The s and α will be varied in experiments, including variation of (s, α) constrained to marginal mode stability, to determine the effect on stability. Also, each of these parameters will be computed theoretically using the MISK code, including the effects of kinetic stabilization, for the high beta target plasma of interest, and compared to experiment. While both s, α are somewhat complex integral quantities of plasma profiles, one can also consider simpler evaluation of these quantities based on plasma parameters (e.g. plasma β_N, and measured mode phase) in real time which would be implemented in the RWMSC in later years of the five year period. Along with plasma stability, the (s, α) strongly affect the plasma response and therefore the total measured perturbed field helicity in the unstable region. This response will be compared directly to the measured mode helicity.

Experimental results to date have only considered a plasma mode that is theoretically predicted to be least stable, and has a single toroidal mode number. The physics model already incorporates the capability of increasing the mode spectrum, which is an important next-step to the controller development and is considered in the next section.

2.2.1.3.2 Active control development, testing, and physics advancements

Although the RWMSC algorithm was written generally for the initial controller, several elements of the control system will be upgraded and expanded, based on both new hardware capabilities and physics advancements. These are briefly summarized below, and addressed individually in the following text. Some of these enhancements will be completed and tested before NSTX-U first plasma, both on offline and real-time implementations:

- independent control of each midplane RWM actuator coil using the new switching power amplifier power supplies
- fully generalize input to allow expanded sensors of any orientation to allow dual component field input
- implement and test n > 1 feedback capability
- implement and test multi-mode spectrum for a given n number

The six midplane coil power supplies, already installed, will be available on Day 0. The plasma control system with the RWMSC will allow full-bandwidth physics applications ranging from open-loop (pre-programmed) error field correction, medium bandwidth ($f << 1/\tau_W$) dynamic error field correction, and high bandwidth ($f \sim 1/\tau_W$) active mode control. The new capability will also allow physics studies of the impact of partial sensor and actuator coil coverage in fulfilling these roles.

In addition to the off-line multi-mode analysis capabilities used on NSTX with the VALEN code (Section 2.4.8), which is directly applicable to NSTX-U, the present model-based RWM state space control system that reached very high values of key stability parameters ($\beta_N > 6.4$, $\beta_N / l_i > 13$) will enable the use of the multi-mode spectrum in real-time global mode control (including 3D mode effects) and 3D detail of the device conducting structure to improve disruption avoidance by improved mode control. Computation of the multi-mode spectrum of NSTX (Section 2.2.1.2.2) has shown that these plasmas exhibit a broader mode spectrum beyond the standard "single-mode" analysis that is typically conducted and that is used in tokamak mode control systems. Operation of NSTX-U plasmas in the high beta operational space accessible by the device will allow testing of the importance of this expanded mode spectrum to further improve active mode control. To support this, the RWMSC will be upgraded to include n > 1 eigenfunctions, and multi-mode capability at constant n number. Use of state space control in a tokamak device was pioneered by NSTX, and these upgrades will take the physics of this control system to unexplored territory. Open-loop testing on existing NSTX data will be possible to test the effectiveness of the added physics before first plasma on NSTX-U.

The addition of the present radial field sensors and the planned magnetic sensor upgrade will also provide additional physics research capabilities for NSTX-U, including the comparison of using radial field sensors alone versus dual-field components in feedback with the RWMSC vessel model included in the calculation. Such testing will be important to determine sensor and actuator needs for future devices, especially where additional shielding of sensors will be needed, such as in ITER.

2.2.1.3.3 Summary of research plans by year

Year 1 (2014):

- Expand RWMSC real-time control software to allow independent actuation of six RWM control coils, and a more general sensor input scheme, for Day 0 plasma operations.
- Implement and perform open-loop tests of n > 1 feedback capability.

Year 2:

- Examine effectiveness of n =1 RWM model-based state space control with independent actuation of six midplane control coils for initial high β_N plasmas in NSTX-U.
- Compare RWMSC modeled sensor signals (controller observer model) with experiment for single mode n = 1 eigenfunction and examine theoretically expected control improvements by adding n = 2 eigenfunctions to the controller.
- Determine optimizations of RWMSC control by varying the amount of plasma rotation-induced stabilization in the controller guided by MISK kinetic stabilization calculations.

- Conduct initial tests on the observer physics model by adding dual-component sensors in RWM feedback, comparing experiment to theory.

Year 3:

- Examine RWMSC multi-mode control with n up to 3 and determine improvements of theory / measurement comparison shown by the controller observer.
- Test optimizations of RWMSC control by varying the amount of plasma rotation-induced stabilization in the controller and compare to MISK kinetic stabilization expectations and experimentally examine effectiveness of the RWMSC as a function of plasma rotation.
- Theoretically determine improvements to the RWMSC by adding the partial NCC (planned for addition to NSTX-U in Year 4) and an extended RWM sensor set (planned for addition to NSTX-U in Year 5).
- Theoretically assess the importance of real-time variation of plasma response parameters in the RWMSC based on experimental studies conducted in Year 2.

Year 4:

- Perform initial investigation RWMSC active control using the newly-installed partial NCC, including variations feedback phase (varied applied control field helicity with respect to mode helicity).
- Determine effectiveness of RWMSC active control during closed-loop feedback of plasma rotation profile, and q_{min} control in plasmas with non-inductive current fraction approaching, or at 100%.
- Examine the effect of varying kinetic RWM stabilization in the RWMSC by varying RWMSC control inputs via multi-phase PCS operation based on real-time β_N calculation

Year 5:

- Test the RWMSC observer physics model by adding a newly-installed expanded RWM sensor set providing improved diagnosis of the mode spectrum in the poloidal direction.
- Examine superior RWMSC settings and multi-mode active control with n up to 3 and the partial NCC to demonstrate improved global MHD mode stability in 100% non-inductive plasmas, demonstrating very low plasma disruptivity in dedicated experiments.

2.2.1.4 Internal kink/ballooning mode control scoping study

The macroscopic mode control research described so far includes activity that yields significant perturbations measurable by external magnetic sensors. However, internal mode activity, which by definition yields small, or immeasurable external magnetic perturbations must also be addressed. Measurement of these modes must be accomplished via non-magnetic means, which

is separately important for mode control systems to be used in future devices with high fusion neutron fluence, such as ITER or FNSF.

Such modes can occur, for example, at the extremes of l_i, or with high pressure peakedness (as can occur, for instance, in a transient H-L back transition). Additionally, coupled m/n=1/1 and 2/1 modes limited many long-pulse scenarios in NSTX. A database of 138 MSE constrained equilibrium reconstructions showed that EPM and ELM triggers cause modes to onset at large values of q_{min}, with rotation shear at q = 2 likely playing a role. There were also "triggerless" modes, that were probably initiated by internal kink or infernal modes as q_{min} approached 1. However, it was also possible to have discharges that have q_{min} just above one for long periods. In NSTX-U, NBCD will be used to understand what the required increment of q_{min} above rational values is to avoid internal/infernal modes.

2.2.1.4.1 Using the RWM state-space observer

An advantage of a model-based controller is that it provides an expectation of how global mode activity will behave in the device as a function of the plasma target. This includes computation of diagnostic measurements in real time. A Kalman filter approach is used to advance the state vector in the presence of noise $\dot{\hat{x}} = (I_r + B_r K_c)^{-1} A\vec{x} + K_o\left(\vec{y}_m - \vec{y}\right)$, where $\vec{y}_m$ is the measured magnetic flux in the RWM sensors, $\vec{y} = C\vec{x} + D\vec{I}_f$, is the controller observer computation of the measurements, I_r is the identity matrix, A and B are the plant and control matrices, and the remaining matrices are the computed controller and observer gain matrices determined by the optimal control algorithm. Subscript "r" is used to denote the reduced order system matrices. It is clear that the second term represents a correction to the plant matrix evolution of the state vector. While typically used to correct the state in active feedback, it can also be used in real time to determine how incorrect the observer is in reproducing the measurements. Therefore, this difference can be used as a criterion of how incorrect the observer is allowed to be in any given sensor, or collection of sensors, and used as input to a disruption warning system. This application can be applied generally, or more specifically as in this instance. In this case, the modeled global mode will have a significant external component, so $\vec{y}_i$ will have significantly larger amplitude than the equivalent sensor measurement.

2.2.1.4.2 Using non-magnetic RWM sensor mode characterization to include sensors in feedback

The multi-energy soft X-ray diagnostic on NSTX was successful in measuring low frequency (less than 500 Hz) mode activity (Figure 2.2.1.4.2-1). Similar, non-magnetic measurement of

global mode activity with multi-energy soft X-rays has been proposed by the Johns-Hopkins group for NSTX-U (see also Section 10.6.1.3). When available, these measurements will be used directly to determine mode amplitude, and in conjunction with the external magnetic sensors to determine the degree to which the mode is internal. Empirical and theoretical criteria can be used to determine and a threshold for these measures, for use as input to the disruption warning system.

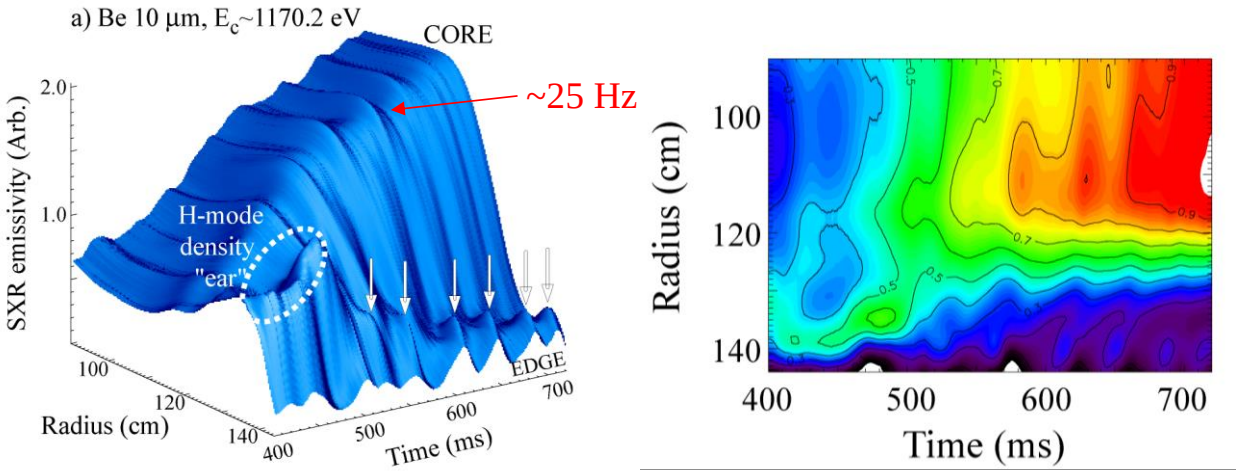

Figure 2.2.1.4.2-1: Low frequency (~ 25Hz) global mode activity measured using multi-energy soft X-ray detectors.

2.2.1.4.3 Summary of research plans by year

Year 2:

- Examine the real-time difference between the n = 1 RWMSC observer and measured RWM poloidal field sensors to evaluate observer physics model and determine thresholds for disruption detection appropriate for use in the NSTX-U disruption warning system.
- Utilize initial NSTX-U ME-SXR and poloidal USXR diagnostics to characterize the RWM eigenfunction by non-magnetic means.

Year 3:

- Examine improvements to disruption detection via the RWMSC based on multi-mode capability of the observer.
- Examine changes to ME-SXR/poloidal USXR measured RWM eigenfunction as a function of plasma rotation.
- Determine the degree of global mode internalization by comparing diagnosis by magnetic and SXR means as a function of proximity to the mode marginal stability point.

- Implement real-time RWMSC observer into disruption warning system.

Year 4:

- Use RWMSC observer in disruption warning system during closed-loop feedback of plasma rotation profile, and q_{min} control in plasmas with non-inductive current fraction approaching, or at 100%.
- Examine time-evolution of global mode internalization using newly-installed, additional toroidally-displaced ME-SXR diagnostic and prepare for real-time input to disruption warning system.

Year 5:

- Determine physics improvements to RWMSC observer for disruption detection and implement to demonstrate reduced disruptivity to internal modes in 100% non-inductive, high β_N plasmas.

2.2.1.5 Use of NCC for mode control and integration of stability control elements

The installation of the NCC will allow studies of NTV physics, and v_φ control with $n \leq 6$. Building off of previous years' research (see Section 2.2.1.1.2), unfavorable rotation profiles can be avoided, and favorable profiles maintained with this capability. Another particularly exciting aspect of this research is the possibility of increasing v_φ via $n > 1$ toroidal propagation with the NCC.

Studies of RWM kinetic stabilization physics can be enhanced by the NCC by exploring such issues as:

1. What are the optimal rotation profiles for RWM kinetic stabilization allowed by adding the NCC field spectra?

2. Can an optimized NCC field spectrum change edge fast ion profiles for RWM stability alteration?

These topics would be explored experimentally and compared to theoretical calculations using the MISK code.

Building upon the experiences of previous years' operation, by the fourth year of NSTX-U operation, a good working understanding of the various feedback and control mechanisms should allow all of them to be used in concert to sustain high performance discharges. Rotation and beta feedback will be used to avoid unfavorable stability conditions while advanced active feedback

systems will be used to control the plasma in the case of excursions from optimal operating regimes. The overall goal is to investigate the combination of v_ϕ-profile, q profile, β-feedback, and active mode control to improve RWM/TM/internal MHD mode stability and to sustain high performance plasmas.

The proposed NCC can be used to demonstrate simultaneous use of actuators sharing multiple control roles. In other words, can the proposed NCC achieve RWM control, ELM control, rotation control, and error field correction simultaneously? Exploring this unique physics coupling in control systems is key for ITER. For example, RWM and NTM stability depend on v_φ, q, n, and T profiles, while v_φ control will depend on NTV (which itself depends on v_φ, q, n, and T profiles). The NCC may improve such control compared to use of the midplane RWM coil alone. A control model must be tested that utilizes the NCC in coupled systems: for v_φ control, β_N control, RWM control (and passive stability), and dynamic error field correction.

The NCC will be extremely useful in the area of RWM active control. Calculations with the VALEN code (Section 2.4.8) indicate that the full option for the NCC coils can provide active RWM control to achieve β_N near the n = 1 ideal wall limit (see Figure 2.2.1.5).

Additionally, the NCC will be used in combination with a model-based RWM state space controller, providing multi-mode RWM control and dynamic error field correction (DEFC). The RWM state-space controller allows far greater flexibility of global mode stabilization physics studies with these coils, with a relatively simple control software upgrade. With the NCC, NSTX-U will be able to demonstrate RWM state space control of ITER-similar coil set.

The NCC can provide quantitative evaluation of the importance of the multi-mode spectrum (n and m) for RWM control and DEFC. The n > 1 mode spectrum has been observed but the importance of control / dynamic correction has never been tested. The performance gained from the added n = 2-3 RWM active control will be evaluated. Also the spectrum will gain helicity, which is important to expand the research.

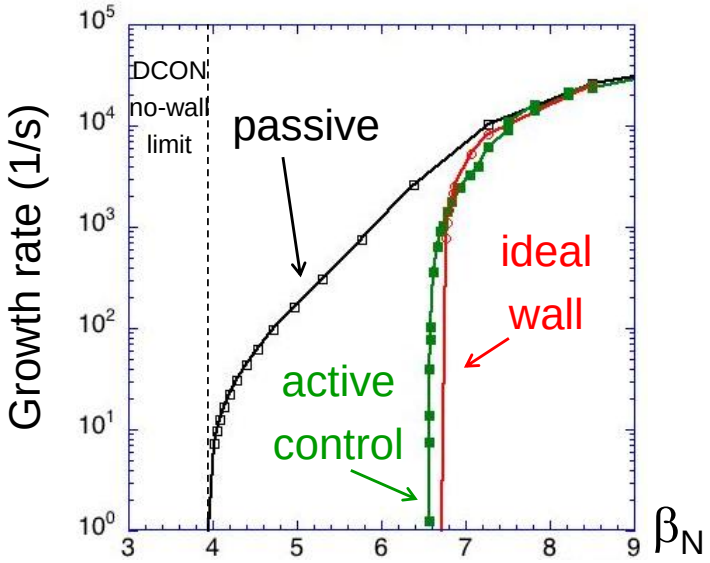

Figure 2.2.1.5: VALEN calculation of RWM active control capability with the full NCC coil set with optimal sensors and optimal gain.

Finally, the NCC will be instrumental in two additional topics of RWM control. First, one can investigate the physics and control of "nonrigid" mode evolution. Second, an important practical topic for ITER is how to prepare to compensate random coil failures in RWM active control. The combination of NSTX-U's RWM state space controller and the flexibility of the NCC allows these issues to be addressed.

2.2.1.5.1 Summary of research plans by year

Year 3:

- Determine improvements to kinetic RWM and NTM stability possible by utilizing expanded capability for non-resonant rotation control by the enhanced 3D field spectrum afforded by the partial NCC, based on theory and the first 2 years of NSTX-U operation.
- Determine improvements to active feedback of n > 0 modes via PID and RWMSC control allowed by the partial NCC, and implement control system changes to test theory in Year 4 device operation.

Year 4:

- Utilize the newly-installed partial NCC to expand plasma rotation profile variation and control, with the goal of improving RWM and NTM stability, with comparison to theory.
- Conduct active n > 0 feedback research using the partial NCC to uniquely address physics for ITER and future STs and tokamaks (e.g. JT-60SA), including (i) mode control with partial toroidal / poloidal coverage of the control coils, (ii) robustness of model based RWM state space control with reduced sensor / control coil availability, (iii) relative importance of midplane vs. off-midplane control coil arrays.
- Determine importance of adding partial NCC capabilities for rotation and mode control in reducing disruptions in high β_N plasmas with non-inductive current fraction approaching, or at 100%.

- Analyze the effect of the partial NCC spectrum on fast ion profiles to determine the effect on RWM stability.

Year 5:

- Utilize the added profile control capabilities allowed by the partial NCC with closed-loop plasma rotation profile control to demonstrate, based on kinetic stabilization theory, reduced disruptivity by actively avoiding global instabilities.
- Employ superior multi-mode physics model settings for n > 0 active control with the partial NCC to demonstrate improved global MHD mode stability in high β_N, 100% non-inductive plasmas scenarios, demonstrating very low plasma disruptivity in dedicated experiments.
- Provide FNSF/Pilot projection on macroscopic stability.

Four years of operation with NSTX-U will culminate in the ability to make projections to next step ST devices, such as FNSF, in the area of macroscopic stability. Specifically, RWM stability as a function of collisionality, rotation, and energetic particle profiles will have been explored and compared to theoretical projections, and experience with advanced active feedback systems operating at the same time as various other control systems (rotation, beta…) will inform schemes for next step devices. Of particular importance to FNSF is whether the integrated controllability is largely changed in fully non-inductive operation.

2.2.2 Thrust MS-2 – Understand 3D field effects and provide physics basis for optimizing stability through equilibrium profile control by 3D fields

2.2.2.1 Error field and tearing mode dynamics

Tokamaks have nested flux surfaces everywhere inside the separatrix and thereby suppress neoclassical transport and provide good confinement. However, flux surfaces can be broken and reconnected to form magnetic islands at the rational surfaces through perturbations unless the plasma is perfectly ideal. Magnetic islands can be more easily formed by external perturbations, can lock to the lab frame by drag due to device error fields, and can also be seeded by internal perturbations and non-linearly grown by changing equilibrium profiles, as called tearing modes.

As mode locking by error fields can be detrimental and lead to a disruption [15,16,17], it is critical to predict the tolerance of the locking of saturated islands and their onset to error fields. This is not a simple task since error fields and plasma responses are intrinsically three dimensional. Recently its understanding has been largely improved, by ideal plasma response calculations, which in fact greatly simplified the view on the interaction between error field and plasmas by finding the dominant field structure [12]. One can call the dominant field affecting the island simply a resonant error field, and the other orthogonal field structure, which can be simply called a non-resonant error field, is predicted to be less influential on the rational surfaces. However, the non-resonant error field can change the island dynamics indirectly through NTV [27,28,29] or possibly directly through non-ideal or non-linear coupling [33]. A number of dedicated experiments will be required to understand the interaction among locking islands, and resonant and non-resonant error fields.

Another important subject is the modification of existing islands, or tearing modes, by error fields. Error fields, or 3D fields in general, can indirectly influence tearing mode dynamics by inducing NTV and thus by altering plasma rotation [13], but also can directly provide the seed island [35,75]. Applied 3D fields can suppress tearing modes by introducing compensating external fields to internal fields arising from the modes. In order to predict tearing mode behaviors under 3D fields, first their own island dynamics without 3D fields must be better understood. The island dynamics can be largely different depending on regimes; whether or not it is linear and more classical [76], or non-linear and neoclassical [77]. The so-called neoclassical tearing mode (NTM) with self-regulating bootstrap currents is itself one of critical issues for the next-step device, as they often limit the achievable β [21,22]. The study of these tearing and neoclassical tearing modes, without and with 3D fields, in NSTX-U, will truly advance the understanding of island dynamics in 3D.

NSTX-U will provide unique environmental elements in this research area, with the low aspect ratio, strong shaping, and high-β. The basic features of resonant and non-resonant error field effects can be well explored with the 6 SPAs, and further comprehensive understanding will be possible when NCC is equipped in later years. The combination of NCC with the 2nd neutral beam will provide various rotation and rotational shear profiles, which are important variables on locking and tearing mode stabilization. The NTM dynamics has never been explored in advanced ST regimes, to which NSTX-U will uniquely contribute. Also, the NSTX-U team can readily use many advanced theoretical and computational tools, such as IPEC and GPEC (Section 2.4.3), MARS-K (Section 2.4.9), and M3D-C[1] (Section 2.4.10), to understand and analyze NSTX-U experiments, and finally to develop predictive capability for locking and tearing modes with 3D fields.

2.2.2.1.1 Error field correction to reduce mode locking

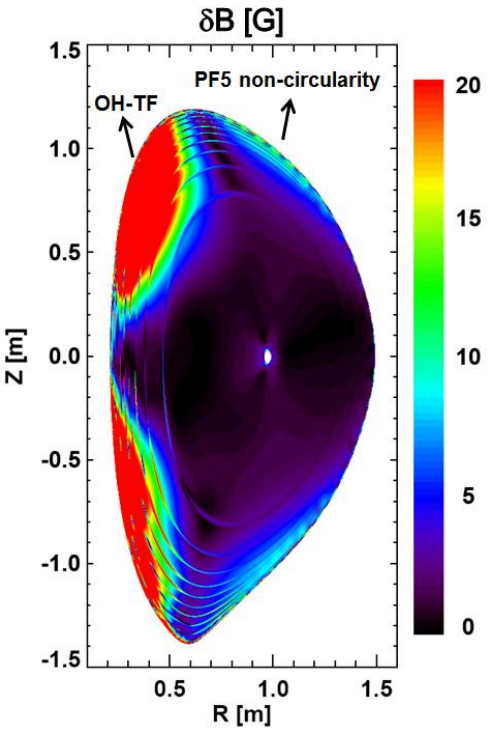

Figure 2.2.2.1.1-1: The perturbed n=1 field strength (calculated by IPEC) due to intrinsic error fields in NSTX.

NSTX-U will be significantly modified in some machine components such as the center-stack and NBI beam ports, and may have different intrinsic error fields. NSTX had two main components of intrinsic errors: (1) n = 1 by OH-TF joint distortion and PF5 non-circularity, as shown in Figure 2.2.2.1.1-1, and also (2) n = 3 by PF5 [23]. The same PF5 coils will be used for NSTX-U and may produce similar error fields, although the coupling to the plasma and the optimal correction against error fields will be different. The OH-TF joint error is not expected to be as substantial as in NSTX, but nevertheless will be investigated since mechanical forces on the center-stack are substantial in ST devices. This investigation will require dedicated effort and time in the first-year NSTX-U operation, since the identification and correction of intrinsic error fields is critical for studies of 3D field physics and for optimal performance.

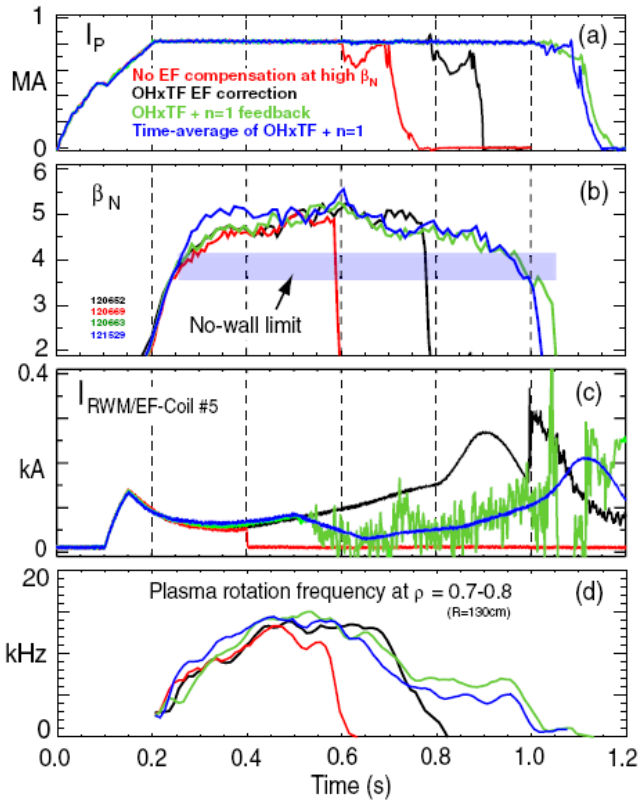

Figure 2.2.2.1.1-2: Various successful error field correction, including the dynamic error field correction in green, which sustained plasma above the no-wall limit and substantial toroidal rotation.

The plan is first to charge the OH, TF, PF coils independently and to measure the vacuum field using magnetic sensors to see the relevance of the previous error field model, such as PF5-triangularity, in NSTX. The model will be revised for NSTX-U as necessary. With updated error field model, IPEC prediction for locking and NTV will be tested with n = 1 ~ 3 compass scan in 4-6 different toroidal phases to optimize static error field correction, which will be important for 3D field physics studies in general. The 6 independent switching power amplifiers (SPAs) will enable n = 2 field rotation for shot to shot, and n = 3 field can also be rotated if the full NCC is installed.

Active mode control and dynamic error field correction are also important especially for high-β since various MHD modes, including the RWM, can arise in typical operation envisioned above ideal no-wall limits. Also the OH-TF error field can be time-dependent and the correction can become more uncertain in high-β due to strong interaction with the plasma. The n = 1 active and dynamic control algorithms were highly successful in NSTX [23] as shown in Figure 2.2.2.1.1-2 and so the plan for the first year is to restore and explore the n = 1 active mode and dynamic error field correction capability in NSTX with the 6 independent SPAs.

The 6 independent SPAs will make any n = 1-3 combination of static and dynamic error field correction possible during operation. Based on the exploratory study for the n = 1 dynamic error field correction in the first year, the optimization of the algorithm will be studied at the interim between experimental campaigns and will be tested in the second year. The optimized n = 1 dynamic correction will be first compared with the pre-programmed static n = 1 error field correction. Next the combination of the dynamic and static correction will be tested with different weighting factors and optimized for the best n = 1 error field correction. The n > 1 dynamic correction will be challenging due to weak plasma response and weak coupling between plasma and magnetic sensors. However, NSTX studies show that n = 2 - 3 RWMs have been

detected [78], and so the possibility for n > 1 dynamic correction will be tested by applying the n = 2 or n = 3 EFC currents to see if the correction algorithm can detect and actuate the proper responses back.

2.2.2.1.2 Study on non-resonant error field effects

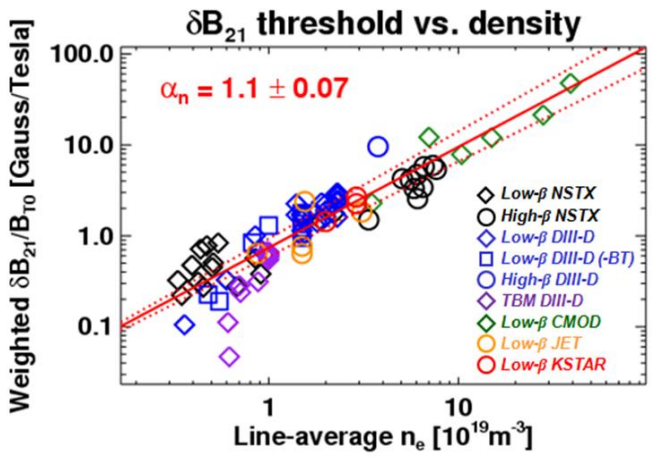

Figure 2.2.2.1.2-1: Error field threshold vs. locking density, constructed using IPEC for five different devices. The coefficient is the power for the density scaling, indicating almost a linear correlation.

Studies of intrinsic error fields have been focused on the resonant component and its compensation to avoid locking. Modeling based on the ideal plasma response has been largely successful across many different devices, including NSTX [12], DIII-D [79], CMOD, JET, and KSTAR, as shown in Figure 2.2.2.1.2-1 The new scaling for error field threshold at locking is still being updated and will be continued with new data and new devices, and will be used to predict the tolerance of error fields in next step devices including ITER.

On the other hand, recent studies with both resonant and non-resonant field applications show that the resonant error field threshold can be significantly altered if the non-resonant error field is substantial. Figure 2.2.2.1.2-2 shows the comparison between the resonant field vs. locking scaling including rotation in NSTX high-β locking experiments [27]. Here the n = 1 resonant field thresholds are significantly lower in the blue cases, due to the additionally applied n = 3 fields that decrease the rotation. The importance of the non-resonant error field correction is clearly demonstrated by recent experiments in DIII-D [28]. In these experiments, the error field was created by external midplane coils (C-coils), and the correction was added with the off-midplane, internal coils (I-coils). The I-coil correction is optimized with conventional compass scans and

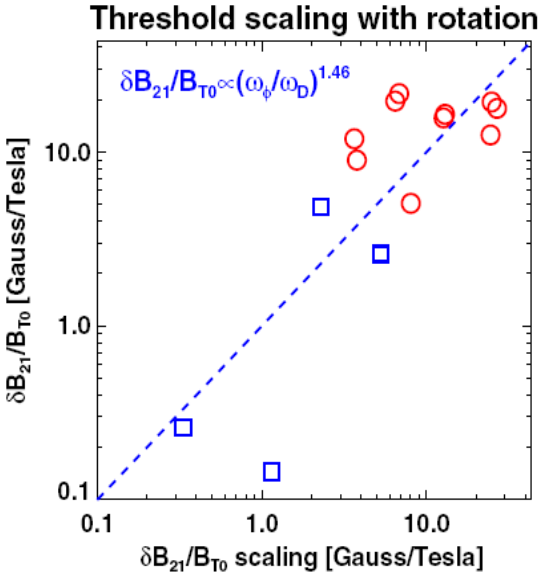

Figure 2.2.2.1.2-2: Comparison between the resonant field (Y) vs. resonant field scaling. Rotation scaling is additionally required for blue points, which included n=3 rotation braking.

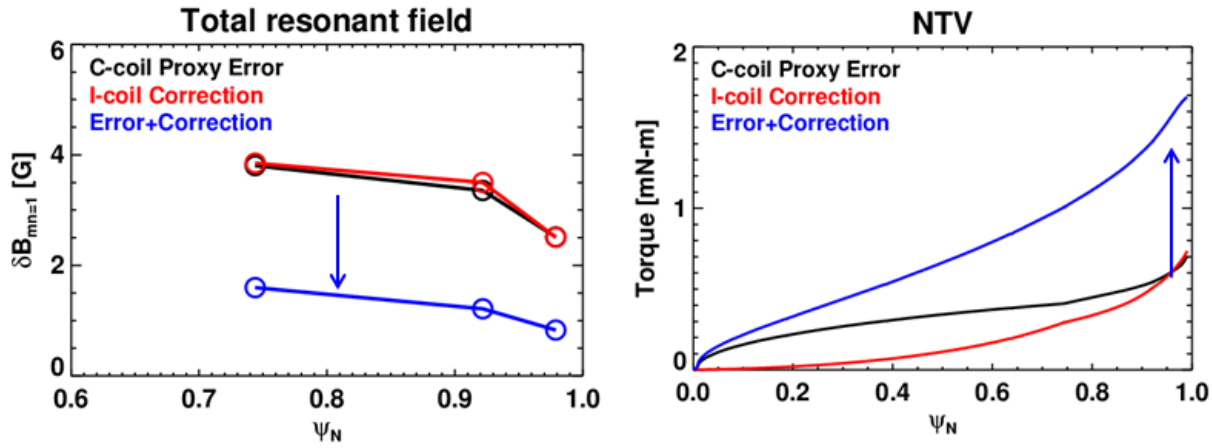

Figure 2.2.2.1.2-3: Total resonant field and NTV in proxy error field experiments in DIII-D. One can see C-coil + I-coil correction reduced the total resonant field, but substantially increased NTV.

this optimization is expected to remove the resonant error field irrespective of the error field sources. However, the optimization for the proxy C-coil error field was not as successful as the intrinsic error field, which may be due to much larger non-resonant components remaining after the correction. Indeed, IPEC and NTV analysis showed that NTV was increased even more than the linear sum of NTV by the C-coil and I-coil fields, while the resonant field was greatly reduced, as shown in Figure 2.2.2.1.2-3. However, although the NTV analysis for the proxy cases shows that the possible resolution may be found in NTV, it is still not clear if the non-resonant component directly influences locking, or indirectly through the NTV rotational damping.

NSTX-U will provide a highly favorable environment to study these non-resonant error field effects, especially when the NCC is installed, but even before then by utilizing the 6 independent midplane RWM coils. In the third year of NSTX-U operation, the study of non-resonant error field effects will be initiated by investigating the n=1 locking threshold by changing n > 1 error fields. The goal is to see if the resonant locking threshold can be modified differently when similar rotation braking is obtained but with different non-resonant fields using n = 2 or n = 3.

The NCC will enable fully systematic investigations of non-resonant and resonant error field effects as a function of plasma rotation. Figure 2.2.2.1.2-4 shows the producible n = 1 resonant field per 1kAt in NSTX-U using different choices of the NCC design; 12U, 2×6-Odd with 6 different phases between upper and lower coils (open red circles) and 2×12 with 12 different phases (filled red circles), compared to the PF5 error field (black) and the midplane field (blue). The resonant fields are the root-mean-square sum of the resonant fields at $\psi_N < 0.85$. The results

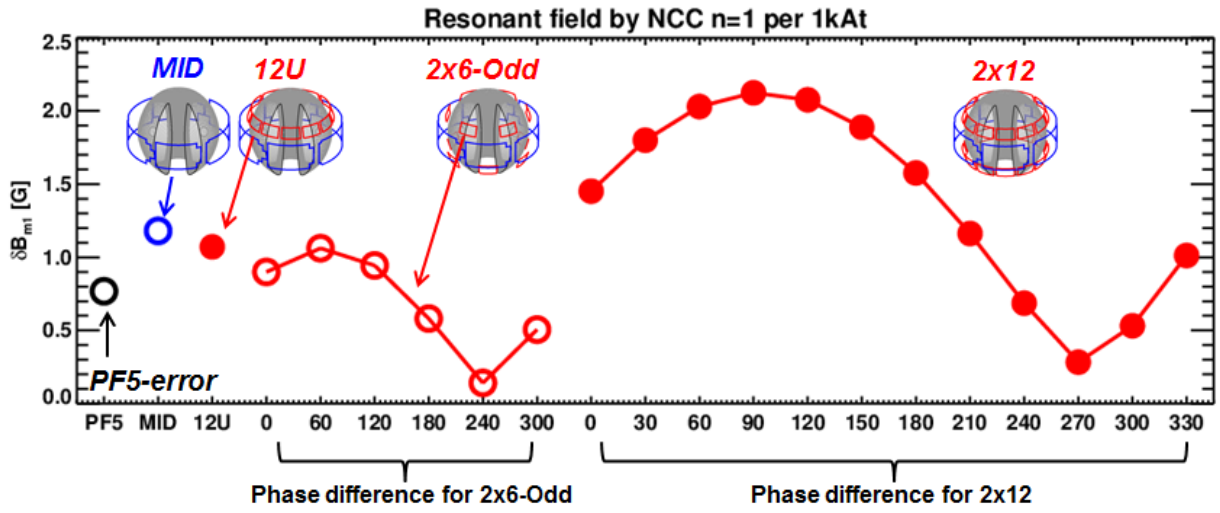

Figure 2.2.2.1.2-4: Resonant fields that can be produced by partial and full NCC coils by 1kAt; 12U, 2x6-Odd with 6 different phases (Open red circles), and 2x12 with 12 different phases (Filled red circles), compared to the present midplane coils (Blue). The resonant field by PF5 coils with 20kA is also shown (Black), which needs to be minimized by error field correction.

show that the proposed NCCs can basically produce a resonant field comparable to the midplane coils, and so they can correct PF5 error fields for example, while at the same time they can provide different poloidal field spectra. This is calculated with the error field figure-of-merit factor (FOM), $F_{N-R} = T_{NTV} \Big/ \sum_{\psi_N<0.85} \delta B_{mn}^2$, which is defined to quantify the ratio of the non-resonant field components to the resonant field components. Neoclassical toroidal viscosity (NTV) torque T_{NTV} was used to represent the physics associated with the non-resonant fields, as well as to give proper weighting on each non-resonant field component. The results are shown in Figure

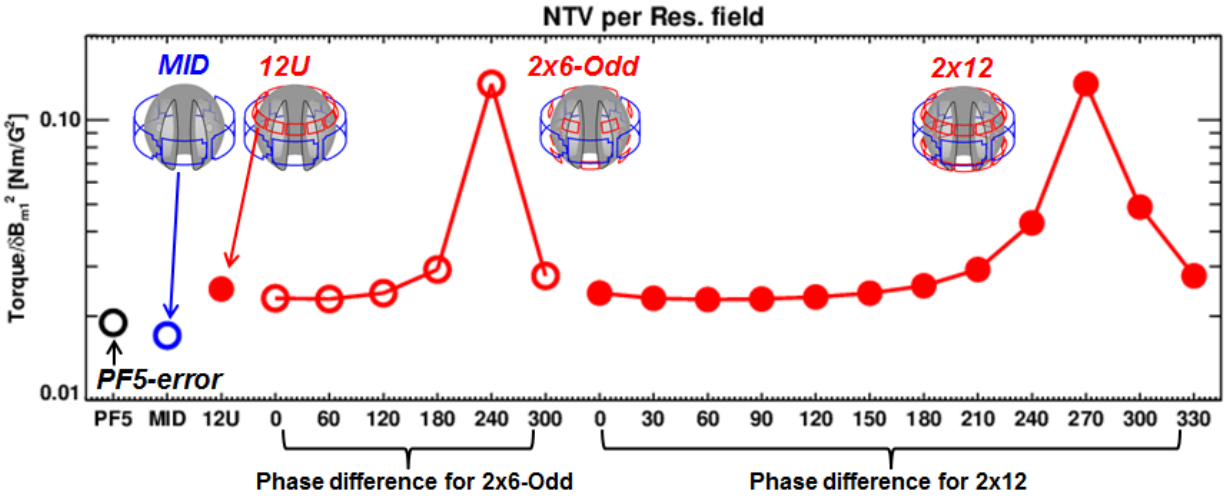

Figure 2.2.2.1.2-5: The NTV per resonant fields for NCCs, which is defined to assess the figure of merit for the error field control. The same labels are used as Figure 2.2.2.1.2-4.

2.2.2.1.2-5, for each NCC configuration. One can see the partial 2x6-odd NCC configuration can give a high FOM as well as variability of the FOM, comparable to the full 2x12 NCC. A high FOM implies that the coils can induce highly non-resonant fields and thus only NTV braking without exciting locking or tearing modes. In contrast, a low FOM means the field is highly resonant, which shows that this particular coil design will allow conclusions regarding the comparison of resonant and non-resonant applied 3D field effects on mode stability and plasma rotation.

Based on the prediction, it will be possible to use the partial NCC configuration to compensate the resonant field produced by the midplane coils, with different ratios of non-resonant vs. resonant field, so that the non-resonant error field effects on locking can be systematically studied. The plasma response, that affects the locking thresholds, will be studied as a function of non-resonant field spectrum and separately as a function of the toroidal rotation. The study will be extended by attempting to produce similar toroidal rotation profiles using different toroidal harmonic perturbations, such as n = 2 or n = 3. This will enable conclusions on whether the non-resonant error field influences the resonant braking directly, or indirectly by toroidal rotation modification.

2.2.2.1.3 Understanding of (neoclassical) tearing mode dynamics in ST

Tearing modes (TMs) and neoclassical tearing modes (NTMs) can be destabilized in the advanced ST regime despite the favorable Glasser [76] and curvature effects [21], by high-β and high bootstrap current fraction in non-inductive operation, and so should be better understood and controlled in NSTX-U. Tearing mode dynamics has some common physics with error field and locking issues, as both are associated with 3D island dynamics. However, different research elements are also required since locking by error fields is external, static, and controllable in ideal and linear regimes, but tearing modes are internal, rotating, and in mostly non-ideal and non-linear regimes. The non-ideal and non-linear nature requires understanding of various second-order physics in the island region including resistivity, viscosity, and two-fluid effects. NSTX-U can provide important regimes with various unique features such as strong shaping and therefore different ion gyro and drift orbits.

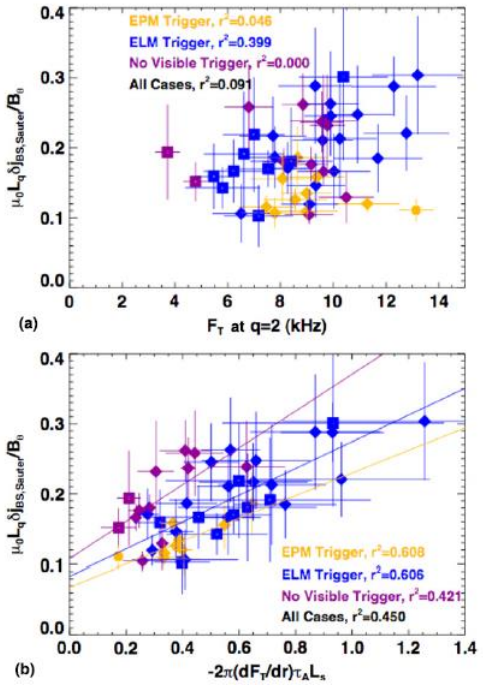

Figure 2.2.2.1.3-1, Onset bootstrap drive at the NTM onset vs. (a) rotation and (b) rotational shear.

The ability of fine rotation control, performed with pre-programmed 3D fields in NSTX, and planned in closed-loop feedback in NSTX-U using NTV, will also be very useful for tearing mode studies. In NSTX, it was shown that rotational shear is a more important variable than the rotation itself in determining NTM onset and stabilizing NTMs [13], as shown in Figure 2.2.2.1.3-1. These correlations between TM/NTM with the rotation profiles will be revised with better separation between the rotation and the rotational shear using the 6 SPAs and three additional NBI sources, and more deeply investigated using NTV braking with NCC in the later years of NSTX-U. The low collisionality and non-inductive operation aimed for NSTX-U can largely modify bootstrap currents, and therefore their effects on NTM stabilization will be extensively studied. Advanced 3D diagnostics such as ME-SXR will also be critical to understand details of island dynamics.

The important dynamics for TM/NTM occur in a narrow island layer, especially at the mode onset, and thus the development of theoretical and numerical understanding of the layer physics is essential to verify and validate TM/NTM physics with available measurements. The development of linear layer calculations with full geometry, such as MARS-K or resistive DCON, will be continued to clearly separate classical effects from neoclassical effects. The layer physics in both codes can be modified to include other non-ideal effects, even non-linearly but coupled to linear treatments for outer-layers. Recent and future theory developments will be used to extend layer calculations [32,33,34]. The fully non-linear codes such as M3D-C1, and particle simulations such as the XGC0 code will also be used to comprehensively understand neoclassical effects, including NTV, on the layer physics. These theoretical and numerical calculations will be tested against experiments, to achieve better predictability and scaling for next-step devices.

2.2.2.1.4 Error field control to stabilize (neoclassical) tearing modes

Tearing modes and neoclassical tearing modes can be modified interactively by both resonant and non-resonant error fields. The non-resonant error field effects are more indirect but better known as the rotation modification by NTV can change TM/NTM stability. Figure 2.2.2.1.4-1 shows the change of the β_N threshold of the NTM onset as a function of rotation, which is varied by non-resonant braking. The trend simply shows the β_N threshold will be decreased if magnetic braking is introduced with non-resonant error fields. However, the interaction can be more complicated if resonant error fields are also applied. Figure 2.2.2.1.4-2 shows the behavior of NTM onset and locking when n = 1 resonant and n = 3 non-resonant

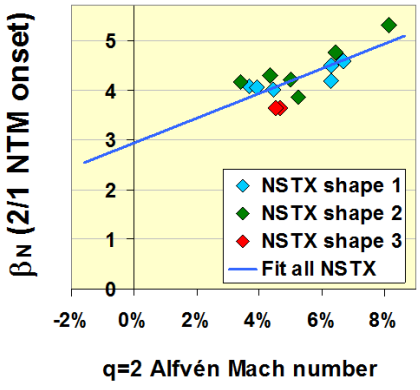

Figure 2.2.2.1.4-1: 2/1 NTM limit as a function of q=2 rotation.

error fields are simultaneously applied. The X-axis is the n = 1 field amplitude, and one can see the rotation (blue vertical lines attached to the data point) is not a strong function of the n = 1 field but the β_N limit (red horizontal lines) is substantially reduced. When the n = 1 field is strong enough, one can see that conventional locking occurred (green data points).

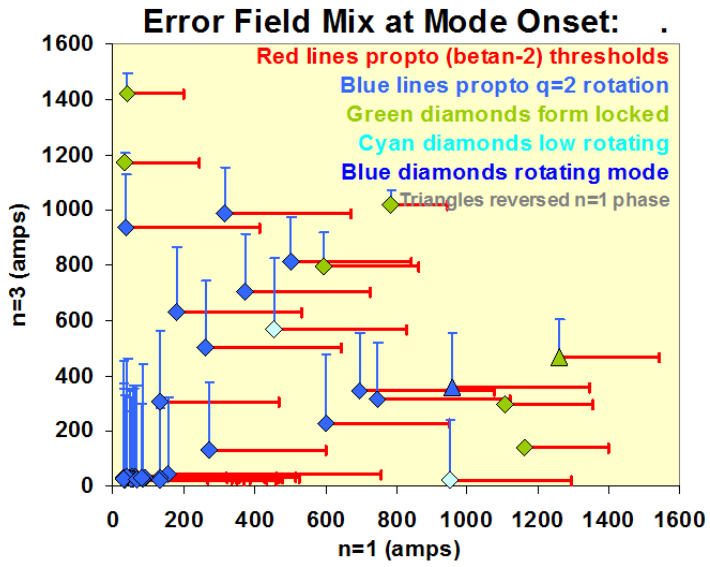

Figure 2.2.2.1.4-2: 2/1 NTM limit as a function of n=1 and n=3 applied fields. Blue points are tearing, green points are locking, blue vertical lines indicate the rotation speed, and red horizontal lines indicate the β_N limit.

There must be a seeding effect by the n = 1 resonant field, and so the research will be continued to improve understanding of the resonant field effect on TM/NTM. This will be started from the third year of NSTX-U operation (Year 4), as the understanding of the intrinsic component of error fields and stable q-profile control is critical for the successful performance of these experiments.

When the partial NCC is available, from the third year of NSTX-U operation (Year 4), the TM/NTM onset by resonant error fields can be fully studied on the two dimensional parametric spaces (β_N,v_ϕ). The rotational shear effect and the direct coupling between non-resonant error fields and tearing modes will be investigated, as the NCC will be able to provide different torque and rotational damping profiles while the same resonant error field is applied. This will allow us to achieve comprehensive understanding of the interaction among locking and tearing islands, and resonant and non-resonant error fields. The detailed dynamics of island onset, suppression, or development, will be attempted using advanced diagnostics such as two toroidally displaced ME-SXR (Section 10.6.1.3), and various real-time measurements planned in NSTX-U.

2.2.2.1.5 Summary of research plans by year

Year 1 (2014):

- Compile resonant error field threshold data from other tokamaks, such as DIII-D, C-MOD, KSTAR, JET, and combine them with NSTX to further support the scaling to ITER.
- Investigate non-resonant error field effects on mode locking based on past NSTX high-beta experiments and DIII-D error field proxy and TBM mock-up experiments.

- Develop numerical codes such as resistive DCON, first to separate linear classical tearing modes from neoclassical tearing modes, and continue to improve layer model.
- Analyze NSTX TM/NTMs in NSTX-U with developed and advanced numerical codes such as resistive DCON, MARS-K, M3D-C1.

Year 2:

- Identify n = 1-3 intrinsic error fields with magnetic sensors, compare to the existing error field model, and update the model as needed.
- Based on the field model and IPEC modeling, optimize the n = 1-3 error field correction using 6 independent SPAs.
- Explore upgraded 3D capabilities of active mode control and dynamic error field correction.
- Investigate the rotation and rotational shear vs. TM/NTM in NSTX-U, compared with NSTX.

Year 3:

- Optimize and combine dynamic error field correction with intrinsic error field correction.
- Initiate the investigation of non-resonant vs. resonant error field effects, by inducing n = 2 and n = 3 fields separately upon the same n = 1 error fields. Vary the rotation profiles using the off-axis NBI with the same 3D field applications, to compare the direct coupling of the non-resonant field components to the resonant fields.
- Investigate the β limit for TM/NTM onsets with varied rotation and rotation-shear.
- Utilize the n = 1 resonant error fields to vary (neoclassical) tearing mode onset.

Year 4:

- Utilize the partial NCC to induce applications of n = 1 non-resonant fields with varied spectra, while the n = 1 resonant field is fixed. Compare the results with the n = 2-3 non-resonant field applications in Year 3 to understand non-resonant and resonant error field effects vs. v_ϕ and the applied field spectra.
- Use the partial NCC and the 2nd NBI beam to study TM/NTM dynamics as a function of (β_N,v_ϕ).
- Investigate the n = 1 non-resonant error field effects on TM/NTM onset and stability, and separate non-linear coupling effects from rotational braking effects.

Year 5:

- Understand error field physics using up-to-date layer theories, and GPEC, M3D-C1, or XGC0 modeling incorporating layer physics across the rational surfaces.
- Understand 3D island dynamics including 3D error fields in tokamaks.

- Develop error field correction predictability for FNSF, ST-Pilot, ITER.
- Develop TM/NTM predictability, including 3D error fields, for FNSF, ST-Pilot, ITER

2.2.2.2 Neoclassical toroidal viscosity at reduced collisionality and applicability to an ST-FNSF and ITER

Neoclassical toroidal viscosity (NTV) [80] is a plasma characteristic resulting from a force created by non-ambipolar particle diffusion. It is an inherently non-axisymmetric (3D) effect, created by intrinsic or applied non-axisymmetric fields, and ideal and resistive MHD instabilities [81,82] which create 3D magnetic field perturbations. The theory of NTV has been developed substantially in the last decade, with extensive work conducted by Shaing, et al., with much work focusing on analytic theory in a variety of collisionality regimes, with smooth connection between these regimes [36-51].

Strong, precise, and controllable neoclassical toroidal viscosity (NTV) effects were observed in NSTX [78,83-85] with direct quantitative comparison to theory of the resultant magnetic torque profile due to applied n = 1 and n = 3 fields, and n = 1 resonant field amplification and resistive wall modes [86]. This extensive study and reliable and reproducible effect has allowed routine open-loop v_φ profile alteration on NSTX. Such rotation control, which is not routinely performed on other devices, places NSTX-U in a position to not only study NTV physics at all levels of plasma rotation, but to also uniquely provide closed-loop plasma rotation control by novel means (e.g. using non-resonant 3D fields to change plasma rotation with feedback) and so allow greater control in studies of the impact of plasma rotation profile on plasma stability. Closed-loop rotation control will be used in the later years of the present NSTX-U five year plan for disruption avoidance and to maintain optimized rotation profiles for plasma stability. This is particularly well-suited for non-resonant NTV rotation control. NSTX has accessed very low plasma velocity (approximately zero over half of the plasma minor radial coordinate, ψ_N) utilizing open-loop plasma control using NTV.

Several aspects of NTV physics are not yet well understood, and this understanding is important for future fusion devices, including an ST-FNSF, and ITER. This physics is summarized in the next several sections, including the potentially important effects of particle resonances, and the nature and scaling of the neoclassical offset velocity – an intrinsic rotation set by NTV. Arguably, the most basic and important dependencies of NTV are on the plasma collisionality and the plasma rotation. For instance, the scaling of NTV in the superbanana plateau (SBP) regime can be very different as NTV is additionally increased when the plasma ExB frequency becomes comparable to the ∇B drift (e.g. when the plasma rotation is sufficiently small). The superbanana plateau regime has been accessed in both NSTX [85] and DIII-D [87]. Similarly,

NTV can be greatly enhanced when the plasma ExB frequency becomes comparable to the bounce motion of trapped particles, called bounce-harmonic (BH) resonances, as predicted by theory [16], shown in simulations [17,18], and may help to explain NSTX [24] and KSTAR [59] results.

NSTX-U provides a significant opportunity to study NTV physics, especially the dependence on collisionality and rotation, for NSTX-U, ST-FNSF and ITER. The dependence of NTV on plasma collisionality is important for NSTX-U, as it is needed to define simple models for the real-time plasma rotation controller. For ITER and FNSF, the strength of NTV needs to be evaluated to understand potential locked mode thresholds for ITER, and the impact of applied 3D fields that will be used for ELM and RWM control. The same applies for an ST-FNSF, except this device is expected to operate at higher plasma rotation. Because of the different expected plasma rotation profiles and speeds, ITER and ST-FNSF are expected to operate with the low torque and rotation, respectively, making the physics understanding in low rotation, e. g. in the superbana plateau regime, of particular importance.

2.2.2.2.1 Comparison of the theoretical dependence on collisionality and rotation to experiment

In the second year of NSTX-U operation, the focus of NTV physics studies will be to understand certain parametric dependencies, especially the dependence on collisionality and rotation. Standard combinations between the n = 3 (or n = 2) applied field, and NBI configurations will be used to test theory with different heating powers and plasma density.

The theoretical dependence of the NTV torque on collisionality and rotation, is given [18] by

$$T_{NTV} \propto \sum_{\ell n m m'} \frac{\nu_{eff}}{(\ell\omega_b - n\omega_{E\times B} - n\omega_B)^2 + \nu_{eff}^2}(\omega - \omega_N)\left[\delta B_m \delta B_{m'} W_{mm'}\right], \quad (1)$$

where ω_b is the bounce frequency, $\omega_{E\times B}$ and ω_B are electric precession and magnetic precession frequency, ν_{eff} is the collisionality, $(\omega - \omega_N)$ is the rotation with neoclassical offset, and the last term contains a quadratic dependence on the variation in the field strength. Depending on the plasma collisionality and the resonances between particle orbits, which are expressed by $\ell\omega_b - n\omega_{E\times B} - n\omega_B$, the NTV torque can vary significantly in theory. Particularly important is how the NTV torque will vary as the collisionality is reduced to levels accessible in NSTX-U. A transition to the superbanana (SBP) regime occurs if the collisionality is sufficiently low and the rotation, or similarly electric precession, is low enough to give $\omega_{E\times B} - \omega_B \approx 0$. Also, in plasmas

with sufficiently fast rotation up to $\ell\omega_b - n\omega_{E\times B} \approx 0$, theory predicts that the NTV can be significantly enhanced by bounce-harmonic (BH) resonances.

The operational regime of NSTX bridging to the lower collisionality of NSTX-U, an ST-FNSF, and ITER takes NTV from Shaing's analysis regimes named the "1/ν" to the "ν – sqrt(ν)" regimes [36,43]. The superbanana plateau regime exists for all three devices at lower collisionality, with $\nu^*_i < 1$. These three regimes have three distinct dependences on plasma collisionality, summarized as follows for ions: the torque due to NTV, $\tau_{NTVi} \propto n_i^{K1} T_i^{K2}$, where K1 = 0, K2 = 5/2 for the "1/ν" regime, K1 = 3/2, K2 = 1/4 for the "ν – sqrt(ν)" regime, and K1 = 1, K2 = 0 for the superbanana plateau regime. Simplified, these scalings show a strong increase in the strength of τ_{NTVi} as the plasma becomes collisionless (here defined as collisionality falls below $\nu_i^* < 1$), then saturates at lower ν. The extended theory states that at sufficiently low ν, τ_{NTVi} will begin to decrease with decreasing ν. Of particular note is that when the superbanana plateau criterion is met, the τ_{NTVi} dependence on ν changes significantly, and increases in magnitude, even though the plasma rotation may be small. This characteristic was found for the SBP regime in NSTX (shown in Figure 2.2.2.2.1-1).

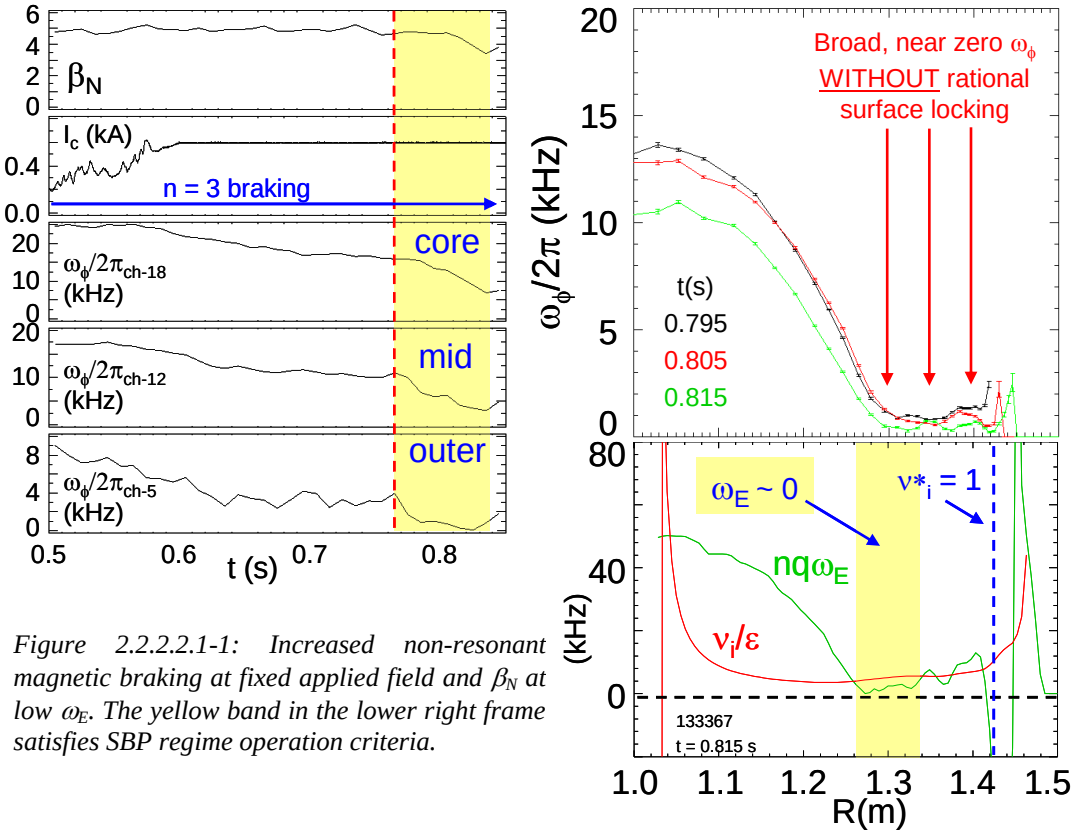

Figure 2.2.2.2.1-1: Increased non-resonant magnetic braking at fixed applied field and β_N at low ω_E. The yellow band in the lower right frame satisfies SBP regime operation criteria.

The dependencies of the NTV torque given by Equation 1 for NSTX plasma parameters, varied over substantial ranges of the plasma collisionality and rotation, are illustrated in Figure 2.2.2.2.1-2.

These theoretical calculations show that NTV torque increases in general when the collisionality decreases, but this fundamental 1/ν behavior becomes more apparent through the rotational resonances. This prediction is qualitatively equivalent to the n = 1 kinetic RWM prediction shown in Figure 2.1.1.3-1, as the kinetic dissipation is the origin of NTV transport in essence [88]. The trend for applied n = 3 magnetic braking is different than the trend for n = 1, as one can see the clear separation between the theoretically computed rotational resonances only for n = 1. This is due to narrower gaps by 1/n between the SBP and BH resonances at higher n. This also implies very different selectivity of the n = 1 and n = 3 NTV torque. With n = 3, the rotation can be decreased until passing the SBP regime at low rotation if the n = 3 field is continuously applied, as found in NSTX [85] (Figure 2.2.2.2.1-1). The calculations also indicate that the 1/ν dependency can be weakened when the collsionality decreases by an order of magnitude.

A simplified expression derivable from Equation 1 for the force on each flux surface due to NTV in the collisionless "1/ν" regime is

$$\left\langle \hat{e}_t \bullet \vec{\nabla} \bullet \overleftrightarrow{\Pi} \right\rangle_{(1/\nu)} = B_t R \left\langle \frac{1}{B_t} \right\rangle \left\langle \frac{1}{R^2} \right\rangle \frac{\lambda_{1i} p_i}{\pi^{3/2} \nu_i} \varepsilon^{3/2} (\omega_\varphi - \omega_N) I_\lambda \quad . \tag{2}$$

This expression scales as $T_i^{(5/2)}$, which is consistent with braking of plasmas with varied T_i in NSTX [89], as well as the plasma inverse aspect ratio, ε, and depends on the neoclassical offset velocity, ω_N. I_λ depends on the spectrum of the 3D field, and other quantities (See Reference [86] for the full definition of other variables). The first key study is the dependence on plasma

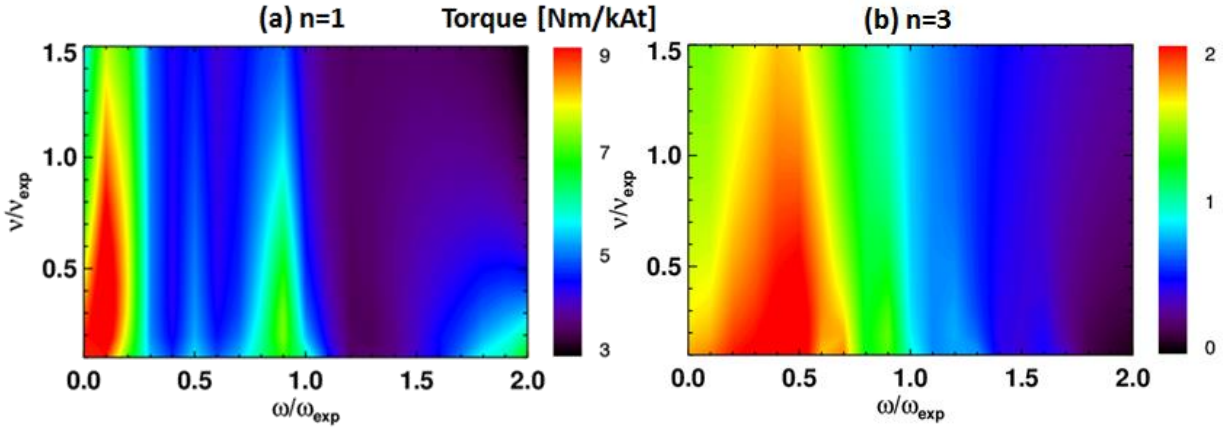

Figure 2.2.2.2.1-2: Analytic NTV calculations for (a) n=1 and (b) n=3 magnetic braking in NSTX, as a function of plasma collisionality and rotation.

collisionality. The collisionality in NSTX-U may be decreased by up to an order of magnitude compared to NSTX. Since the strength of the NTV torque in NSTX was sufficiently large to bring the plasma rotation to near zero on a 100 ms timescale non-resonantly with an applied n = 3 field from the midplane coils, there will clearly be sufficient non-resonant braking in NSTX-U in this regime to quickly access the low rotation regime. The very strong inverse theoretical scaling of τ_{NTVi} with ν will allow a clear test to the present theory, even if collisionality is reduced by a more modest factor of 2 or 3.

Additional elements of NTV theory in connection to plasma collisionality will be explored in the model discussed above. First, the SBP regime at reduced plasma rotation will be able to be accessed similarly as it was in NSTX. The more complex dependencies associated with the various resonances shown in Equation 1 will be examined at the reduced collisionality of NSTX-U. As this regime theoretically has no dependence on T_i, the scaling can be tested experimentally and distinguished from the "1/ν" regime formulation. Second, the theoretically expected saturation of τ_{NTVi} at sufficiently low ν can be examined at the lowest attainable collisionality accessible in NSTX. The lowest plasma collisionality will be accessed once the upward-pointing lithium evaporator system and cryopump are installed.

2.2.2.2.2 Experimental investigation of important theoretical NTV characteristics

Experimental investigations of NTV to date, such as the studies performed on NSTX [83-86], MAST [90], DIII-D [91], and JET [92] have shown general agreement with different aspects of NTV theory, however, the elements have been varied, and are not always consistent among devices. For example, while the neoclassical offset rotation, ω_{NC}, has been observed as significant and consistent with NTV dominated by the ion channel in DIII-D, experiments, results on NSTX show ω_{NC} to be close to zero. In fact, before the NSTX publication of quantitative experimental agreement of the NTV torque profile with theory [86], prior published work at best found qualitative agreement between experiment and theory, and predominantly stated that rotation damping by NTV theory was too weak to explain experiments quantitatively.

The enhanced capabilities of NSTX-U will allow a significantly expanded study of NTV to best leverage and test NTV theory, with the research aiming to unify results across devices. Our collaboration to study NTV on the KSTAR superconducting tokamak will also support this research. As mentioned above, an extensive test of the dependence of NTV on collisionality will be carried out on NSTX-U. Long-pulse aspects, including the evaluation of ω_{NC} will be greatly enhanced by the factor 5 – 10 increase in pulse length of NSTX-U, with analogous comparison with KSTAR long-pulse plasmas. KSTAR also offers the largest aspect ratio difference to NSTX-U, to evaluate the theoretical dependence of NTV on aspect ratio (see equation 2). At

lower collisionality, the effects of the electrons in NTV can be increased, as expected for ITER [93], and this will be examined at the lowest collisionality in NSTX-U. The q-profile is not directly linked to NTV physics, but it can alter the non-axisymmetric variation in the field strength through the plasma response and can result in a strongly modified NTV torque profile. The q-profile will be varied primarily by different combinations of neutral beam current drive (NBCD). Since NBCD will also affect the rotation profile, the rotation and q-profile effects on NTV will be studied together.

The enhanced capability of varying the applied 3D field spectrum utilizing independent control of the midplane RWM coils will allow further testing of the NTV dependence on 3D field configuration on Day 0 of operation. This capability will be significantly enhanced when the partial NCC is installed and operated in Year 4. These additional off-midplane coils will allow applied field spectra that attempt to match or oppose the main plasma field helicity, which will help determine the effects of plasma response and resonant vs. non-resonant damping effects. Further analysis of the expected alteration of NTV by the NCC is given in Section 2.2.2.2.5. All of these aspects will be important for future devices including ITER.

2.2.2.2.3 Comparison of NTV theories and computations

NTV theory continues to be developed and ranges from models formulated in certain asymptotic limits with connection formulae bridging these limits (e.g. the Shaing model), to the solution of the bounce-averaged drift kinetic equation with various collision operators, to particle code simulations. Our present computational toolset spans this range of numerical approaches and includes the NTVTOK code [93], NTV modules included with the IPEC code, and the POCA and FORTEC-3D codes, all of which are described briefly in Section 2.3.

This full range of code capability and analytic models is important for NTV studies in NSTX-U, since the research requires models of varying depth and complexity. For instance, particle simulations (POCA) allow fewer assumptions in the modeling, while analytic

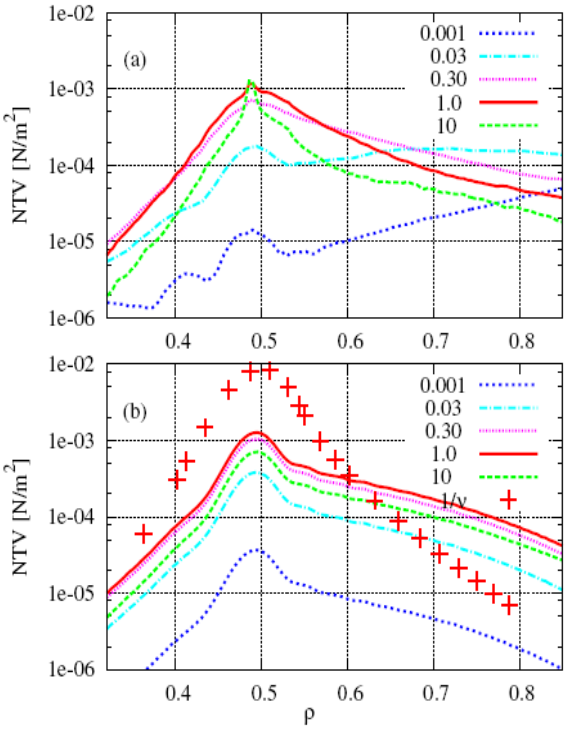

Figure 2.2.2.2.3-1: Comparison between FORTEC-3D (Upper) and analytic NTV (Lower) for different collisionality. One can see good agreements in general, but also a substantial discrepancy in the lowest collisionality.

solutions to the drift kinetic equation allow easier understanding of key scalings for ST-FNSF and ITER. Corrections to analytic models that bridge different operational conditions (e.g. collisionality) can be evaluated by solution of the drift kinetic equation in the various regimes. Factors of 2 to 3 difference between these two types of solutions have been found in the transition regions between the regimes evaluated [93]. Finally, highly simplified models that can be computed in real-time will be needed for use in the plasma rotation control system. These models will be improved as the NSTX-U NTV research develops and updated/tested throughout the five year research period.

In the third year of NSTX-U operation, the study of the NTV dependence on the collisionality will be extended by achieving the lowest density and collisionality regime, which will be directly relevant to future ST applications. The prediction of the analytic theory is a large increase of NTV through the rotational resonances. However, simulations using the global code FORTEC-3D (Section 2.4.12) shows that the analytic NTV may be underestimating the effects of non-resonant field components, as illustrated in Figure 2.2.2.2.3-1. Therefore, NTV validation in the lowest collisionality regimes will be especially important to resolve the different predictions between the numerical and analytic computations.

2.2.2.2.4 Development and testing of models appropriate for closed-loop rotation control

Open-loop rotation control has been routinely conducted on NSTX using non-resonant NTV to alter the rotation profile. This technique has allowed much finer control of the plasma rotation levels than using individual NBI sources, since small changes to the applied 3D field can be made by making small changes to the midplane coil currents. Closed-loop rotation control on NSTX-U will be unique in the world ST and tokamak program, as it will use a combination of NBI source control and NTV via applied 3D field spectra as actuators.

Non-resonant NTV magnetic braking profiles have been experimentally produced for n = 2 and n = 3 applied field configurations in NSTX [84], and results using the n = 1 and n = 3 fields have been quantitatively compared to theory [86]. These results will be used to generate the real-time NTV profile for n = 1, 2, and 3 field “configurations”. Here, the quotes indicate that these configurations are not purely n = 1, 2, and 3, but have higher-n components due to the full 3D configuration of the coils, which are used in the NTV calculations.

Open-loop control of the plasma rotation will be available from the start of NSTX-U operation, utilizing independent control of the 6 midplane coils for the first time. NSTX-U will have greater flexibility to change the toroidal torque than in past NSTX operation, since the 6 independent SPAs will allow the application and switching of n = 1-3 fields simultaneously, and also the 2nd

off-axis NBI system will produce various profiles of injection torques. The experimental quantification of injection torques will be important prior to the NTV study. The total input torques including the intrinsic part and momentum exchanges such as diffusion and convection will be balanced with induced NTV transport, creating the rotational equilibrium.

Closed-loop control, which is expected to start in Year 4, will additionally require a real-time model of the NTV torque profile as a function of applied 3D field current, spectrum, and plasma parameters appropriate to NTV. Real-time 3D coil currents and NTV profiles for closed-loop control for the main n = 2 and 3 non-resonant field configurations will already be available on Day 0. Additional plasma information important to NTV (e.g. plasma rotation speed at several radial positions, real-time evaluation of plasma temperature and density) will be added to the model as they become available in real-time. A real-time toroidal velocity (RTV) measurement system that has been successfully installed in NSTX (and is described in detail in Section 10.6.3.2) will be utilized for rotation feedback control. The neutral beams and 3D fields with the 6 independent SPAs will be used as actuators, to control the input torque and rotation in closed-loop feedback. In this beginning step, the goal is to explore the roughly accessible level of rotation at the center of the plasma and in the pedestal region using NBI. Within the accessible levels of the rotation, the rotation feedback system with RTV and NBIs will be tested to improve RWM/TM stability by altering both rotation and its shear. The ability to control rotation shear will improve during the five years of planned research as additional real-time rotation channels become available.

2.2.2.2.5 NTV theoretical analysis for the NCC physics design

The partial or full NCC coils, available by the third year of NSTX-U operation (Year 4) will provide a more powerful 3D-field actuator for rotation control. This includes the possibility of increasing v_φ via n > 1 toroidal propagation. Figure 2.2.2.2.5-1 shows the integrated NTV torque profiles for the partial and full coil set options, compared to the existing midplane coil. Here $F_{N-N} = T_{NTV}(\psi_N < 0.5) \big/ T_{NTV}(\psi_N < 1)$ is used and a figure-of-merit for NTV is defined as ΔF_{N-N}. The variability can be increased by an order of magnitude with the partial NCCs, ΔF_{N-N}=10~20, and by another order of magnitude with the full NCC, ΔF_{N-N}~200. This means that the NCCs can exert larger torque on the core rather than the edge by 1~2 orders of magnitudes, and thus possibly will produce much stronger rotational shear as well.

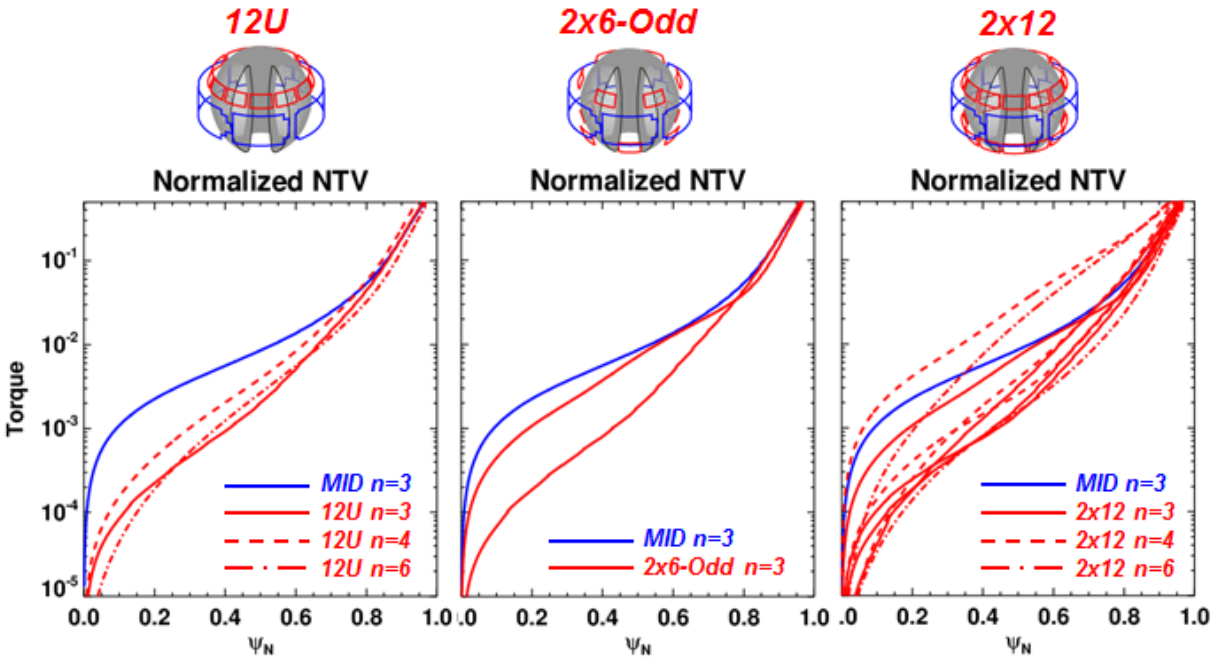

Figure 2.2.2.2.5-1. The torque profiles integrated from the core, for the partial 12U, 2x6-Odd NCC, and for the full 2x12 NCC. One can see that the torque values can be changed in the core by an order of magnitude with the partial NCCs, and by another order of magnitude with the full NCC using high n perturbations.

The variability of the NTV torque profiles will be even greater when the NCC and midplane coils are combined. Examples are shown in Figure 2.2.2.2.5-2, where n = 1 and n = 3 are combined using NCC or midplane coils. The left shows the integrated torque profiles, and the figure on the right shows the damping rates. One easily can see 3~4 orders of magnitude can be produced and can expect that NCC will give indeed unprecedented flexibility of the NTV braking and rotation controllability if truly optimized. Note the examples with the partial NCC, 2x6-Odd configuration, illustrate the powerful n = 1 capability when three rows of coils are used, allowing greater control of the poloidal mode spectra at the outboard side.

The NCC will also allow the expanded investigation of varying rotation in the same q-profile and β, by fully utilizing both NBIs and 3D fields. In particular, the q-profiles and β values favorable to RWM, TM, and internal MHD mode stability will be selected and maintained while the rotation is changed. Next the variation of the q-profiles or β values will be varied while the rotation is held fixed to optimize tradeoffs to improve MHD stability. Rotation (and shear) profile control will be attempted using real-time plasma rotation measurements and improved understanding of the intrinsic torque and NTV braking. This is indeed a research area and capability that will be used by many different topical science groups in NSTX-U, as an optimal rotation profile will be determined to stabilize instabilities from microscopic scale to macroscopic scale and the rotation profile will be controlled using the rotation control system with 3D fields and NBI. Producing and understanding the physics behind optimal and robustly stable rotation profiles will be strongly enabled by the large flexibility of 3D field spectra produced by the NCC. It will enable improved understanding and predictability of the NTV

braking physics and the rotation control capability for the next-step devices such as FNSF, ST-Pilot, and ITER.

Another important issue is whether or not NCC can provide better particle control and also ELM control. As described earlier in Section 2.1.4.1, the 3D field effects on ELMs are not yet fully understood, although various experimental demonstrations have been achieved in different devices. One of the well-known empirical criteria for ELM suppression is the vacuum Chirikov overlap condition for resonant magnetic perturbation (RMP) [19], which partially represents the

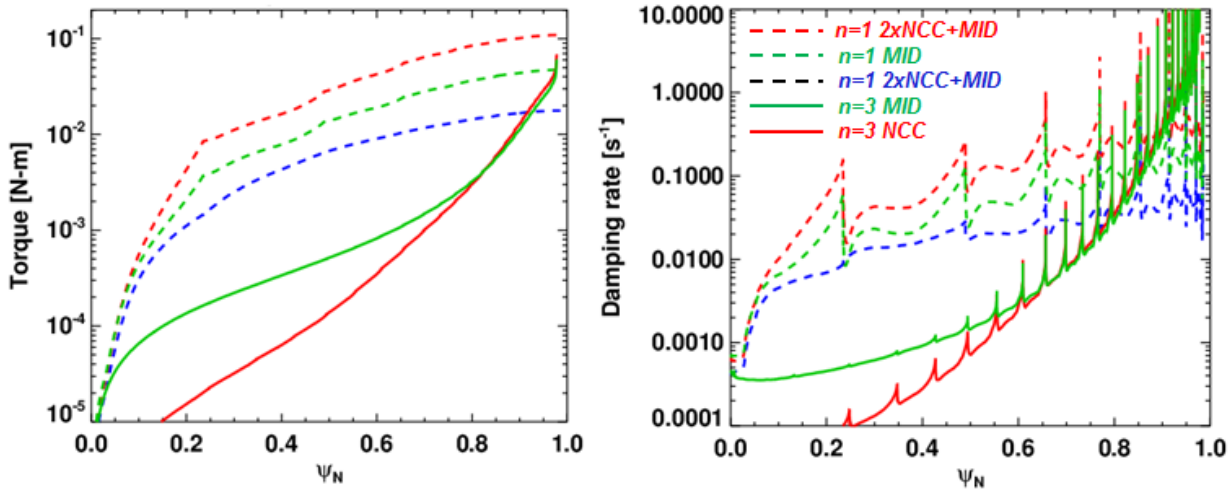

Figure 2.2.2.2.5-2. The torque profiles integrated from the core (on the left) and damping profiles (on the right) when n=1 and n=3 perturbations are used by combining partial NCC (2x6-Odd) and midplane coils. 2xNCC means that the NCC coil currents are twice larger than currents in the midplane coils.

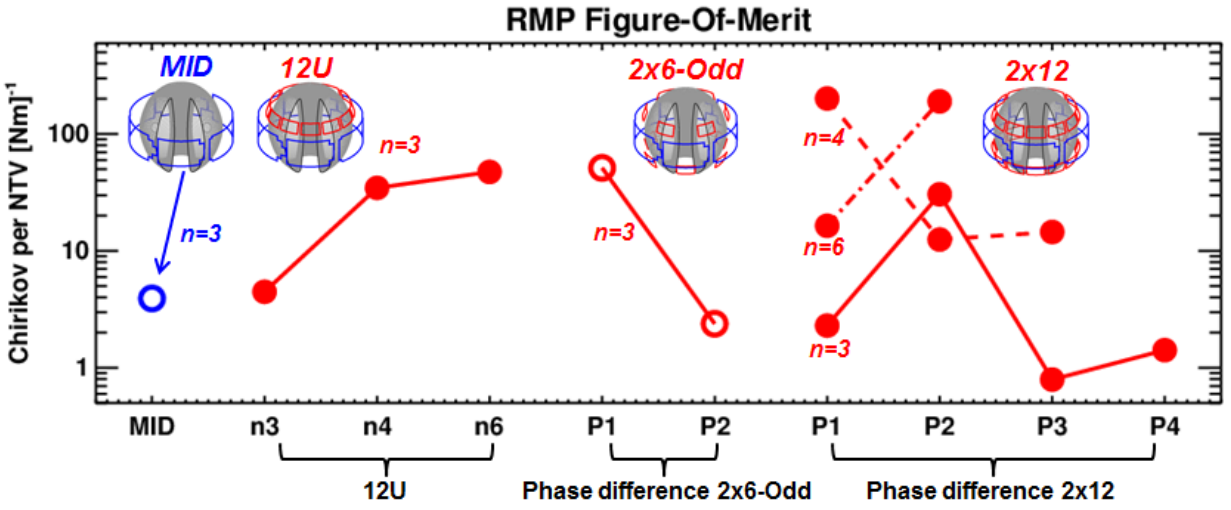

Figure 2.2.2.2.5-3. Comparison for figure-of-merit parameters for ELM control, among existing midplane coils, the two partial NCC options, and the full NCC. (NOTE this figure will be updated consistently with new FOMs.

resonant coupling between 3D fields and rational surfaces in the edge. Another condition is the pitch-alignment condition, and this represents the minimized non-resonant field components other than the edge-resonant components. However, the pitch-alignment condition is qualitative, and a more quantitative condition is needed for actual assessment. The figure-of-merit for RMP ELM control here is defined as $F_{N-C} = (C_{vacuum}, \psi_{N=0.85})^4 / T_{NTV}$, where the numerator is the vacuum Chirikov overlap parameter (with fourth-power to make the FOM independent of field strength), and the denominator represents the non-resonant field components, similarly to the pitch-alignment condition, but quantitatively by NTV strength. The subject of ELM control using 3D fields will be discussed more extensively in Chapter 4, but this FOM assessment related to NTV is shown here in Figure 2.2.2.2.5-3. One can see that this FOM can be increased by an order of magnitude with the partial NCC, and even another order of magnitude when the high n = 4 or 6 is utilized with the full NCC. Although no single criterion, including this FOM parameter, has been found to explain RMP ELM control, this analysis indicates that the NCC will enable significantly expanded testing of RMP ELM control over wide ranges of field spectra to improve the physics understanding of ELM mitigation physics.

2.2.2.2.6 Summary of research plans by year

Year 1 (2014):

- Complete analysis of existing NSTX data from specific experiments investigating NTV. This existing data includes an investigation of NTV vs. plasma collisionality over the range attainable in NSTX, past operation in the superbanana plateau regime, magnetic braking by dominant n = 2 and n = 3 field configurations, and the dependence on plasma rotation speed.
- Update all NTV experimental analysis tools to allow processing suitable for NSTX-U capabilities (e.g. independent control of the midplane coils).
- Continue the design of the NCC with respect to the resonant and non-resonant physics of rotation control.

Year 2:

- Make initial assessment of the dependence of NTV profile and strength as a function of plasma collisionality, and examine the NTV offset rotation utilizing HHFW heated plasmas.
- Prepare an initial simplified real-time model of NTV profile as a function of applied field and available plasma parameters for use in initial tests of the plasma rotation control system (this development carries forward to future years as new real-time diagnostics become available and NTV models improve.)

- Begin verification of the newly developed codes POCA and FORTEC-3D using initial NSTX-U experimental data.
- Investigate NTV effects by intrinsic error fields and find optimal corrections to minimize unexpected rotation braking if needed. Interact with the T&T Topical Science group to best identify intrinsic torque in NSTX-U.
- Investigate NTV physics vs. v_ϕ and q-profile with new NBIs and independent actuator coils.

Year 3:

- Evaluate the neoclassical offset rotation as a function of plasma parameters in long-pulse, steady-state plasmas.
- Determine the experimental dependence of the superbanana plateau NTV on plasma collisionality and compare to theory.
- Utilize real-time model of NTV profile as a function of applied field configuration, strength, and plasma rotation in the plasma rotation control system and evaluate model performance in closed-loop feedback.
- Combine low n perturbations with n = 2, 3 braking and investigate the variability of the rotation and rotation shear profiles using various NBI sources.

Year 4:

- Experimentally determine the dependence of NTV profile and strength as a function of plasma collisionality at the highest ion temperatures, and evaluate the role of electron NTV in this condition.
- Utilize closed-loop rotation control, including initial use of the partial NCC, to produce the broadest and most peaked rotation profiles possible, and high, intermediate, and low rotation levels, comparing offline and real-time rotation models to theory.
- Make initial use of the partial NCC to test theoretical expectations of applied 3D fields as their helicity is varied compared to the equilibrium plasma field helicity.
- Investigate the extended controllability of the rotation using the NCCs. The predicted variability by various phasing between rows will be tested and compared.
- Utilize the NCCs to assess and optimize tradeoffs between v_ϕ, q-profile, β to improve RWM/TM/internal MHD mode stability.

Year 5:

- Examine NTV at the lowest plasma collisionality possible in the device to determine if a saturation of NTV at low collisionality can be found, as expected by theory.
- Demonstrate low rotation profile operation in steady-state with closed-loop rotation control, producing plasma rotation most applicable to ITER and utilizing the partial NCC, with comparison to theory.

- Experimentally determine optimal 3D field spectra, including use of the partial NCC, for minimizing or maximizing NTV vs. applied current and compare to theory.
- Fully utilize and develop the rotation control system to maintain optimized v_ϕ and its profiles for sustained microscopic and macroscopic mode stability.

2.2.3 Thrust MS-3 – Understand disruption dynamics and develop techniques for disruption prediction, avoidance, and mitigation in high-performance ST plasmas

The subsections of this thrust are divided into four main areas for disruption research: prediction, avoidance, mitigation, and characterization.

2.2.3.1 Stability physics for disruption prediction

Next-step STs and steady-state advanced tokamaks both aim to operate continuously at high normalized beta, $\beta_N \equiv 10^8 <\beta_t> aB_0/I_p$, ($\beta_t \equiv 2\mu_0 <p>/B_0^2$) and high non-inductive current fraction. A high bootstrap current fraction yields a broad current profile, corresponding to low plasma internal inductance, l_i. This is favorable for efficient non-inductive operation, but is generally unfavorable for global MHD mode stability, reducing the ideal n = 1 no-wall beta limit, $\beta_N^{\text{no-wall}}$. Past high β_N operation with l_i typically in the range $0.6 < l_i < 0.8$ has an n = 1 $\beta_N^{\text{no-wall}}$ computed by the DCON code (Section 2.4.2) to be 4.2 – 4.4 [7]. Operation at $\beta_N > 7$ and $\beta_N/l_i > 13.5$ has now been demonstrated transiently, with pulse-averaged β_N (averaged over constant plasma current), $<\beta_N>_{\text{pulse}} > 5.5$ in low l_i plasmas in the range $0.4 < l_i < 0.6$ with active n =1 mode control (Figure 2.2.3.1-1). Pulse-averaged values of (l_i, β_N) now intercept the higher l_i portion of the planned operational ranges for ST-CTF and ST Pilot plants. Especially important is that the ideal n = 1 no-wall stability limit is significantly reduced at these low l_i values, so that β_N now exceeds the DCON computed $\beta_N^{\text{no-wall}}$ for equilibrium reconstructions of these plasmas by up to a factor of two. In addition, synthetic variations of the pressure profile for plasmas with $l_i \sim 0.38$ show these equilibria to be at the purely current-driven ideal kink stability limit, as they are computed to be ideal unstable at all values of $\beta_N > 0$. In this operational regime, passive or active kink and resistive wall mode (RWM) stabilization is therefore critical. The disruption probability due to unstable RWMs was reduced from 48% in initial low l_i experiments to 14% with this control, but remarkably, the reduced disruption probability was observed mostly in plasmas at high $\beta_N/l_i > 11$. Disruptions occurred more frequently at intermediate values of β_N/l_i. This agrees with active MHD spectroscopy diagnosis, used to determine the proximity to marginal stability [65] (Figure 2.2.3.1-2). The resonant field amplification (RFA) of an applied 40 Hz co-NBI rotating n =1 seed field shows an increase in RFA to a broad peak near $\beta_N/l_i = 10$. This decrease in RWM stability, shown by the increase in RFA, is expected as β_N increases, and has been as reported for DIII-D [94] and NSTX [7] at lower β_N values. In contrast, and remarkably, RFA is found to decrease at higher values of β_N/l_i in NSTX, indicating increased mode stability (Figure 2.2.3.1-2). This positive result is presently not thought to be a second stability region for the

RWM, but is more likely related to proximity to broad resonances in plasma rotation providing kinetic stabilization of the RWM [8,9]. The result of decreased disruptivity at higher β_N/l_i is also consistent with analysis of the wider NSTX database spanning 2006 – 2010 [95]: no clear increase is found in disruptivity at increased β_N and $l_i < 0.8$.

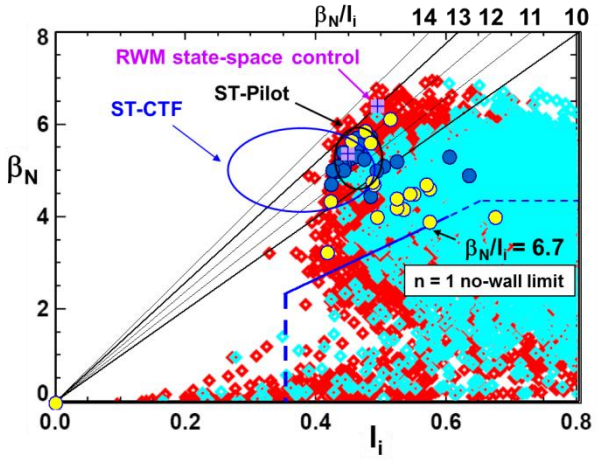

Figure 2.2.3.1-1: High β_N, low l_i operational space. Red/cyan points indicate plasmas with/without n = 1 active RWM control. Blue circles indicate stable long pulse plasmas with active RWM control; yellow indicates disruptions.

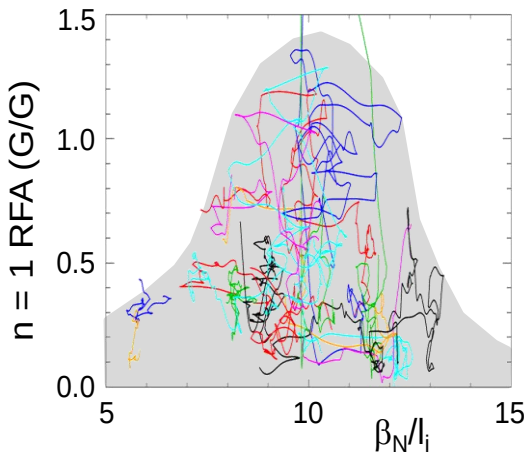

Figure 2.2.3.1-2: n = 1 resonant field amplification during high β discharges using active MHD spectroscopy, indicating improved stability at high β_N/l_i.

2.2.3.1.1 Establish and test approach to marginal stability based on kinetic stabilization for disruption prediction

NSTX research established that global mode stabilization physics is more complex than having a small level of plasma rotation present to ensure stability. Quantitative comparisons of kinetic stabilization theory to experiment [8,9] have shown that unstable bands of rotation can exist at relative high rotation. These bands are defined by the plasma crossing an unstable boundary, rather than a lack of torque balance as can occur for modes (such as tearing modes) that exhibit resonant braking torques. Sections 2.2.1.1.3 and 2.2.1.1.4 discuss and illustrate the physics analysis that motivates a real-time model to predict the proximity to marginal instability. This information can be used in a staged manner to (i) attempt to alter key profiles such as plasma rotation, or NBI heating to move away from a marginal boundary, and (ii) issue a plasma shutdown command if the marginal boundary is very close, or reached.

Simple models will be supplied to the NSTX-U disruption warning system, which will continue to be developed as real-time diagnostics implantation allows. For example, the simple criterion

$|\omega_E - \omega_D| < K$, where K is a constant (see Section 2.2.1.1.4) can be implemented once real-time rotation measurements are available, making very simple approximations for ω_D – even using a fixed ω_D profile based on routine high beta H-mode operation will be enough to start the real-time study. As additional information becomes available (e.g. real-time Thomson scattering, real-time estimates for T_i profile from CHERS), the parameters in the physics model will be known to greater certainty.

2.2.3.1.2 Testing low frequency MHD spectroscopy for active disruption prediction

Low frequency MHD spectroscopy has been used in NSTX and DIII-D to determine global mode stability in stable plasmas, and will be further developed as an important tool for disruption prediction and avoidance in NSTX-U. The striking results of increased stability at increased β_N/l_i shown in Section 2.2.3.1 (Figure 2.2.3.1-2) and dependence of RFA amplitude on collisionality shown in Section 2.2.1.1.3 show how the RFA amplitude correlates well with the complex stability space in NSTX, and is a good detector for the proximity to marginal stability. The present offline analysis is being converted to allow real-time application for disruption prediction.

While the physics of low frequency MHD spectroscopy using single mode RFA amplitude is well known, this technique leaves out at least two important physics aspects that require further research to improve the single mode analysis. First, the single-mode RFA phase carried important information for NSTX plasmas. For example, the transition of the single mode RFA phase from being stationary to rotating in the rest frame of the applied field is a key early warning indicator that the amplification of the applied field is transitioning into a mode. This event is due to the NTV drag of the plasma on the amplified applied field and happens while the plasma is still stable. This event in itself could be used to predict disruption. However, if the mode spins up to sufficiently high rotation frequency, it is strongly damped. Intermediate rotation frequencies are most dangerous and indicate disruption. Second, the multi-mode spectrum of NSTX (Section 2.2.1.2.2) shows that a multi-mode RFA analysis should be used at sufficient β_N. The new capabilities of NSTX-U will allow the application of applied field with different n numbers, and the additional information provided by the upgraded sensors with positions closer to the divertor may provide further mode discrimination.

2.2.3.1.3 Use of RWM state-space controller observer for disruption prediction

The specific use of the RWM state-space controller observer for detecting internal modes was discussed in Section 2.2.1.4.1. This is actually a specific use of the observer, where the correction term $K_o\left(\vec{y}_m - \vec{y}\right)$ becomes large due to $\vec{y}_m$ becoming small. However, this concept can be used more generally, in that sufficiently large $|K_o\left(\vec{y}_m - \vec{y}\right)|$ can be used to predict

disruptions. This difference is already computed in real-time in the RWMSC. It is also important to realize that this difference depends upon how well the physics model reproduces the measurements. If the physics model reproduced the mode dynamics with 100% accuracy at each step, then the observer and measurements would be equal, and the difference would be zero. Therefore, the planned improvement of the physics model in the RWMSC will affect this disruption indicator. The research will begin before the start of NSTX-U by assessing how large this difference becomes before the onset of disruptions in the present NSTX database.

2.2.3.1.4 Summary of research plans by year

Year 1 (2014):

- Evaluate simple physics criteria (suitable for real-time use) for the approach to global mode marginal stability based on ideal (e.g. pressure peaking, β_N/l_i) and kinetic stability physics using initial high performance NSTX-U plasmas, emphasizing rotation profile and speed.
- Initially compare the degree of mismatch between the initial RWMSC observer model and sensor measurements and the occurrence of plasma disruptions from the existing NSTX database to evaluate future use in the disruption warning system.

Year 2:

- Construct an initial MHD spectroscopy database for high performance NSTX-U plasmas to determine the measured variation of global mode stability as a function of key parameters including plasma rotation, energetic particle profile and distribution, q_{min}, and β_N. Determine if results are consistent with past NSTX experimental results.
- Improve simple physics criteria used to determine global mode marginal stability adding energetic particle stabilization and expanding the kinetic stabilization model.
- Determine the applicability of single mode RFA phase information in low frequency MHD spectroscopy measurements to supplement amplification in determining proximity to global mode stability boundaries.
- Improve disruption prediction using the RWMSC observer model and sensor measurements by improving the model and/or sensor mismatch criteria used.

Year 3:

- Determine and implement a real-time evaluation of a simple global mode marginal stability model including important parameters (e.g. plasma rotation speed and profile, q_{min}, T_e, n_e) that will be available in real-time during Years 4-5.
- Determine single mode RFA amplitude and phase criteria that predict disruptions, and evaluate possible improvements afforded by multi-mode RFA.

Year 4:

- Add and use real-time rotation and q_{min} measurements and evaluations for determining global mode marginal stability boundaries, enabling improved evaluation of physics model.
- Examine real-time low frequency MHD spectroscopy in determining global mode stability boundaries for input to stability profile control systems (e.g. rotation, q).

Year 5:

- Add and use real-time Thomson scattering data to improve the simple kinetic stabilization physics criterion used for determining global mode marginal stability boundaries.
- Improve disruption prediction using the RWMSC observer by the addition of the newly-installed expanded RWM sensor set.

2.2.3.2 Stability control for disruption avoidance

Once the physics elements of the disruption prediction are established as discussed in Section 2.2.3.1, the actuators and algorithms to avoid disruption must be defined and implemented. This task will be a joint effort between the Macroscopic Stability and the Advanced Scenarios and Control topical science groups. The elements described here focus on the task elements of the Macroscopic Stability group.

Note that in all examples below, a flag that predicts an approach to an instability boundary can be made to trigger a plasma shutdown, or triggering of the disruption mitigation system, using the NSTX-U disruption warning system. These results are taken as a last resort, based on the most critical disruption prediction flags. The plasma disruption mitigation system is described in Section 2.2.3.3 and plasma shutdown techniques are described in Section 9.2.3.2.

2.2.3.2.1 Rotation and heating control to test kinetic RWM marginal stability, and to maintain r/t stability

Kinetic stabilization of global modes presently has the greatest physics content and understanding in the underlying models. Therefore, the theory guides the relevant actuators. In this case, actuators that affect both the ideal and kinetic stability contributions to δW are relevant, which covers the majority of the real-time actuators planned for the next five year period. For example, once real-time MSE becomes available, it can be matched to the operation of specific NBI sources to change q. The pressure peaking factor is also another basic parameter that affects ideal stability. TRANSP runs provide guidance on NBI deposition, but only NSTX-U operation will determine how the three new NBI sources will specifically alter the pressure

peaking in NSTX-U. Generally, they should broaden the profile, which would provide a more stable profile to global modes. The impact on ELM stability based on these changes will also need to be determined to find optimal profiles in the broadest sense.

The key actuators affecting the kinetic stability will be the rotation control system, and choice of NBI sources. The former itself will use both the NTV from applied non-axisymmetric fields, and the NBI source input to control the plasma rotation with active feedback. Therefore, one input to the real-time rotation control system will be a series of target rotation profiles generated by the kinetic stabilization physics model in real-time. The simple models developed for real-time use (Section 2.2.3.1.1) will output these target profiles. As shown in Section 2.2.1.1.3, these favorable profiles will depend on plasma parameters such as collisionality, and so real-time evaluation of temperature and density will be used in the algorithm as they become available. Since β_N itself has been found to not be a useful indicator of mode stability (higher β_N was *more* stabilizing in NSTX – see Section 2.2.3.1), NBI actuation is planned to be based more on momentum input, energetic particle profile, and pressure peaking alteration than overall input power. However the ability to limit β_N in real-time through total NBI power will be an option in NSTX-U. As shown in this example, some actuators will become overloaded (i.e. asked to perform conflicting action simultaneously). Prioritizing the actuation based on the physics study or stabilization goal in question will be an important aspect of the research.

2.2.3.2.2 Real-time MHD spectroscopy for active disruption avoidance

Real-time low frequency MHD spectroscopy (i.e. RFA amplitude magnitude and phase dynamics) can be used in the simplest ways (e.g. limit β_N) for disruption avoidance. However, this technique has far greater potential for disruption avoidance when used in conjunction with other physics models that predict mode stability in real time. This is state-of-the-art research that will be pioneered in NSTX-U. The plan is to couple the RFA output to the kinetic stabilization (Section 2.2.3.1.2) and RWMSC observer (Section 2.2.3.1.3) models. As each of these models evaluates new criteria for improved stabilization, the real-time low-frequency MHD spectroscopy system can determine whether or not these models are indeed improving stability. This information can be used not only to alter the output of the physics models, but also to catalog a very large database of how successful the physics models are in guiding the control system toward greater stability. This latter aspect will allow a greatly accelerated understanding of what changes in the control lead to improvements in stability well before marginal stability points are approached.

The number of possible variations using this approach is large, so theory will guide the research plan, and experiment will determine how well the approaches actually work. Theory will then be improved if needed until successful approaches are found. One concrete example is the alteration

of the rotation profile. Kinetic stabilization theory will produce real-time rotation profile targets, and the low frequency MHD spectroscopy system will determine in real-time if the change made is superior, or inferior (the change may be inferior simply because the model is approximate and incomplete). Changes to the target rotation profile can then be made solely on the change that is measured from MHD spectroscopy *without* updating the target profile as indicated by kinetic stabilization model. Variations of applied non-resonant 3D fields, NBI momentum input, q profile, and density are four examples of actuators that could be directly guided by real-time MHD spectroscopy.

2.2.3.2.3 RWM state-space controller observer development for RWM avoidance

The RWMSC observer can also guide variations to actuators in a similar fashion to low frequency MHD spectroscopy. For instance, of a set of target rotation profiles from the kinetic stabilization model lead to an increasing difference in $|K_o(\vec{y}_m - \vec{y})|$, perturbations around these profiles can be considered by altering them and observing if $|K_o(\vec{y}_m - \vec{y})|$ decreases. This approach can be used for as long as desired before using a new target rotation profile based on the kinetic stabilization model. Additionally, monitoring the RWMSC observer during disruption avoidance will quickly generate a large database showing how well the difference $|K_o(\vec{y}_m - \vec{y})|$ correlates with favorable stability changes as measured by low frequency MHD spectroscopy. This data can be used to guide improvements to the observer physics model.

2.2.3.2.4 Rotation control to run at ITER-relevant low rotation

Non-resonant NTV braking of the plasma rotation profile has been used in NSTX to produce very low levels of plasma rotation, creating target plasma that are more applicable to rotation conditions expected for ITER. The plasma rotation profile and level alters plasma stability, and so alters demands on the active mode control system, and changes the stability and stability gradients. NSTX-U will provide unique capabilities to study this operational regime for ITER, as it will have an extensive set of actuators and real-time disruption prediction and avoidance tools to study the low rotation plasma state in a tokamak device.

2.2.3.2.5 Coupling of stability and control to ITER and ST-FNSF scenarios

The kinetic stabilization physics model has been used to compute the stability of ITER advanced scenarios, and has drawn important conclusions. Most importantly, present models show that ITER plasmas that are just a few percent over the ideal marginal stability point will be unstable unless a significant alpha particle population is present [66]. As shown in NSTX, even with large plasma rotation, global instability can cause disruptions in ST plasmas. Therefore it is critical that the stability and disruption prediction and avoidance research be conducted in NSTX-U

scenarios that best emulate ST-FNSF operation. Significant development of these stability tools along with the production of the ST-FNSF scenarios are expected synergistically join in the later years of the 5 year period to directly test the physics and control tools in these scenarios, along with scenarios at low rotation to best support ITER.

2.2.3.2.6 Summary of research plans by year

Year 2:

- Perform initial experiments using open-loop plasma rotation, current profile, and energetic particle control to demonstrate the ability to avoid encountering disruptive global mode stability boundaries based on kinetic RWM stabilization models.
- Test stability physics expectations of increased global mode stability at the highest β_N/l_i in NSTX-U plasmas, and compare to positive results found in NSTX, examining potential differences due to aspect ratio.
- Determine physics implications of scenarios that over-constrain 3D field and NBI actuators for simultaneous use in meeting open-loop requests for plasma profile targets for rotation, q, energetic particle population, β_N, and other key parameters in the goal of disruption avoidance.
- Implement and test initial disruption avoidance using the RWMSC observer model in real-time, including open-loop disruption avoidance criteria in low rotation plasmas (most ITER relevant).

Year 3:

- Implement results from a real-time evaluation of the simple global mode marginal stability model into plasma rotation and q profile control systems that will be available in real-time during Years 4-5.
- Implement single mode RFA amplitude and phase as input to profile control systems and disruption warning system.
- Combine physics criteria for disruption avoidance systems (profile control and disruption warning systems) allowing variable prioritization of control to avoid physics request conflicts and to avoid actuator overloading.

Year 4:

- Evaluate and study the stability physics response of real-time rotation and *q* profile control using the simple kinetic stabilization physics criteria and real-time low frequency MHD spectroscopy for avoiding global mode marginal stability boundaries, including initial use of the partial NCC as an actuator for rotation control.

- Test coupling of real-time RFA, simple physics model, and RWMSC observer systems in providing simultaneous actuation of stability profile for avoiding global mode stability boundaries.
- Apply combined disruption avoidance control to high β_N plasmas with non-inductive current fraction approaching, or at 100%.

Year 5:

- Combine disruption avoidance control with simultaneous use of n > 0 active feedback and the partial NCC, determining physics implications of this combination and potential control conflicts.
- Demonstrate improved global MHD mode stability and very low plasma disruptivity in dedicated experiments using ITER-relevant (low rotation), high rotation inductive scenarios, and 100% non-inductive ST-FNSF scenarios.
- Determine the physics and controllability implications of using/omitting upgrades to the combined control systems, including the partial NCC, expanded RWM sensor set, real-time Thomson scattering, and real-time ME-SXR data.

2.2.3.3 Rapid shutdown techniques via mass injection for disruption avoidance

When disruption prediction and avoidance techniques fail, a fast discharge termination method is needed to minimize the deleterious effects of the disruption, particularly the large heat loading from the thermal quench and the generation of large populations of runaway electrons. Massive Gas Injection (MGI) is one approach to addressing this difficult issue for ITER. Research in NSTX-U will compare MGI from different poloidal locations to assess the gas penetration efficiency from each of these locations. NSTX-U researchers have begun modeling gas penetration using the DEGAS-2 code (Section 2.4.11) to quantify the gas penetration past the SOL for NSTX-U. For disruptions in ITER that have short warning times of less than 10ms, the MGI system may not perform satisfactorily. For these extreme cases, for which the ITER disruption mitigation system (DMS) must be designed, more rapid impurity injection systems, such as the Electromagnetic Particle Injector (EPI) planned for NSTX-U might be used.

Note that realtime disruption detection methods are described in Sections 2.2.3.1 and 9.2.3.1. Those methods will be used to trigger these mitigation technologies in NSTX-U to test real-time disruption mitigation.

An important goal of these studies is to assess reductions to the divertor heat loads during an unmitigated vs. mitigated disruption and the radiated power profile during the thermal quench phase. Many of the diagnostics that will be used for these and other measurements (soft X-ray

and VUV measurements, bolometer arrays, Thomson scattering, visible cameras, interferometer, divertor diagnostics including halo current sensors, multi-color IR cameras and divertor thermocouples) are described in Chapter 10 Also, specifically, the instrumented tile diagnostics required for disruption mitigation studies in NSTX-U will be described in Section 2.2.3.4.2. Finally, a description of a dedicated fast diode based XUV radiometer to diagnose impurity dynamics during the disruption mitigation experiments is included in Section 10.6.3.6.

2.2.3.3.1 Massive gas injection experimental development

At present, massive gas injection (MGI) appears to be the most promising method for safely terminating most discharges in ITER [96-100]. MGI involves the rapid injection of large quantities of gas into the tokamak discharge; the quantity of gas is typically several times the inventory of the plasma discharge. Usually some fraction of the injected gas has a high-Z component such as argon or neon. Requirements for the mitigation of disruption effects fall into three categories: (1) Reducing thermal loads on the first wall and the divertor; (2) reducing electromagnetic forces associated with "halo" currents, i.e. currents flowing on open field lines in the plasma scrape-off layer; and (3) suppressing runaway electron (RE) conversion during the current quench phase of the disruption. To accomplish these in ITER, it is projected that about 500 kPa-m^3 of helium with some noble gas fraction will be required.

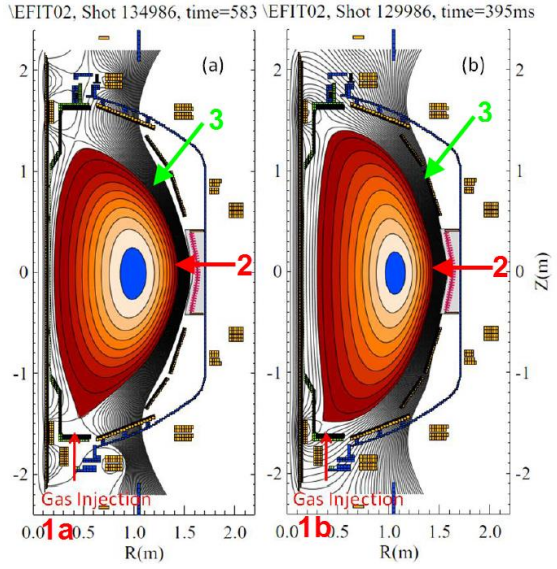

Figure 2.2.3.3.1-1: Shown are the planned Massive Gas Injection locations on NSTX-U. (1a) Private flux region, (2) mid-plane injection, (1b) high field lower SOL region and (3) outer SOL above the mid-plane.

The present understanding of disruption mitigation using massive gas jets is based on work conducted on DIII-D, Alcator C-MOD, ASDEX-U, JET, Tore Supra and other large tokamaks, and is summarized in References [96-100]. Recent experimental results have shown that the cold front from the edge, which has been cooled by an MGI pulse, needs to reach the q = 2 surface for the onset of rapid core cooling to occur. On ITER, it is not known if a simple MGI pulse from multiple locations would be adequate because of its larger minor radius, the increased transit times for the neutral gas, and the larger expected scrape-off-layer (SOL) flows. Insight into ways for reducing the total amount of injected gas and optimizing the injection locations would provide critical help to the design of a suitable system for ITER.

NSTX-U can offer new insight by injecting gas into the private flux and lower x-point regions of divertor discharges to determine if this is a more desirable location for massive gas injection. Injection from this new location has two advantages. First, gas injected directly into the private flux region does not need to penetrate the scrape-off-layer. Second, because the injection location is nearer the high-field side in standard D-shaped cross-sections, the injected gas should be more rapidly transported to the interior as known from high-field side pellet injection [101] and from high-field side gas injection work on NSTX [102]. By comparing massive gas injection from this new location to injection of a similar amount of gas from the outer mid-plane, NSTX-U can improve the knowledge of disruption mitigation physics and thus improve the disruption mitigation system (DMS) design for ITER (provided the NSTX-U results are obtained early in the 5 year plan).

To put the gas penetration issue in perspective, the private flux region in ITER is predicted to have an electron temperature of less than 2eV and an electron density below $2x10^{20}$ m^{-3} [103], and for detached DIII-D plasmas less than 1eV and less than $5x10^{19}m^{-3}$ [104]. The relatively low electron temperature in the private flux region in both ITER and DIII-D is due to active gas puffing in the divertor region to obtain a detached divertor configuration, which is necessary to reduce divertor heat loads. The electron temperature and electron density in the SOL at the mid-plane region of ITER is predicted to be about 100eV and $2x10^{19}m^{-3}$ [105], and for DIII-D less than 20eV and less than $3x10^{18}$ m^{-3} [106]. The parameters for NSTX-U could be expected to similar to those for DIII-D.

These numbers show that plasma parameters in the SOL region for present large tokamaks as well as the projected SOL parameters for ITER are much more challenging for neutral gas penetration compared to the parameters in the private flux region. This is the motivation for proposed experimental work on NSTX-U. These parameters will be used as input in DEGAS-2 simulations to theoretically assess the gas penetration efficiency as a function of SOL and private flux region parameters and will eventually be compared to experimental observations from NSTX-U.

The primary goal of the MGI experiments in NSTX-U is to compare the gas penetration efficiency as gas is injected from the different poloidal locations shown in Figure 2.2.3.3.1-1. These are (1a) the private flux region, (2) the mid-plane region, (1b) high-field side outer SOL region, high-field side inner SOL region and (3) outer SOL region above the mid-plane. A second objective is to determine the uniformity of the radiated power profile. The third objective is to assess the reduction in divertor heat loads and halo currents. The importance of the q = 2 surface proximity to the plasma edge will be studied by gas injection at different times during the discharge as the q = 2 surface evolves. The eventual goal of these studies would be to design a system for NSTX-U that can automatically trigger the MGI system based on input received from

sensor-provided data on an impending disruption. For these up-coming experiments on NSTX-U four ports have been assigned for MGI. The green arrows in Figure 2.2.3.3.1-2 show these MGI port locations.

The gas assimilation efficiency will be measured by obtaining closely spaced (in time) Thomson scattering density profiles just prior to and after the MGI gas begins to interact with the edge plasma but before the thermal quench phase has initiated. EFIT reconstructions would provide the plasma shape and volume. H-alpha detectors would be used to establish the time of contact of the MGI gas with the edge plasma. The time delay between this and the time when the individual MGI valve is triggered would provide the overall system response time for each gas injector. Starting from the time when the MGI gas first makes contact with the edge plasma, the Thomson scattering system would be triggered (at 0.5, 1, 1.5ms) to obtain density profiles before the plasma shape begins to significantly distort or before the Thomson scattering system detectors saturate. Since the Thomson scattering system measures local density this is preferred over the NSTX-U multichord interferometer system as it avoids the issue of profiles obtained using Abel inversion from a few interferometer chords. However, depending on the amount of injected and assimilated gas, both systems will be needed to obtain reasonable estimates for the amount of gas assimilated by the plasma discharge. Measuring this parameter has been challenging in other tokamaks and will prove to be challenging on NSTX-U as well since these diagnostics are not designed for the very high density plasmas that result from assimilation of large quantities of gas.

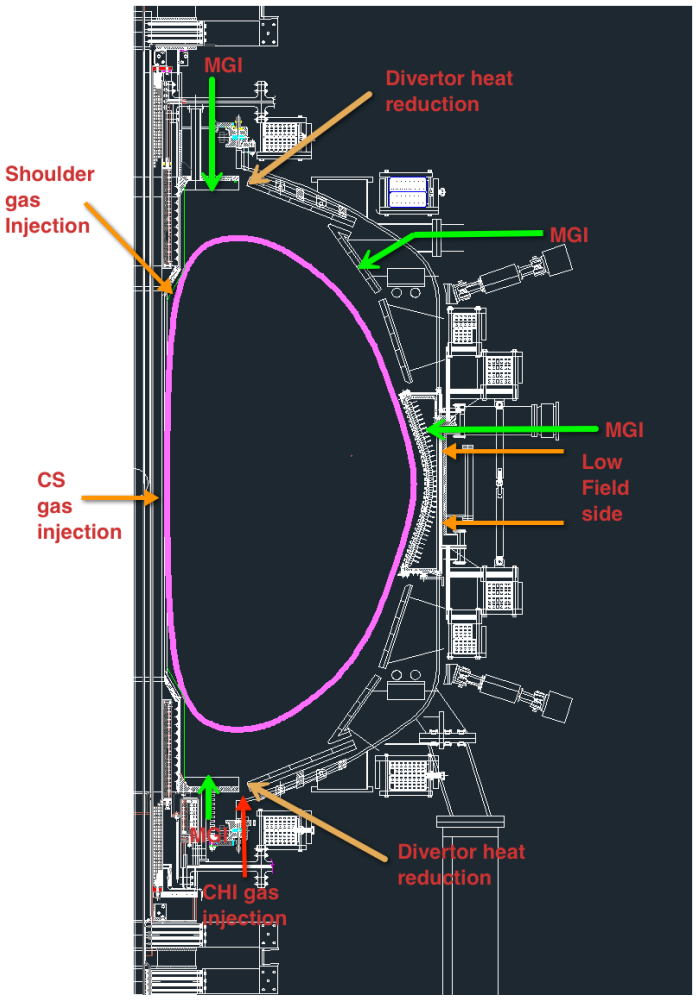

Figure 2.2.3.3.1-2: MGI gas injection locations on NSTX-U are shown by the green arrows.

A concern with localized gas injection for ITER is that the radiation profile could be toroidally localized to a region near the gas injection port. Depending on the plasma parameters, this could lead to localized heat deposition on nearby walls leading to localized melting. Thus measurement of the radiated power profile at three or more toroidal locations is important. This is discussed in detail in a subsequent section, including the need for a new-dedicated diagnostic. Here the NSTX-U multi-chord bolometer array and the multi-chord soft X-ray arrays will be used to obtain the radiated power and soft X-ray emission profiles using an Abel inversion method from a dense array of chords.

The spatial distribution of the divertor heat loads will be measured with two color divertor fast infrared cameras. These were successfully used during the FY2010 NSTX run campaign to measure divertor plate temperatures during the snowflake divertor experiments. These will be complemented with eroding thermocouples that would provide an independent measurement of the divertor plate radial temperature profile at a few toroidal locations. Halo current sensors on the divertor plates will provide data on the extent of halo currents during the different disruption mitigation scenarios and during unmitigated disruptions.

2.2.3.3.2 MGI simulations using the DEGAS-2 code

In support of Massive Gas Injection (MGI) studies on NSTX-U, DEGAS-2 simulations [107,108] are being conducted to better characterize the gas penetration physics and to improve the design of the MGI gas delivery system on NSTX-U.

There are two requirements for successful implementation of MGI in ITER. The first requirement is that an adequate amount of injected gas penetrates past the separatrix. This is related to the physics of neutral gas penetration through an energetic edge plasma region and the SOL. The ratio of the injected gas that couples to the tokamak discharge to the total amount of injected gas is referred to as the gas assimilation or gas penetration efficiency. The second part involves the physics of how the gas that penetrates past the separatrix distributes within the plasma discharge. The dynamics of the gas mixing is responsible for the resulting thermal quench timescales and radiated power profiles. This is referred to as gas dissipation physics inside the separtrix. While much work is in progress to understand the gas dissipation physics, for example through the use of the NIMROD code [109] the more fundamental gas penetration issue is still poorly understood.

A review of the literature [96-99] shows that the amount of gas injected in MGI experiments in present tokamaks varies from 100 $Pa.m^3$ to over 2000 $Pa.m^3$, considerably less than the projections for ITER. The fraction of this gas that penetrates past the separatrix also varies widely, with penetration efficiencies of over 20% being reported for cases that have a short MGI

pulse. To better quantify the amount of gas required in a MGI pulse a DEGAS-2 Monte-Carlo code simulation effort has been initiated to understand the extent of gas penetration through the SOL region and private flux regions. In addition to supporting NSTX-U needs, this simulation effort focuses on studying the fundamental issues of edge penetration to the separatrix, which is needed for predicting gas penetration efficiencies in ITER. This work complements other 3-D MHD modeling (such as with the NIMROD code), initiated by the ITER organization, of the gas dissipation physics inside the separatrix.

Full DEGAS-2 model: For a full detailed simulation of the involved gas penetration physics, both the DEGAS-2 and UEDGE codes are required. The planned simulations will start with plasma parameters from a suitable NSTX-U discharge with neutral beam heating. The computational mesh needed for DEGAS-2 to model the region outside the separatrix region would be generated by the UEDGE code [110,111,112].

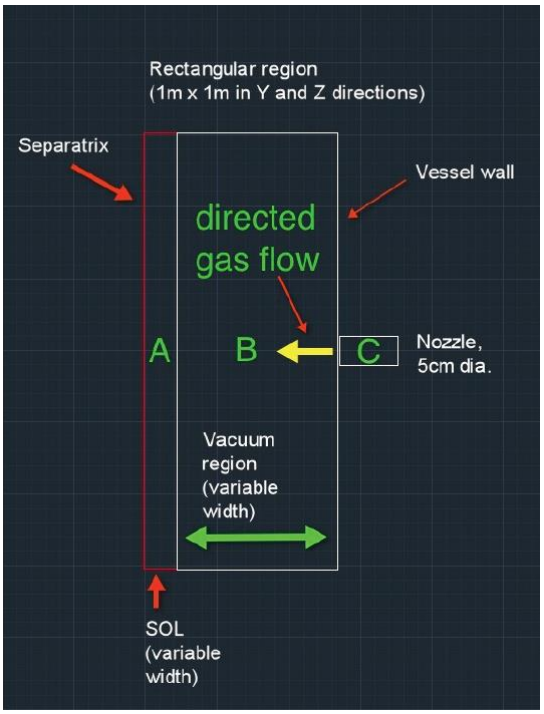

Figure 2.2.3.3.2-1: Simplified rectangular 3-D mode for DEGAS-2 simulations.

As the molecules penetrate the plasma, they would undergo ionization, dissociation, and elastic scattering; resulting molecular ions would undergo ionization, dissociation, or recombination. Any product atoms would then be tracked through the plasma and can undergo ionization and charge exchange. The particle track terminates upon ionization of the atom. Along the particles' paths, the volumetric source of plasma ions is accumulated in each computational zone. The penetration fraction is then the ratio of the volume-integrated sum of those source rates over zones inside the separatrix to the gas puff rate.

Simplified DEGAS-2 model: While we are interested in conducting this full model study during the 5 year period, due to present man-power limitations, we have considerably simplified this model to understand a smaller part of the important gas penetration physics that is relevant to the up-coming NSTX-U MGI experiments. To carry out this simplified study we have used a simple rectangular geometry. In this simplified rectangular geometry, shown in Figure 2.2.3.3.2-1, a 1m x 1m (in the y and z directions) region is used. Region A represents the SOL region and its width and plasma parameters (density and temperature) can be arbitrarily varied. Region B is the space between the SOL outer edge and the vessel wall. This is 20cm in width

and contains no plasma. This width could also be varied to reflect the location of the gas valve with respect to the edge of the SOL. The gas valve, labeled C, is located at the vessel wall.

In this simplified model, the SOL and private flux regions can be modeled by varying the length of the dimension A and the corresponding plasma parameters in region A. Thus depending on the choice of the parameters, region A would represent either the SOL or the private flux region. With the proper choice of the plasma parameters in region A, it should also be possible to obtain estimates for the gas penetration fractions that could be expected in ITER. These simplified DEGAS-2 simulations are planned to be completed before year 2 of NSTX-U operation.

This model will provide a lower bound for the gas penetration efficiency that can then be compared to observed results from DIII-D, C-MOD and other tokamaks. It will also provide guidance for the gas penetration efficiencies for NSTX-U mid-plane and private flux region conditions. Based on the extent of differences between the simplified DEGAS-2 results and experimental observations form present machines as well as from NSTX-U, a full DEGAS-2 simulation could be considered during years 2 to 4 of NSTX-U operations.

These simulations can also be extended to cases where smaller fractions of high-Z gases (neon, argon) are introduced into a carrier He gas to assess the ratio of high-Z to He gas fractions that allow the high-Z component to retain a high velocity. These will be incorporated into the model during years 2 and 3 of NSTX-U operations.

These planned experiments and simulations are expected to contribute to the understanding of important physics questions related to the MGI experiments in support of NSTX-U, ITER and future ST and tokamak based machines. The primary study to be conducted would be to understand the gas penetration efficiency as a function of poloidal gas injection location and variations in plasma parameters, especially at the edge. Supporting DEGAS-2 studies would contribute to quantifying the MGI system requirements aimed at minimizing the gas throughput and maximizing the gas penetration through the separatrix.

2.2.3.3.3 Novel mitigation technologies: electromagnetic particle injector

This section describes our on-going work for developing a new system for safely terminating discharges in ITER and FNSF. The system, referred to as an Electromagnetic Particle Injector (EPI) propels a coaxial projectile, containing particulate matter of various sizes and composition, in a coaxial electromagnetic rail gun, then shatters it in order to inject the smaller sized particles into the tokamak, as shown in Figure 2.2.3.3.3-1. While experiments on NSTX-U would likely shatter the pellet, the system for ITER may choose to inject the capsule intact.

The following observations can be made concerning MGI. First, it is generally agreed that the Massive Gas Injection system is the best understood system for safely terminating discharges in ITER. Second, the time response of this system and the controllability of the amount of gas and impurities injected by this system for variations in the initial plasma current at which a disruption initiates may be inadequate. Third, it may not be possible to fully rely on this system for forced thermal quenches that have less than 10 ms of warning time. Thus, it is generally agreed that other faster acting systems should be tested and developed. The EPI concept was presented at the U.S. Disruption Mitigation Workshop held at General Atomics on March 12-13, 2012. It was noted that this system was more complex as compared to a conventional gas gun, but no technical flaws were identified. It was also suggested that a proto-type should be built and tested before considering it for ITER.

At present the design parameters for such an injector for NSTX-U have been established. We plan to build a proto-type during the second quarter of 2013, and conduct off-line testing during the fourth quarter of 2013.

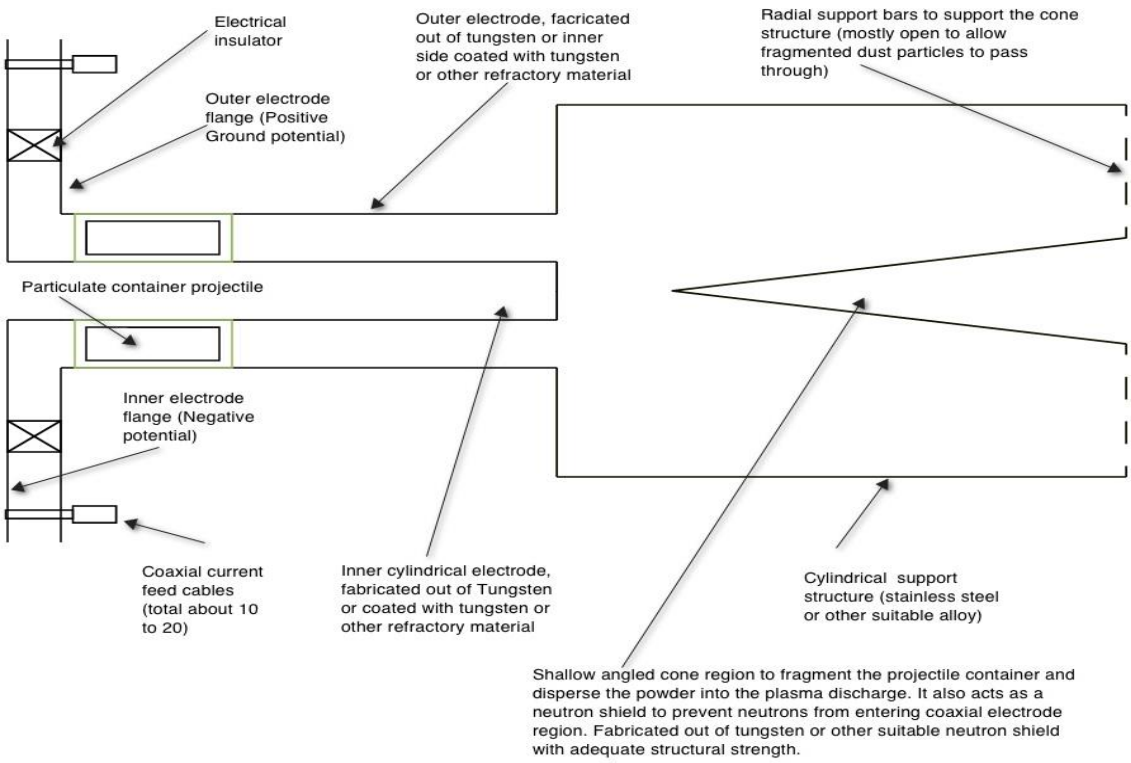

Figure 2.2.3.3.3-1: Electromagnetic Particle Injector (EPI) using a coaxial electromagnetic rail gun.

The proposed system, shown in Figure 2.2.3.3.3-1 and Figure 2.2.3.3.3-2, is now under detailed design. The EPI system has several advantages over other disruption mitigation systems being considered for ITER. These are:

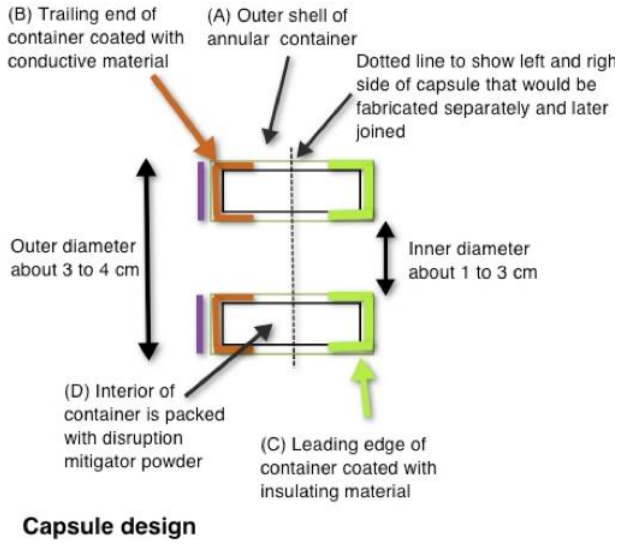

Figure 2.2.3.3.3-2: Shown are the primary elements of the capsule design. The purple ring at the trailing end of the capsule serves two purposes. In an electromagnetic accelerator it is used to increase the inertial strength of the capsule. If the capsule is used in a conventional gas gun it could be fabricated out of a non-conductive material.

- It is capable of delivering a highly tailored mass inventory with:

- A large particle inventory,

- All particles delivered at nearly the same time,

- Particles tailored to contain multiple elements in different fractions and sizes, and

- Particles that are fully ionized only in higher current discharges (to control current quench rates).

- The toroidal structure and conical disperser ensures that:

- For smaller machines, the capsule does not enter the tokamak intact,

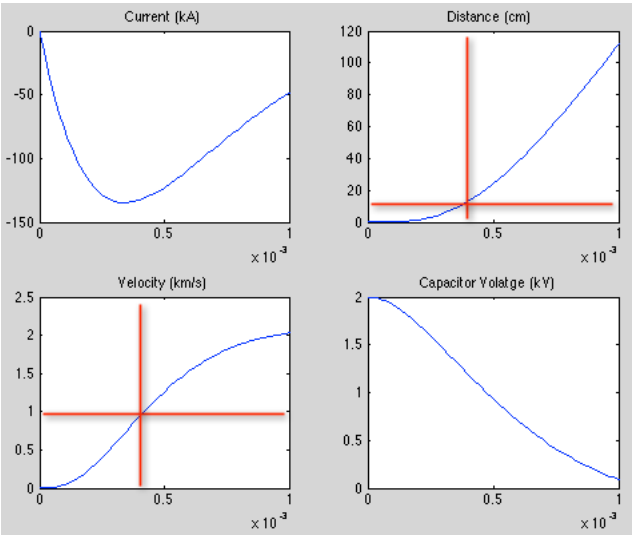

Figure 2.2.3.3.3-3: Accelerator current, capsule velocity, distance traveled by the capsule, and the capacitor bank voltage history all as a function of time after discharge of the capacitor bank.

Figure 2.2.3.3.3-4: The NSTX CHI capacitor bank system is well suited to powering the EPI injector for NSTX-U.

- The capsule will fragment symmetrically and deliver a uniform distribution of particles (or via. tapered final section),

- For larger machines, the capsule can also be injected intact without fragmentation, and

- Particle penetration is not impeded by magnetic fields

- A coaxial rail gun is a fully electromagnetic system with no moving parts, so should have high reliability from long stand-by mode to operate on demand.
- Conventional gas guns will inject gas before capsule and will trigger a pre-mature thermal quench.

Design studies for NSTX-U have now converged on an attractive and viable system. Table 2.2.3.3.3 contains the specifications for the capsule and injector. The capsule volume is about 0.5 to 1.5 cm^3. For present machines, the capsule would be fabricated out of graphite particles compression packed with a bonding agent. The purple ring shown in Figure 2.2.3.3.3-2 would be fabricated out of a layer of conductive graphite. For NSTX-U the capsule would have a mass of about 2-3g and contain enough carbon atoms to equal about 20% of the required impurity atom content for a forced thermal quench in ITER. The inner and outer diameter of the accelerator would be 1 and 2cm respectively. The overall injector length would be 20cm for a final velocity of 1km/s. As shown in Figure 2.2.3.3.3-3 which contains results from rail-gun simulations, by

Capsule Parameters	Injector Parameters
Inner and Outer Radius: 0.5cm and 1cm	Accelerator Length: 0.2 to 1m
Length and Volume: 0.5-1.5cm and 1-3cc	Capacitor bank voltage: 1-2kV
Capsule Mass: 2.8g	Bank Capacitance: 50mF
No. of Carbon atoms: 1.5×10^{23}	Capacitor bank energy: 100kJ
No. of electrons: 9.2×10^{23}	External inductance: 2μH
Electrons in capsule/ITER TQ needs: ~0.2	Accelerator inductance: <1μH

Table 2.2.3.3.3: Capsule and EPI Injector Parameters for NSTX-U

extending the accelerator length to 1m, velocities as high as 2km/s could be achieved. The simulations also show that the velocity of 1km/s is achieved in less than 0.5ms after the discharge of the power supply. In systems such as this, it is the power supply that is the high-cost component. Fortunately, because of CHI research on NSTX, the capacitor bank used for CHI research (shown in Figure 2.2.3.3.3-) is well suited for powering the EPI injector for NSTX-U. The system capacitance is 50mF and it will be operated at 2kV. The RG218 power cables that

feed power into the CHI current bus at the machine would be disconnected and could be connected to the EPI injector bus during disruption mitigation studies.

Given that the high-cost components will be in an operational state during year 1 operations to support the CHI program, what remains is the fabrication and testing of a prototype injector which as mentioned above, will be completed before the start of NSTX-U operations.

2.2.3.3.4 Summary of research plans by year

Year 1 (2014):

- Continue DEGAS-2 modeling of gas penetration physics for NSTX-U.
- Prepare MGI system for operation.

Year 2:

MGI program goals: Test hardware and commission MGI diagnostics

- Using a low triangularity discharge as shown in Figure 2.2.3.3.1-1a, a comparison will be made of massive gas injection (using a combination of deuterium and helium) of gas injected into the lower X-point and private flux region to that from the vessel mid-plane. This is a comparison of locations 1a and 2 in Figure 2.2.3.3.1-1a.
- The shape of the plasma will be varied to make it highly triangular so that the outer strike point rests on the inner divertor plate and at a radius less than the radius of the gas injection port (Figure 2.2.3.3.1-1b). Gas will then be injected into the scrape-off-layer region near the divertor, which is now located in a region of high toroidal field (location 1b in Figure 2.2.3.3.1-1b). This injection location will be compared to mid-plane injection (location 2, in Figure 2.2.3.3.1-1b) to understand the effects of gas penetration through the scrape-off layer that is located in regions of high vs. low toroidal field. The same combination of deuterium and helium will be used for these experiments to compare these results to those for the low triangularity discharges.
- During the first year of NSTX-U operations, much of the MGI studies will use a combination of deuterium and helium primarily to gain experience in conducting these studies on NSTX-U for the first time and to commission the diagnostics that will support MGI studies. Towards the end of Year 2 operations test will be conducted in which neon is introduced as an additional impurity gas in the deuterium/helium gas mix used above to gain experience with the use of high-Z gas and to develop experiments for Year 3 that will begin to use high-Z gasses.

Year 3:

MGI program goals: Increase high-Z gas fraction to satisfy milestone 3a (quantify MGI results from NSTX-U). Systems that were installed, tested and improved during the previous two years

will this year be used to obtain sufficient quantitative results in support of this Milestone, including the following research tasks:

- Based on previous results, a desired fraction of neon (in a combination of deuterium/helium carrier gas) will be used for all subsequent comparison experiments to be conducted this year.
- Compare: (1) the gas transit and system response times, (2) propagation time for the cold front to reach the q = 2 surface, (3) the amount of gas required for initiating a rapid thermal quench and (4) symmetry of the radiated power profile.
- Determine if a cold mantle can be continually maintained around disrupting plasmas by simultaneously injecting gas from three locations (bottom, mid-plane and top. Assess the benefits of multiple injection location for reducing localized radiation thermal loading.
- Replace neon with argon to assess the benefits of each of these gases and to select the gas combination for further experiments.
- Quantify the gas assimilation fraction for variations in the gas injection location and compare to DEGAS-2 modeling results. Assess if a full DEGAS-2 model is required for future work.
- Assess reduction in divertor heat loads and reduction in divertor halo currents for variations in the gas injection location.
- Measure asymmetries in the radiated power profile for variations in the gas injection location and for simultaneous gas injection from multiple locations.

EPI program goals: The primary objective for the EPI system (planned for Year 3) is to assess the EPI injector system's capability to initiate a forced thermal quench in less than 10ms after the system is triggered. This is for assessing its potential to meet ITER needs.

- Conduct an initial commissioning test of EPI injected capsule into energetic NSTX-U plasma so as to obtain sufficient information to assess its potential as a disruption mitigation system for ITER. Parameters of interest would be (1) time when the projectile particles contact the plasma after system trigger time, (2) time for the resulting thermal quench and (3) reliability of the system. For NSTX-U experiments, the system will be designed to inject the capsule at a velocity of 1 km/s. At this velocity, in principle, the particles should reach the NSTX-U core plasma 3-4 ms after the system is triggered. These initial experiments will be used to guide the capsule velocity requirements for ITER and for Year 5 NSTX-U EPI experiments.
- Obtain additional measurements using the EPI system to assess its potential benefits over the MGI system.

Year 4:
Compare MGI and EPI systems in NSTX-U: Characteristics of the thermal and current quench phases for MGI and EPI triggered disruptions will be compared.

- Inject MGI at different times into a discharge in which the q-profile is evolving to understand the importance of the location of the q = 2 surface to the plasma edge.
- Compare the thermal and current quench rates for forced disruptions using MGI and EPI in a high-powered NSTX-U discharge.
- Work with groups using NIMROD, KPRAD, and if possible the EIRENE-SOLPS codes to simulate NSTX-U experimental observations. This is work that will have been initiated during Year 1 of NSTX-U operations.
- Continue to include the NSTX-U MGI and EPI data into the ITER database to contribute to the continued understanding of these systems for ITER, future tokamaks and STs.

Year 5:
Integrate DMS to DM Sensors: Obtain other needed data from the MGI and EPI systems and to test their reliability to trigger on demand using signals provided by disruption detection sensors in NSTX-U.

- Trigger the MGI system based on input from the disruption warning system (see thrust MS-1). Additionally, it will be determined if the DM control system is capable of triggering a specific MGI valve based on the plasma configuration (i.e., downward vs. upward moving disruption).
- Trigger the EPI system based on input from the disruption warning system.

See Section 9.2.3.1 for additional information of the systems for synthesizing NSTX diagnostic data in order to provide pre-disruption triggers to these systems.

2.2.3.4 Disruption physics

The topic of disruption physics captures a number of topics critical for the reliable operation and design of future tokamaks. In general, these include the physics of:

- transport during the thermal quench, and associated power loading of the PFCs,
- the current quench,
- the generation of halo currents,
- the generation of runaway electrons (REs).

Of these topics, the current quench will be studied extensively as part of the mitigation research described in Section 2.2.3.3, and will not be addressed here. Due to the strong shaping and lower toroidal field, disruption RE generation is not expected in NSTX-U (the RE studies in Section 2.2.3.3.3 are proposed to be performed on an RE population generated by low-density Ohmic operation, not disruptions). Hence, the research program described here will focus on the thermal quench and halo current generation.

2.2.3.4.1 Improving understanding of thermal quench physics and transient disruption heat loads

In the chain of disruption consequences, the first event is the thermal quench. The impulsive thermal loading associated with the quench can lead to severe damage to the plasma facing components. The magnitude of this problem can be viewed in Table 2.2.3.4.1, where the thermal quench heat loads are projected using the methodology from Table 5 of Reference [113]. The pre-disruption thermal energy is used for projecting the thermal loads. The divertor area is taken from Reference [113] for ITER, and as $2\pi R_0 \lambda_{mid} f_{exp}$, where λ_{mid} [cm] = max(0.2,1.0/$I_p^{1.6}$) [114] and a flux expansion f_{exp}=30 is assumed for NSTX-U and 60 for the next step STs. Furthermore it is assumed that the SOL expands by a factor of seven during the disruption process, yielding a similar expansion in the wetted area of the divertor. Finally, the time-scale of the heat pulse (τ_{div}) is assumed to be similar to the time-scale of the thermal collapse, and is of order 1 ms. A thermal loading parameter is then estimated as $W/7A_{div}\tau_{div}^{1/2}$.

	ITER	NSTX-U	ST-Pilot	Power Reactor
R [m]	6.2	1	2.2	3.2
I_p [MA]	15	2	19	29
l_{mid} [mm]	*	3.299	2.000	2.000
W [MJ]	350	1.5	282	1100
A_{div} [m]	3.50	0.62	1.66	2.41
t_{TQ} [ms]	0.7	0.5	1	1
Loading [$MJm^2s^{-1/2}$]	540	15	768	2061

Table 2.2.3.4.1: Disruption thermal loading estimated for ITER, NSTX-Upgrade, an ST-Pilot facility, and an ST power reactor.

The results in the table show that for ITER, a thermal load parameter of roughly 540 $MJm^2s^{-1/2}$ is expected, which is much larger than the C or W ablation/melting threshold of 40-60 $MJm^2s^{-1/2}$ [113]. This clearly illustrates why mitigation of the thermal quench is critical for ITER. The NSTX-U disruption thermal loading is significantly smaller than this threshold, and disruption damage to potential metal PFCs is only expected if the PFC temperature is already significantly

elevated. The ST pilot plant, taken from Reference [4] shows thermal loading approximately 30% larger than that projected for ITER. The ST power reactor, whose parameters are loosely based on ARIES-ST, shows thermal loading more than a factor of five greater than ITER and 50 times larger than the melting threshold for tungsten, even with the large divertor area generated by operating at f_{exp}=60 and a further factor of seven increase during the disruption.

The research proposed for this area in the NSTX-U research program is based on examining the assumptions made in constructing this table, and then providing an experimental basis for improving them.

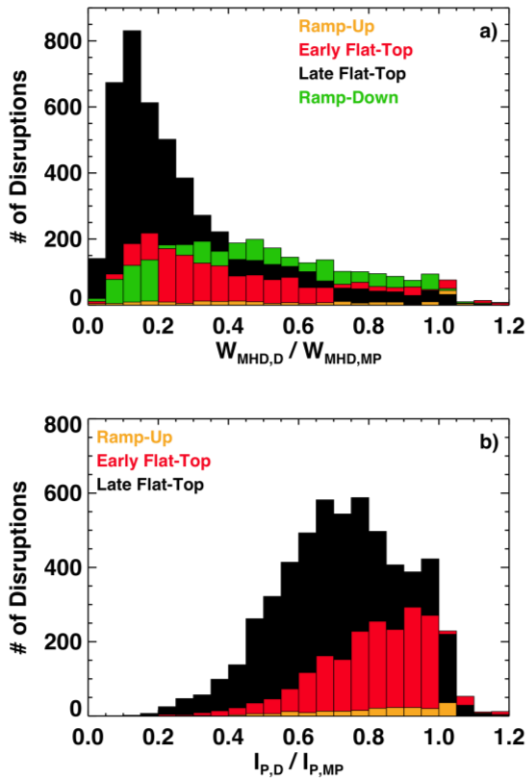

Figure 2.2.3.4.1-2: Histograms of the of a) stored energy, and b) current left at the time of disruption vs. at the time of maximum performance. The data is broken into the current ramp, the period between the start of flat-top (SoFT) and SoFT+250 ms, the later flat-top, and the rampdown. Figure from Reference [95].

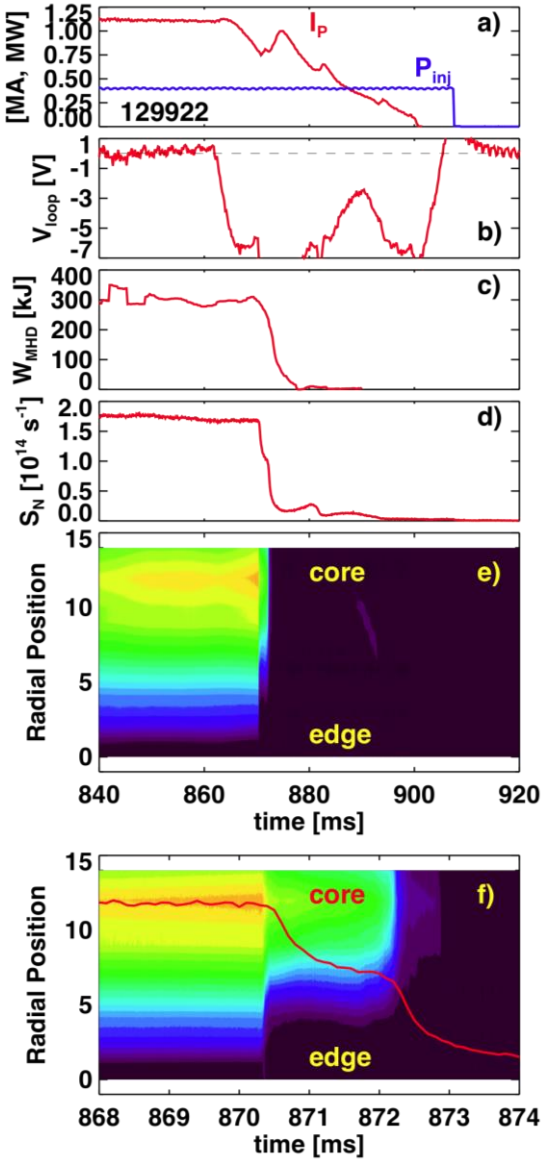

Figure 2.2.3.4.1-1: Time evolution of quantities during a plasma with an extremely rapid thermal quench. Shown are a) the plasma current and injected power, b) the applied loop voltage, c) the stored energy, d) the neutron emission, e) the soft X-ray profile, and f) the neutron and soft X-ray emission zoomed in to the region surrounding the thermal quench. Figure from Reference [95].

This process illuminates the key physics assumptions and processes that must be understood to make improved projections to next step STs.

The first physics assumption in these estimates is that stored energy at the time of the thermal quench is equal to the value during the high performance phase. In fact, as shown in Reference [115] for JET and Figure 2.2.3.4.1-2a for NSTX data [95], there is typically a rather large fractional loss of stored energy during the low confinement phase preceding the thermal quench. For instance, for disruptions in the later flat-top, the most likely case has a stored energy equal to 15-20% of the stored energy at the time of maximum performance. Similarly, Figure 2.2.3.4.1-2b shows that there is typically a loss of plasma current in the phase leading up to the disruption. Both of these effects can help to mitigate the dangerous aspects of the disruption.

Note, however, that there are many examples in Figure 2.2.3.4.1-2a with minimal fractional stored energy loss preceding the disruption. These cases are often among the highest stored energy disruptions in NSTX. An example of such a disruption is shown in Figure 2.2.3.4.1-1, where frames a) through e) share a common time-base, and frame f) zooms in on the soft X-ray emission dynamics during the thermal quench. In this case, the disruption is triggered by a reversal of the loop voltage in Figure 2.2.3.4.1-1b, as the plasma current is ramped down without first reducing the stored energy. The stored energy of 320 kJ at the time of the thermal collapse is quite large by NSTX standards, and shows no substantial reduction in the phase leading up to the thermal quench. In fact, 21 of the 22 largest stored energy disruptions in NSTX were of this variety, where the loop voltage was reversed during the high performance phase. This observation motivates the ramp-down automation tasks described in Section 9.2.3, designed to avoid this occurrence, but also provides a means to generate reproducible disruptions for physics studies, as will be described in the next section.

Research in NSTX-U will continue to examine the typical stored energy losses preceding a disruption. More importantly, it is worth noting that that the levels of energy loss in Figure 2.2.3.4.1-2a are only due to natural plasma processes. Collaborative research between the ASC and MS groups will attempt to actively increase the levels of pre-disruption energy loss by implementing automated soft-stop procedures, as described in Section 9.2.3.2. This will allow a better understanding of the scenarios under which full-energy disruptions are unavoidable.

A second key assumption made in formulating Table 2.2.3.4.1 is that all of the energy present at the time of the thermal quench is conducted to the divertor, and that radiation is not a significant part of the disruption power balance. This assumption will be verified by power balance measurements during disruptions. In particular, a bolometry system will be used to assess the total radiation as a function of time, during both the thermal and current quenches. The fast IR thermography systems and eroding thermocouples will be used to assess the heat conducted to

the PFC surfaces. Measurements of vessel eddy currents will be used to assess the magnetic energy lost to eddy currents. These measurements will be made for both centered major disruptions and vertical displacement event (VDE) disruptions.

The third assumption in Table 2.2.3.4.1 is with regard to the temporal scale of the thermal collapse and the thermal loading. At conventional aspect ratio, a two-stage thermal quench sequence has often been discussed [113], where there is first flattening of the thermal profiles within the q = 2 surface, followed by a complete collapse of the remaining thermal energy. The time-scale of the second collapse is used as a worst-case proxy for the time-scale of the thermal loading in the calculation of Table 2.2.3.4.1, though some measurements from AUG [113] indicate that this may be too conservative.

The largest stored energy disruptions in NSTX are also observed to have a two stage thermal collapse. For instance, the neutral emission trace in Figure 2.2.3.4.1-1d shows a two stage collapse, as does the profile of soft X-ray emissivity in Figure 2.2.3.4.1-1e. The dynamics of this two-stage collapse can be seen most clearly in Figure 2.2.3.4.1-1f, where the neutron and X-ray signals have been expanded around the time of the thermal quench. It is clear that, unlike the conventional aspect ratio case, the first collapse occurs at the edge of the plasma. This collapse takes place over 40-60 ms, followed by a nearly constant phase of 1500 ms duration, and the core thermal energy collapse on a time scale of ~200 ms.

The fast IR thermography and eroding thermocouples will be used in conjunction with the core diagnostics to assess the relative timing between the core thermal collapses and the arrival of heat at the divertor surface. These measurements will be conducted for “hot plasma VDEs”, where there is minimal thermal energy loss preceding the vertical motion, and centered disruptions such as that in Figure 2.2.3.4.1-1, where there is minimal plasma motion preceding or during the thermal quench. The presence of multiple time-scales in the thermal collapse will be documented for the various disruption types, and the levels of thermal loading associated with each time-scale will be documented. The effective duration of the thermal energy pulse will be measured, with a view to determine if various effects such as SOL turbulence or plasma sheath effects [113] result in a temporal spreading of the heat flux compared to the time-scale of the core collapse.

The fourth assumption made in assessing Table 2.2.3.4.1 is that the conducted heat flows along the SOL field in a fashion similar to that during the flat-top phase, but with a factor of seven expansion in the wetted area. Note that significant heat flux is conducted to the inner target during VDEs in DIII-D by poloidal flows and is not fully understood [116]; this effect is potentially more problematic in an ST, given the different divertor areas of the two targets, and must be understood well in order to project for future devices. The IR thermography diagnostics

will be used to assess the spatial extent of the conducted heat flux, to determine the correct area expansion factor for estimating thermal loads. Furthermore, the split between the inner- and outer-divertor legs will be assessed, to determine which locations receive the largest energy loading. As with the time-scale studies, these experiments will be conducted in both hot-plasma VDEs and centered, high-energy disruptions.

The fifth and final assumption involved in Table 2.2.3.4.1 involves the assumption of axisymmetry. The axisymmetry of the heat flux could be violated because of helical distortions of the plasma boundary due to MHD activity, or due to enhanced sheath conduction if thermal electron emission occurs on very hot PFC surfaces [117]. This latter effect could be relevant to cases where the PFC temperatures are already highly elevated when the high-energy disruption occurs, and could be strongly localized. Using the proposed wide-angle IR camera view, NSTX-U researchers will examine the disruption heat fluxes for evidence of strong non-axisymmetry, and quantify those asymmetries if present. The dynamics of those asymmetries will be compared to those for the halo currents, which are the topic of the next section.

2.2.3.4.2 Improving understanding of disruption halo currents

When vertical stability is lost during the disruption process, the plasma typically moves up or down, and comes in contact with the divertors. Large "halo currents" have been observed to flow from the plasma into the divertor structures, through those structures, and then back into the plasma. The part of this current that resides in the structures, when it flows across the magnetic field, can exert damaging forces on those structures.

Much of the early work on "halo currents" focused on the axisymmetric component of those currents, including their inductive coupling to the main plasma current channel [118]; this case corresponds to the currents being driven by a voltage source. More recent work has emphasized the role of halo currents in reducing the otherwise Alfvenic growth of n = 0 and n = 1 instabilities [119,120]; the currents in this case act as if they are driven by a current source. Given incremental funding, halo current research in NSTX-U will attempt to understand the relative importance of these two effects, as well as determine more completely the halo current dynamics in a spherical torus. In particular, the goals for halo current research in NSTX-U are as follows:

- Determine the total halo current fraction in next-step relevant ST conditions.
- Better document the toroidal and poloidal structure of the halo currents, and compare to magnetic measurements of the plasma 3D structure.
- Document the reduction of halo currents with disruption mitigation technologies.

These studies will be made possible by a significant expansion of the halo current measurement systems, as described below.

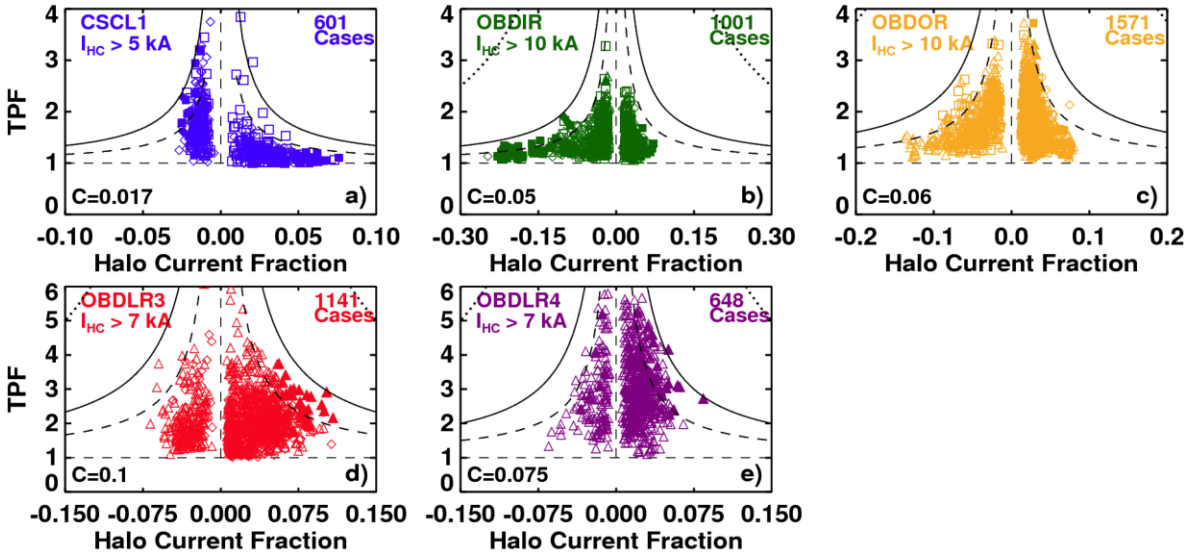

Figure 2.2.3.4.2-1: Halo current fraction vs. toroidal peaking factor, for a series of diagnostics. Frame a) shows data from instrumentation on the center-stack casing, frames b) and c) show data from the lower vessel wall, while frames d) and e) shows data from arrays of tiles located in the outboard divertor. Figure from Reference [122].

NSTX had a significant array of halo current diagnostics: see Reference [121] for a description of the instrumentation, and Refs. [122,123] for example results. However, even with those extensive measurements, it has been impossible to comprehensively measure the total current flowing in the plasma SOL. This can be understood by examining Figure 2.2.3.4.2-1, which shows the halo current fraction vs. toroidal peaking factor for measurements at various positions around the NSTX vessel. The largest halo current fractions are measured at the vessel wall in frames b) and c), where values of up to 25% have been measured. However, this measurement must necessarily underestimate the total halo current, on account of the current which can flow along the copper divertor plates, never entering the vessel wall. Frames d) and e) illustrate the total current flowing into a single row of tiles; both the row 3 and row 4 divertor tiles are illustrated. Unfortunately, the total halo width at the divertor floor can be larger than the poloidal extent of these two tile rows, and the sum of the currents in these two rows thus underestimates the total current.

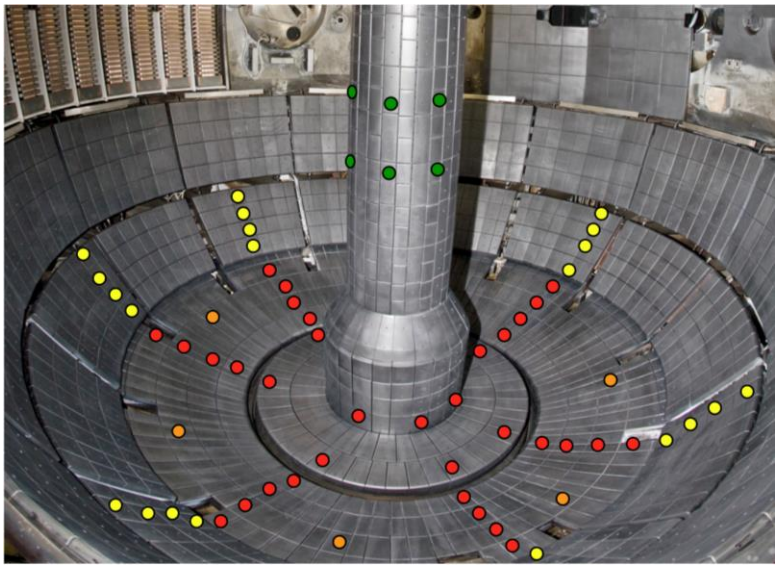

Figure 2.2.3.4.2-2: Proposed expansion of the NSTX-U shunt tile diagnostic set. Each red dot represents a tile which is instrumented with a resistive shunt beneath it. Note that NSTX-U has only a single row of tiles on the inner horizontal target. The colors are explained in the text.

In order to properly measure the total halo current, the shunt tile arrays and other halo current measurements will be significantly expanded. This expansion, indicated conceptually in Figure 2.2.3.4.2-2, will be implemented in a staged way, and if these tiles are eventually replaced by metal PFCs, we will need to reassess our measurement capabilities.

For the ST, the most critical location for halo current loading is possibly the center column, since the toroidal field B_T~1/R is strongest there. Hence, measurements during the first year of operation (Year 2) will focus on diagnosing halo currents at that location, and will utilize an expanded array of sensors on the center column. This includes an array of 12 shunt tiles indicated in green in Figure 2.2.3.4.2-2, as well as a toroidal array of B_T sensors located near the midplane. The shunt tiles will assess the local halo current density in the central region of the center stack, though they may not be sufficiently dense to measure the total current. This measurement will be accomplished using the array of B_T sensors, which act like segments of a partial Rogowski coil and should be able to accurately assess the total vertical current on the center column (though measurements of the peaking factor by this means will be difficult as per the discussion in [121]). These sensors, along with the total and partial Rogowski coils on the upper and lower portions of the center column, should allow a complete inventory of halo currents on the center column.

The next upgrade to the halo current sensor array will involve improved measurements in the outboard divertor, with the goal of significantly improving the toroidal and poloidal resolution. These will include instrumenting all five rows of the outer divertor, as well as the single row of the inner target, with ~6 tiles each; see red circles in Figure 2.2.3.4.2-2 for suggested locations. This toroidal distribution of tiles has proven useful in resolving the approximate toroidal structure of the halo currents in NSTX. Increasing the toroidal coverage in one or two select rows will also be considered, in order to better assess any fine structure in the measurement; the

arrangement in Figure 2.2.3.4.2-2 shows increased toroidal coverage in the third row of divertor tiles as orange circles.

The final upgrade will involve making measurements of the halo currents on the passive plates. While the most common location for the plasma to limit during a VDE is on the divertor floor, plasmas limiting on the secondary passive plates [122] during VDEs were occasionally observed in NSTX. If this type of VDE continues to occur in NSTX-Upgrade, then the tiles on the secondary passive plates will be instrumented in the later years of the five year plan for measurements of currents, as indicated in the yellow circles in Figure 2.2.3.4.2-2. If improvements to the vertical control system described in Section 9.2.2.1.2 eliminate this variety of VDE, then these tiles will not be implemented.

Additional diagnostics will contribute to the understanding of these halo currents. Newly upgraded Langmuir probe diagnostics will facilitate an assessment of the halo electron temperature during the VDE. The new divertor 3D magnetic diagnostics should allow a more precise measurement of the 3D distortions of the configuration during the phase of large currents. These will be used in conjunction with the current measurements to assess the relative phase between the surface distortions and the currents, in order to elucidate the role of the "Hiro current" mechanism [124] in driving these currents. Finally, a divertor Thomson scattering system (incremental) would provide a high-quality measurement of the core and halo temperature density during the VDE.

Using the diagnostic systems described above, it will be possible to measure the total halo current density, at the current entrance and exit points, for a wide range of disrupting plasmas. At a basic level, this diagnostic will provide essential data to project global and local halo current to future ST devices. The scaling of the maximum local and global halo currents with plasma current, toroidal field, and VDE characteristics will be documented. However, beyond this simple parameter, the suggested system will target the following physics issues.

The upgraded halo current sensors will be used to assess the poloidal extent of the halo current channel, known as the halo width. This quantity impacts the total resistance of the halo current path, and thus the current that flows when the halo currents are driven as by a voltage source [117]; this drive term was apparently determined to be dominant in MAST measurements [125]. The width of the halo also impacts the spatial region in the divertor over which the force are applied, and is a key input parameter for many halo current simulation codes. Previous measurements in NSTX have been used to make estimates of the halo width [122], but the present system should resolve it more accurately by providing sufficiently broad poloidal resolution.

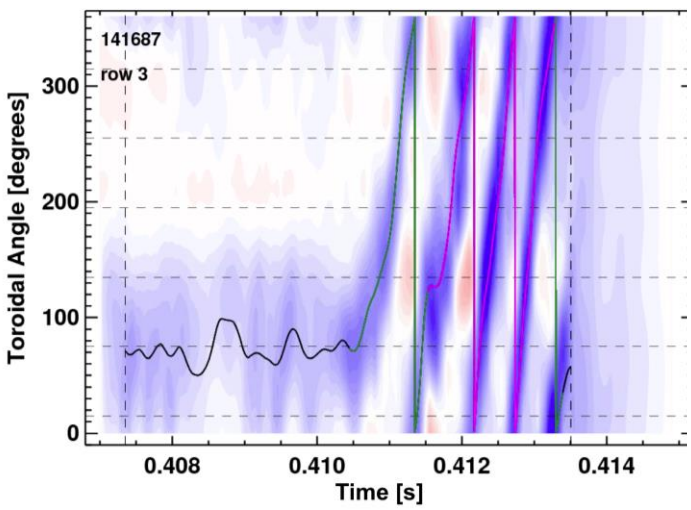

Figure 2.2.3.4.2-3: Evolution of the halo current density as a function of time and toroidal angle but at fixed poloidal angle. Note the strong toroidal rotation of the asymmetry.

NSTX-U studies will also assess the toroidal structure of the halo currents. As shown in Figure 2.2.3.4.2-3, previous measurements using six tiles at a fixed poloidal angle showed that the dominant structure of the halo current tended to be a rotating but toroidally localized lobe [123]. In this particular example, the halo currents flow at largely fixed toroidal angle for ~3 ms, then have a period of ~2.5 ms where they make 4 complete revolutions around the machine. However, previous measurements of the toroidal width of the structure relied on a fitting function that used the intrinsic toroidal rotation of the structure to improve the effective toroidal resolution [123]; the six toroidally distributed tiles were not, in general, sufficient to accurately assess the lobe width using the instantaneous data. This resulted in some uncertainty, especially for cases with little or no toroidal rotation. The system indicated in Figure 2.2.3.4.2-2, if it includes the tiles indicated by the orange circles, should be able to accurately resolve the toroidal structure even in the absence of rotation. Understanding the toroidal structure is critical for determining the potential for severe localization of forces, and can provide key insight into the underlying physics mechanisms generating the currents.

Finally, a key goal of the MGI experiments is to demonstrate a reduction in halo current loading with mitigation. The system described here will be able to comprehensively address this concern, by measuring the total current. With a more sparse measurement set, there is risk that any reduction of current observed with mitigation is simply the result of variations in the VDE dynamics resulting in the location of maximum current moving to a poorly instrumented portion of the divertor.

With regard to the theory of halo currents, there appears to be some consensus that a 3D equilibrium code capable of incorporating the effects of currents in the SOL is required. The development of such a code is beyond the scope of the NSTX-U experimental program. However, should that activity be pursued elsewhere, the NSTX data collected by this diagnostic system would provide a strong constraint on, or test of, those calculations. The research program described above will also produce data for benchmarking simulations of halo currents using extended MHD codes, as described in Reference [126].

If incremental funding is not provided, it is likely that the halo current diagnostics will be significantly more modest, and will be used to provide limited data for the mitigation experiments. The physics research described above would likely not be completed.

2.2.3.4.3 Impact of operating without solenoid induction on disruption physics

NSTX-Upgrade will be able to operate with 100% non-inductive current drive over a range of field, currents, and heating powers; see Chapter 9 or Reference [127] for additional discussion of this operating space. While many scenarios will continue to use the solenoid for I_P feedback control, it is also possible to deliberately disable that feedback loop. This will then duplicate the capabilities envisioned for next-step STs [3,4,5] that do not include an Ohmic solenoid. It is interesting to consider how this modification to the actuator capabilities may modify the disruption characteristics.

Typical H-mode disruptions in NSTX have some precursor modes or event, such as an RWM, locked mode, or H->L transition, that leads to a large drop in stored energy; these are the modes that lead to the large stored energy losses in Figure 2.2.3.4.2-1a. This collapse is typically followed by a 20-100 ms long phase with large loop voltage and, typically, growing vertical instability [95]. The actual thermal and current quenches typically occur only after the solenoid reaches its current limit and begins to ramp down, resulting in a reversal of the loop voltage, or after the plasma is driven into the divertor floor by the uncontrolled vertical motion.

If there were no solenoid induction, the dynamics following the precursor MHD/event would likely be quite different. Rather than responding to the strong inductive edge current drive from the solenoid, the current would begin to decay, though on a time-scale slower than during a true current quench. If the internal inductance were to increase during this process, problems may arise with evolution to unstable current profiles, which could prompt a final disruption. The time available for vertical motion, however, would likely be much less than the cases where induction partially supports the discharge current, and it appears possible that the halo current loading would be reduced in these cases. These various dynamics will be examined in dedicated experiments once 100% non-inductive operations have been established.

2.2.3.4.4 Summary of research plans by year

The timeline for this research is provided below. Note that the halo current research described beyond year 1 will likely require incremental funding, due to the expense of installing the shunt-tile diagnostics.

Year 1 (2014):

- Examine the physics assumptions underlying projections of thermal loading to future devices.

Year 2:

- Investigate halo current loading on the center column, using newly installed center column shunt tiles.

Year 3:

- Upgrade shunt tile diagnostics for complete coverage of the horizontal divertors. Make first assessments of total halo current fraction, toroidal structure, and poloidal width.
- Conduct first experiments on disruption heat loads during VDEs, including studies of spatial extent and timing of the heat deposition.
- Begin assessments of non-axisymmetric heat loading during disruptions, if diagnostic availability permits.

Year 4:

- Extend study of disruption thermal loads to centered major disruptions. Begin efforts to determine the disruption power balance for the various disruption types.
- Complete assessments of halo current scalings using the full field and current capabilities of NSTX-U.
- Conduct experiments examining the impact of fully non-inductive operations, with no loop-voltage feedback, on disruption physics.

Year 5:

- Complete assessments of the disruption power balance for the different disruption types. Complete assessments of 3-D effects in disruptions heat loading
- Utilize upgraded 3D magnetics for comparison of helical distortions and local halo currents.
- Study non-axisymmetric effects on the divertor heat loading.
- Continue support of disruption mitigation experiments by providing data on halo currents and thermal loads. Support halo current and thermal quench modeling activities by providing experimental data.

2.3 Non-axisymmetric control coil (NCC) design and analysis

A non-axisymmetric control coil (NCC) set has been proposed for NSTX-U, to gain understanding of the underlying 3D field physics in many applications in the ST geometry. A more complete overview of the motivation for the NCC was given earlier in Section 2.1.4. In additional, physics design considerations and calculations for the NCC are given in each section describing each of the three Thrusts. In this section, additional design elements are considered, along with a summary of quantitative figures of merit in tabular form, describing the most favorable NCC configurations considered to date.

2.3.1.1 Additional elements of the design motivation

The ST geometry allows the strongest 2D shaping in toroidal confinement, and thus can provide a unique environment to validate 3D field interactions with 2D plasmas. ELM triggering by 3D fields found in NSTX, is a good example illustrating the complexity of 2D shaping itself in 3D field applications. Also, 3D field applications with the snowflake divertor for NSTX-U will help reveal the role of the divertor in ELM applications and the stochastic parallel transport of particles. Non-inductive current drive requires strong bootstrap current with an associated self-consistent q-profile modification, where plasma responses to 3D fields may be very different, but have not yet been explored. Also, it has been shown that the plasma response can become very strong through field amplification at high-β, but amplification effects on resonant and non-resonant interactions between 3D fields and 2D plasmas are not yet fully understood, especially when the high-β is combined with strong bootstrap current in the fully non-inductive scenarios.

The application of 3D fields allows new and selective channels of momentum and particle transport, and thereby can provide rotation, pedestal, and stability control in tokamaks. The modification of the plasma toroidal rotation is a significant capability enabled by 3D field application. Compared to using NBI as the sole actuator, the addition of a 3D field actuator can allow greater and more precise ability to alter plasma rotation and its shear, both of which affect macroscopic and microscopic instabilities in different ways. However, mode stability is not a simple function of rotation or rotational shear, and therefore 3D coils should have sufficient flexibility in the applied field spectrum to finely tune and optimize toroidal rotation and control various instabilities. The particle and ELM control by RMP 3D fields are also complex, as different devices have shown slightly or largely different results on ELM modification. DIII-D has demonstrated complete suppression of ELMs using dominant n = 3 (n is the toroidal harmonic number) RMPs by two off-midplane internal coil sets [128], but in NSTX, n = 2 and 3 fields alone were not successful for ELM suppression and instead showed ELM triggering [19],

although the NSTX midplane n = 3 fields included more non-resonant components than resonant components. The JET tokamak showed that n = 1 fields from external midplane coils can mitigate ELMs by increasing their frequency [129], and the ASDEX-U tokamak showed successful mitigation of ELMs using n = 2 fields by two off-midplane internal coil sets, with the mitigation almost independent of resonant content in the 3D fields [130]. The KSTAR tokamak used three rows of internal coils and showed ELM mitigation and suppression using n = 1 RMPs [131]. Most recently, MAST showed ELM mitigation using n = 6 fields with two off-midplane coil sets [132]. These examples indicate that the present understanding and predictability of the underlying 3D physics are indeed insufficient for low-risk extrapolation to next-step devices.

2.3.1.2 Initial NCC design choices, including partial and full NCC

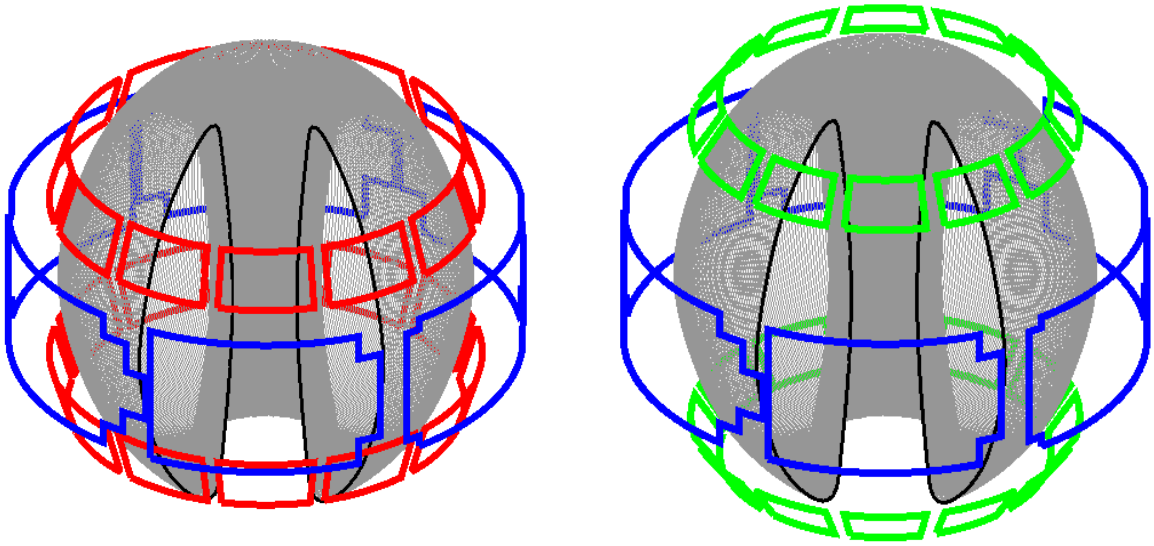

Figure 2.3.1.2-1: The proposed primary (left) and secondary (right) options for the NCC, shown in red (left) and green (right) date back to earlier proposals. Shown in blue are the existing midplane coils.

The physics design of the NCC has been developed over the past few years, and continues to develop as relevant physics understanding in the numerous physics research areas stated above expands. The present designs being considered address these physics topics (see Section 2.1.4) with an aim to maximize research flexibility and effectiveness, given engineering constraints on the coils. Further discussion of the preliminary engineering features of the NCC can be found in Section 10.5.1.2. The present design for the full NCC coil set is planned to have 24 individual coils in total, and our initial NCC design options were correspondingly focused on two sets, called primary and secondary passive plate NCC options, as shown in Figure 2.3.1.2-1 . Both options are two off-midplane rows of 12 coils toroidally, and would be able to generate high toroidal harmonic perturbations up to n = 6, and also up to n = 4 rotating fields. The capability of

3D field rotation is important to enable studies of the toroidal distribution of plasma response using a single toroidal array of diagnostics, such as reflectometry, soft X-ray, or real-time Thomson scattering. Also, these options will add a very different poloidal field spectrum for n = 1-6, compared to the previously limited field spectrum from the midplane coils, and therefore will enable us to better understand, confirm, and extend various unique and interesting physics that has been found in NSTX using only the midplane coil array. However, present physics analyses showed the primary option is superior to the secondary option in many aspects, largely due to its stronger coupling to important plasma modes [12], especially when the coils are operated separately. Therefore, in this section, and also in the remainder of the 5 year plan document, only the primary passive plate NCC option (in the front of the passive plates) will be described to illustrate the NCC utility.

As stated, the total number of the coils in the full NCC will be 24, but for budgetary reasons a staged approach is being considered, with a "partial" NCC set of 12 coils that can be installed in the mid-term of the present five year plan. The NCC design studies, however, will be continued for other full NCC options, including mixed configurations, different coil turns, power supply options, in the next 1~2 years, to achieve the most unique and capable set of 3D coils. The extended NCC design activities will include the most fundamental methods of coil design, based on comprehensive mapping between individual coils and physics advantages. One simple example is to use the coupling matrix $\ddot{C}$ between the 48 coils and the resonant fields at the rational surfaces, which are the critical physics quantities to govern resonant magnetic islands. Once the coupling matrix is developed using available analysis tools, such as the ideal perturbed equilibrium code (IPEC), the singular-value-decomposition (SVD) of the coupling matrix can be used to choose the best coil turns and positions, under constraints such as the total number of coils.

2.3.1.3 Staging of the NCC implementation

As the baseline budget plan does not allow the full implementation of the NCC with independent control of each coil, the performance of partial coil sets have been studied in the present physics design to determine configurations that address as much of the key physics as possible. Presently two partial NCCs options showing the greatest performance and research flexibility: one off-midplane row but with the full set of coils toroidally (named "12"), or two off-midplane rows of 6 coils toroidally (2×6) as shown in Figure 2.3.1.3-1. In these options, the upper and lower arrays are almost identical as NSTX-U plasmas will usually operate near an up-down symmetric configuration. The upper array can be slightly advantageous for the separation of the coils from future enhanced magnetic sensors, which will be largely added in the lower section to detect a higher amplitude of RWM modes near the divertor, and thus "12U", rather than "12L", will be mainly discussed. For the 2×6-coil option, the upper and lower coils can be positioned toroidally

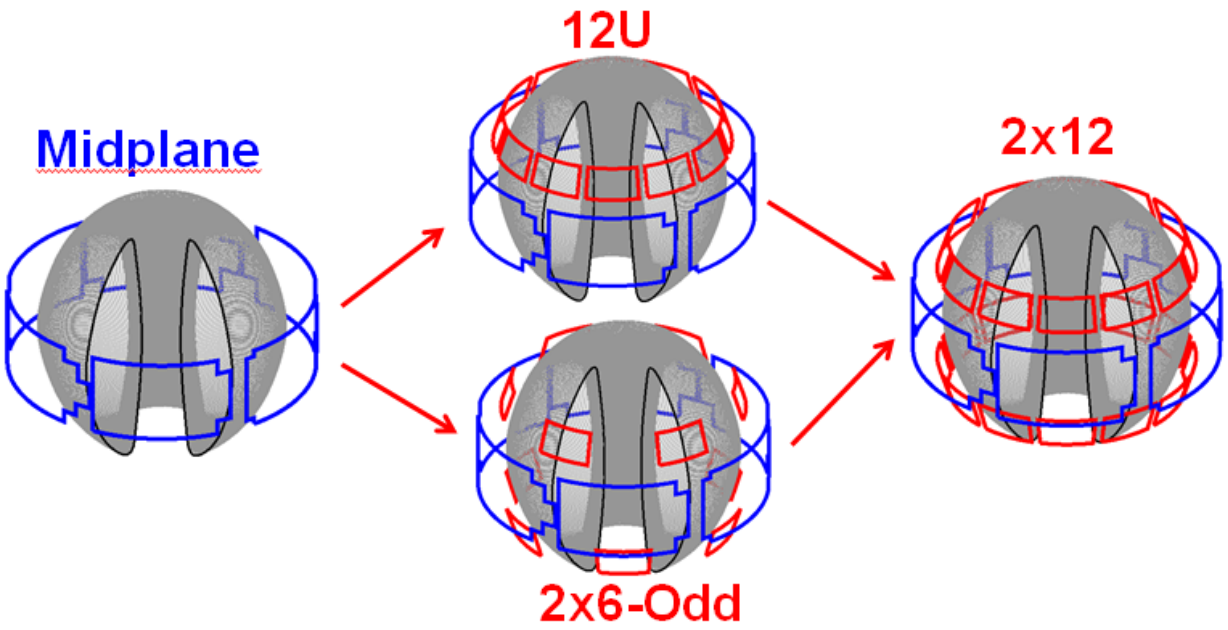

Figure 2.3.1.3-1. Present partial NCCs (12U and 2x6-Odd) and full NCC (2x12), compared to the existing midplane coils. Two partial NCC options will be compared for a staged installation before the full NCC.

in an up-down symmetric (even) or staggering/alternating (odd) configuration. With these options, the goal of design activities is to provide quantified assessment of physics on each as much as possible. As separately described earlier in Sections 2.2.1.5, 2.2.2.1, and 2.2.2.5, present quantitative comparisons of the design choices are based on defined figures-of-merit (FOMs)for each physics element as follows.

- Passive and active RWM control (Section 2.2.1.5):
  The NCC will be extremely useful for both passive and active RWM control. The controllability of toroidal rotation that will be enhanced by NCC will lead us to the best optimization of passive stabilization. Also the NCC will directly add available actuators for expanded physics studies and improve active RWM control. The enhancement of control capability is measured by the RWM FOM, $F_\beta = \beta_{active} / \beta_{no-wall}$, which quantifies the β-gain by the active control, and thus a high F_β value is favorable.

- Error field control (Thrust MS-2):
  Resonant error fields can directly drive mode locking, but non-resonant error fields can also influence locking or tearing, either indirectly by NTV braking of rotation or directly by field coupling. The ratio of the non-resonant error field to the resonant error field is therefore important, which can be quantified by the EF FOM, $F_{N-R} = T_{NTV} / \sum_{\psi_N<0.85} \delta B_{mn}^2$.

Here the non-resonant field effect is measured by the total NTV, and the resonant field effect is measured by the sum of the resonant fields at the rational surfaces, but the rational surfaces $\psi_N > 0.85$ are excluded as they represent the physics outside the pedestal. High F_{N-R} is good to drive the non-resonant field only, but a wide range of ΔF_{N-R} will also be good for related greater range of physics studies.

- Rotation control of NTV braking (Section 2.2.2.5):
  A fundamental motivation for the NCC can be found in rotation control. NSTX-U will uniquely operate in non-inductively driven plasmas and explore the high beta ST operational space. Sustaining this operational regime will require advanced stability control, as for instance disruptivity is not maximized at the highest β_N, or β_N/l_i in such operating space, and therefore will require greater rotation control. The local NTV control capability is measured by the NTV FOM, $F_{N-N} = T_{NTV}(\psi_N < 0.5) \big/ T_{NTV}(\psi_N < 1)$, which quantifies the NTV drive in the core with respect to the total. It is important to have variability of this quantity, and thus it is favorable to have a wide range of ΔF_{N-N}.

- ELM and particle control (Boundary Physics)
  ELM triggering in NSTX using the midplane coils, without clear particle density modification, illustrates the complexity of plasma response to 3D fields and raises concerns on ITER resonant magnetic perturbation (RMP) applications. As this ELM triggering is unique in NSTX, different 3D field applications using NCC in NSTX-U will be extremely beneficial to improve understanding of the mechanism behind ELM modification and particle control by 3D fields. It is not straightforward to quantify the figure of merit for RMP as its understanding is not mature, but the best empirical condition for RMP is the vacuum Chirikov overlap criterion. Also, it may be important to suppress the NTV drive when achieving the condition. This ability is measured by the RMP FOM, $F_{N-C} = (C_{vacuum}, \psi_{N=0.85})^4 \big/ T_{NTV}$,which quantifies the island-overlapping level and thus the degree of stochasticity in a unit NTV strength. The fourth power is needed to make the FOM independent of the applied field strength.

Using the NSTX-U target plasmas and defined FOMs, the up-to-date physics analyses are shown in Table 2.3.1.3, and can be summarized; (1) For the partial NCC options, the 2×6-Odd can provide better variability and gains for active RWM control, error field control, rotation control and ELM control, at most by an order of magnitude for FOMs, compared to existing midplane coils. (2) Full NCC options can provide another order-of-magnitude improvement for FOMs at most, especially for rotation control by high n flexibility, and can provide a significantly

increased capability to study 3D stability. Therefore, presently it has been concluded that the 2×6-Odd option is the best for the partial NCC implementation, and the full NCC will provide further important physics studies if incremental funding resources are available. The final assessment of the coil design will be made based on physics analysis conducted in the next 1~2 years.

Figures of Merit	Favorable values	MID	12U	2x6-Odd	2x12
EF (n=1), $F_{N-R} = \frac{T_{NTV}}{\sum_{\psi_N<0.85} \delta B_{mn}^2}$	High F_{N-R}	0.017	0.025	0.13	0.13
	Wide ΔF_{N-R}	1.00	1.00	5.65	5.65
NTV (n≥3), $F_{N-N} = \frac{T_{NTV}(\psi_N < 0.5)}{T_{NTV}(\psi_N < 1)}$	Wide ΔF_{N-N}	1.00	2.00	3.97	19.6
RMP (n≥3), $F_{N-C} = \frac{T_{NTV}}{(C_{vacuum}, \psi_{N=0.85})^4}$	High F_{N-C}	3.92	47.3	51.3	201.3
	Wide ΔF_{N-C}	1.00	10.5	22.1	252
RWM (n=1), $F_\beta = \frac{\beta_{active}}{\beta_{no-wall}}$	High F_β	1.25	1.54	1.61	1.70

Table 2.3.1.3: NCC performance comparison table, based on defined FOMs. Note here NCCs were used alone without the midplane coils except for the RWM analysis, in which the NCC and the midplane coils were considered.

2.4 Summary of theory and simulation capabilities

Code	*Description*	*Scope*	*Improvements*
DCON	Ideal MHD stability code	Ideal Kink stability analysis with and without the wall up to n=6	Resistive layer physics across rational surfaces (Resistive DCON)
DEGAS-2	Monte Carlo code to compute transport of neutral atoms	Calculation of neutral gas penetration through SOL	Include multiple gas species Use exact NSTX-U SOL conditions from UEDGE
EFIT	Equilibrium reconstruction code	Between-shots equilibrium reconstruction	Higher resolution, auto best level, new diagnostics
FORTEC-3D	Monte-Carlo drift-kinetic physics simulation code	Non-ambipolar transport and NTV physics in general geometry	Continued integration with IPEC and application to NSTX-U
IPEC/GPEC	Ideal and general perturbed equilibrium with 3D fields	Plasma response, locking, and NTV studies with 3D fields	General force balance equation including general jump conditions
M3D-C[1]	Implicit resistive and 2-fluid MHD code	Linear and nonlinear MHD stability	Neoclassical terms, resistive wall being added
MARS-K	Self-consistent kinetic stability calculation	Calculation of RWM stability and plasma response to perturbation	Inclusion of energy dependent collisionality for NTV calculation
MISK	Modifications to ideal stability by kinetic effects	Calculation of resistive wall mode stability	Improved model of energetic particle, anisotropy effects
NTVTOK	Shaing theory NTV computation including ion and electron effects	Calculation for comparison to experiment of NTV in all collisionality regimes	Continued implementation of NTV models, guided by experiment
POCA	δf guiding-center orbit code	Calculation of neoclassical transport, perturbed pressures and NTV	Improved numerical scheme to enhance computation speed
RWMSC	Resistive wall mode state-space controller computations	Generate control matrices for real-time controller, and offline physics studies	Generalization for partial actuator availability, $n > 1$ and multi-mode spectrum
VALEN	Models currents in structures with thin shell finite elements	RWM active feedback simulation, growth rate prediction with 3D walls	Multi-mode effects, study extra time delay in plasma model

Table 2.3: Summary table of the main codes used for theory-experiment comparison on NSTX-U.

2.4.1 EFIT

Accurate equilibrium reconstruction is necessary for experimental analysis as well as input to various other stability codes. In NSTX this capability has been provided automatically between-shots with EFIT [133,134] on two levels: with magnetics only (EFIT01) and with magnetics plus diamagnetic loop plus Thomson electron density and temperature (EFIT02). Additionally, higher levels of reconstruction can be achieved in post-run analysis by including a magnetic field pitch angle constraint from the motional Stark effect (MSE) diagnostic [135] (Section 10.6.1.4). Finally, use of the toroidal plasma rotation (from a charge exchange recombination spectroscopy (CHERS) measurement) is possible. This makes the pressure no longer a flux function, which complicates the reconstruction. Such reconstructions have been successfully generated for NSTX [7].

Plans for EFIT improvements for NSTX-U operation include the following: Higher time and spatial resolution is possible with computer improvements. A scheme for automatically detecting the level of diagnostics available and running up to the highest reconstruction level possible (ie with Thomson, or with Thomson plus MSE, etc…) is planned. Finally, new diagnostics that will be available, such as the motional Stark effect with laser-induced fluorescence (MSE-LIF) diagnostic (Section 10.6.1.5), which has the ability to measure both the magnetic field pitch angle, and the magnitude of the magnetic field, |B| [136], will be incorporated.

Finally, real-time motional Stark effect and Thomson scattering diagnostics are proposed for NSTX-U, and will be incorporated into real-time EFIT reconstructions. These systems are described in detail in Sections 10.6.3.1 and 10.6.3.2.

2.4.2 DCON

Ideal MHD stability is a critical for plasma operation, as the equilibrium states cannot be sustained or need other passive or active stabilizing mechanism if the stability condition is not satisfied. DCON is the fastest stability analysis code by investigating plasma potential energy only, and is also one of the most precise codes with adaptive radial grids. The DCON application to ideal stability will be continued in NSTX-U, and will be extended to higher toroidal harmonic numbers up to n = 6, consistent with the plan for high-n stability studies in NSTX-U.

DCON is an ideal code, but it also has been developed for application to resistive MHD stability analysis. The so-called resistive DCON has been successful for cylindrical geometry, and will be improved and tested for more general toroidal geometry. The resistive DCON code will be very useful to couple and study resistive wall mode and tearing mode physics together in NSTX-U.

2.4.3 IPEC / GPEC

The ideal perturbed equilibrium code (IPEC) has been successfully applied to study the basic feature of plasma responses to small 3D fields in tokamaks. The code utilizes the Euler-Lagrange equation in DCON to solve the ideal force balance and couples solutions to the external 3D field. Various external coils in different devices, NSTX-U, DIII-D, KSTAR, JET, ITER are implemented and IPEC results will be applied to study error field thresholds for locking, plasma response, and neoclassical toroidal viscosity. Recently calculations of neoclassical toroidal viscosity have been implemented into the IPEC code, based on the combined NTV formula without large-aspect-ratio approximation, which will enable us to study NTV more precisely in NSTX-U.

Although the ideal plasma responses are often dominant, non-ideal forces such as NTV torque can modify the 3D equilibrium itself. The general perturbed equilibrium code (GPEC) is under development to incorporate such non-ideal forces in a self-consistent way, as well as more generalized jump conditions across the rational surfaces beyond the ideal constraints. The GPEC code will be highly useful to study plasma responses to 3D fields especially in high-performance plasmas above the no-wall limit and also to investigate the interactions between 3D plasma responses and inner-layer activities when successfully developed.

2.4.4 MISK

The MISK, or Modification to Ideal Stability by Kinetic effects, code [67] calculates the change in potential energy of the plasma due to kinetic effects, δW_K. Along with the fluid δW terms calculated using a marginally stable eigenfunction with the PEST code [137], the dispersion relation or energy principle including kinetic effects is used to predict the growth rate of the resistive wall mode. This approach assumes that kinetic effects do not change the eigenfunction, and that the mode growth rate and frequency are small, so their nonlinear inclusion is unimportant. Cases which are above the ideal no-wall limit, and therefore would be unstable without kinetic effects, are examined. MISK has been used extensively (see Refs. [8,9,68,138,139]) and good agreement between the theory and experimental trends have been found.

MISK will be used in NSTX-U to predict RWM stability dependence on various parameters, such as rotation, the expected reduced collisionality, and the changed energetic particle distribution. Comparisons between experimental results and theoretical expectations will be made.

2.4.5 NTVTOK

The NTVTOK code [93] (NTV computation for TOKamaks) is a code that presently computes the full Shaing model of NTV, including both ions and electrons, across the full collisionality space as theoretically developed over the past decade [36-51], including the superbanana plateau regime. This formulation was used with high success in the initial quantitative comparisons of theory to experiment in NSTX [86] in an initial (unnamed) code, and has been significantly expanded in the NTVTOK incarnation. The code will be used in conjunction with experimental results on NSTX-U to address elements of NTV theory that seem to be disparate among present experimental data, and to test the theory in the important low collisionality regime of NSTX-U. As one example, the theory will be tested to quantitatively determine if NTV begins to decrease at further decreased ν^*, and if so, at what value of ν^* this occurs. The code will be continually developed as needed, to implement additional NTV physics models in the literature, and to correct the theory when experimental results show quantitative disagreement.

2.4.6 POCA

POCA (Particle Orbit Code for Anisotropic pressures) is a newly developed δf particle code to calculate neoclassical transport, perturbed pressures, and NTV in perturbed tokamaks using the δf Monte Carlo method [53]. Every kind of guiding-center motion is tracked by Hamiltonian orbit equations, and the Fokker-Planck equation is solved with a momentum-conserving pitch-angle scattering collision operator. POCA was successfully benchmarked with neoclassical theories, and verified $1/\nu$, $\nu\_\nu^{1/2}$, superbanana plateau regimes, and bounce-harmonic resonances in NTV transport. Good agreement between measured and modeled NTV torques were also obtained with magnetic braking experiments of DIII-D and NSTX [140]. POCA will be extensively used to predict and analyze the non-axisymmetric field effects on neoclassical transport in NSTX-U.

2.4.7 RWMSC

The RWMSC (resistive wall mode state-space controller) code performs the analysis required for both offline physics studies and online real-time RWM state-space control. The code (which continues to expand) presently serves two main roles: (i) it computes the needed input for the real-time controller based on a general implementation optimal control theory and the physics model described earlier, and determines the controller characteristics, most importantly, the controller stability, and (ii) it contains synthetic diagnostics that replicate the expected NSTX-U magnetic sensor measurements, for direct comparison with experiment. The physics model in RWMSC will be continually upgraded both before, and during NSTX-U operation. Simpler

upgrades include the addition of extra sensors, while more sophisticated upgrades include the addition of kinetic measurements to the model.

2.4.8 VALEN

The VALEN code simulates Resistive Wall Mode (RWM) behavior in the presence of 3-D models of conducting structures. The passive growth rate of such an instability is reduced by the interaction of the instability with electrical currents induced in the nearby conducting walls and other structures. The growth rate of the instability can also be altered by additional magnetic fields produced by electrical coils that provide negative feedback. In order to simulate such a problem VALEN models conducting structures, sensor coils, active control coils, power supplies, and a feedback logic in addition to the basic instability.

VALEN will be used in NSTX-U to provide system matrices for the state space controller. Multi-mode VALEN will investigate changes in the plasma mode spectrum due to coils and feedback, plasma wall interaction, and mode to mode interactions.

2.4.9 MARS-K

MARS-F/K (Magnetohydrodynamic resistive spectrum – Fluid/Kinetic code) is a toroidal MHD-kinetic hybrid stability code [141,142] that has been benchmarked with IPEC, MISK and HAGIS codes. The code solves the eigenvalue problem derived from the linearized single-fluid ideal/resistive MHD equations with toroidal flow, self-consistently including the drift kinetic effects in full toroidal geometry. The approach allows the kinetic effects associated with the thermal or energetic particles to consistently modify the mode eigenfunction, which could significantly influence the mode stability and structure in certain circumstances [143,144]. The code simulates a plasma surrounded by a pure vacuum region, includes a set of radially separated, toroidally complete resistive walls and a set of magnetic coils located in the vacuum region. With these features, MARS-F/K has been successfully applied to physical study and support of experiments on various subjects such as MHD instabilities (e.g. resistive wall mode and tearing mode), and plasma response to external fields (e.g. resonant filed amplification and resonant magnetic perturbation).

The MARS-K code has been modified to include the actual collisional frequency with energy dependence and will be used to study perturbed equilibria by including kinetic effects self-consistently. The upgraded MARS-K and the newly developed quasi-linear version MARS-Q will be applied to the calculation of self-consistent kinetic stability and neoclassical toroidal viscosity for NSTX-U plasmas.

2.4.10 M3D-C^1

The M3D-C^1 code [145,146] represents a complete rewrite of the older M3D 3D MHD code. It can be run as resistive MHD or two-fluid MHD, and also can be run as either 2-variable or 4-variable reduced MHD. The code is fully implicit using the split-implicit method and this enables it to take large time steps and run to long time. It uses high-order finite elements in 3 dimensions. These elements force the function and its first derivative to be continuous (C^1-Continuity). This property allows spatial derivatives up to 4th order to be treated when using the Galerkin method. This property is essential for an implicit formulation using the potential/stream function form of the velocity field and magnetic vector potential.

Current emphasis is on modeling sawteeth, snakes, ELMs, the seeding of NTMs, and the effect of rotation on stability, will be applied, as appropriate, to NSTX-U. Future work directly applicable to NSTX-U will be to treat NTMs including neoclassical effects, and to include a resistive wall.

2.4.11 DEGAS-2

DEGAS-2 [107, 108,147] uses Monte Carlo techniques to compute transport of neutral atoms and molecules in the vicinity of material surfaces; general three-dimensional devices can be modeled.

Neutral transport in fusion devices is computed using a Monte Carlo technique in general three-dimensional geometries. DEGAS-2 has been designed as a state-of-the-art code featuring optimized geometry / tracking, dynamic memory allocation, and built-in parallel processing. General methods for handling atomic and surface physics data have been developed to make physics modifications easy. Linear and nonlinear neutral elastic scattering processes have been included. The code is designed to be run in a coupled fashion with fluid plasma codes, as well as in a stand-alone mode. It is intended to be portable with thorough documentation.

DEGAS [148] is the predecessor to DEGAS-2. It uses the pseudo-collision algorithm for scoring, as opposed to the track-length estimator in DEGAS-2. The former works better in a dense plasma; the latter in a vacuum. Unlike DEGAS-2, the surface and atomic physics interactions are hard-wired into the code and are difficult to modify.

DEGAS-2 has been verified against multiple analytic and semi-analytic models. It has been thoroughly compared with original DEGAS and EIRENE, and comprehensively validated against NSTX gas puff imaging experiments.

In NSTX-U, DEGAS-2 will be used extensively for MGI studies, as outlined in detail in Section 2.2.3.3.2.

2.4.12 FORTEC-3D

FORTEC-3D [149-151] is a global Monte-Carlo simulation code, developed to study drift-kinetic physics in fusion devices without any approximation and without any limitation for the geometry. The code can perform the highest level of computations for neoclassical physics, including 3D fields, although the computational cost is quite demanding as it follows 10^7-10^8 particles through the entire region of the plasma. The collision operators are also advanced including energy scattering operator, which may also be important for extremely low collisionality plasmas and non-Maxwellian particles.

The FORTEC-3D code has been extensively benchmarked with other computations and theories. The GAM and basic 3D neoclassical properties have been successfully verified against the GT5D code, which is a gyro-kinetic continuum code in real geometry, for the LHD configuration [118]. Then it has been applied to study non-ambipolar transport in the LHD and in the large-aspect ratio tokamak geometry, and indeed showed almost all essential non-ambipolar transport physics, such as the quadratic δB dependency, $1/\nu$ behavior, superbanana plateau, and neoclassical offset, for the first time by simulation [119]. The actual NTV profiles have been also successfully compared with the combined NTV theory [120], indicating the precision of both methods.

The code is maintained at a different institution, NIFS, but the strong collaboration between PPPL theory and NIFS computation division will be continued. Recently, IPEC inputs were transformed into VMEC-Boozer type data, to enable FORTEC-3D to perform actual NTV calculations in tokamaks. The IPEC coupling to FORTEC-3D will be utilized to investigate NCC capabilities in NSTX-U, by selecting a few limited cases.

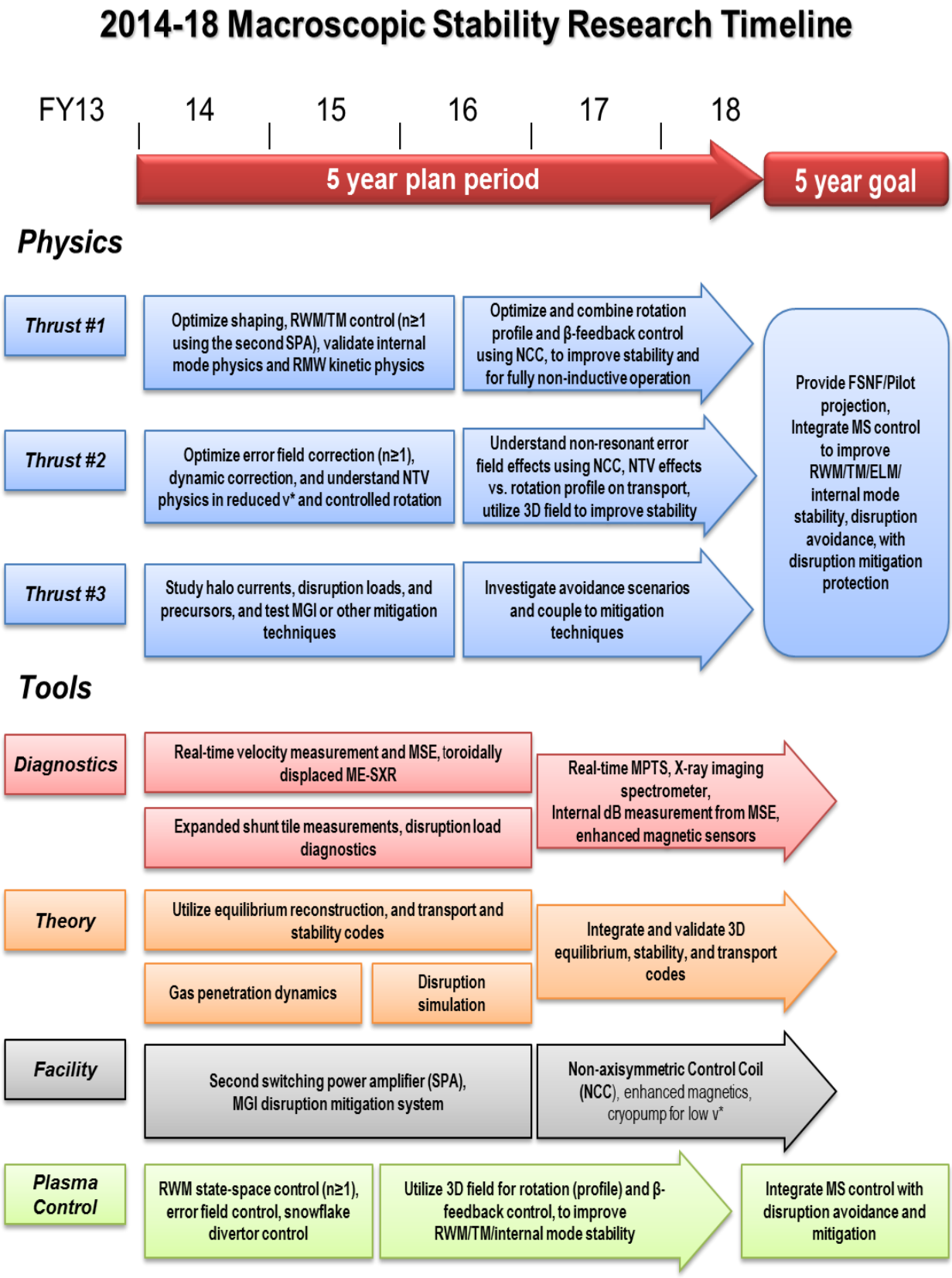
2014-18 Macroscopic Stability Research Timeline
FY13
14
15
16
17
18
5 year plan period
5 year goal
Physics
Thrust #1
Optimize shaping, RWM/TM control (n≥1 using the second SPA), validate internal mode physics and RMW kinetic physics
Optimize and combine rotation profile and β-feedback control using NCC, to improve stability and for fully non-inductive operation
Thrust #2
Optimize error field correction (n≥1), dynamic correction, and understand NTV physics in reduced v* and controlled rotation
Understand non-resonant error field effects using NCC, NTV effects vs. rotation profile on transport, utilize 3D field to improve stability
Thrust #3
Study halo currents, disruption loads, and precursors, and test MGI or other mitigation techniques
Investigate avoidance scenarios and couple to mitigation techniques
Provide FSNF/Pilot projection, Integrate MS control to improve RWM/TM/ELM/ internal mode stability, disruption avoidance, with disruption mitigation protection
Tools
Diagnostics
Real-time velocity measurement and MSE, toroidally displaced ME-SXR
Expanded shunt tile measurements, disruption load diagnostics
Real-time MPTS, X-ray imaging spectrometer, Internal dB measurement from MSE, enhanced magnetic sensors
Theory
Utilize equilibrium reconstruction, and transport and stability codes
Gas penetration dynamics
Disruption simulation
Integrate and validate 3D equilibrium, stability, and transport codes
Facility
Second switching power amplifier (SPA), MGI disruption mitigation system
Non-axisymmetric Control Coil (NCC), enhanced magnetics, cryopump for low v*
Plasma Control
RWM state-space control (n≥1), error field control, snowflake divertor control
Utilize 3D field for rotation (profile) and β-feedback control, to improve RWM/TM/internal mode stability
Integrate MS control with disruption avoidance and mitigation

References

[1] Y.K.-M Peng, et al., Fusion Sci. Technol. **60** (2011) 441.
[2] Y.K.-M Peng, et al., Fusion Sci. Technol. **56** (2009) 957.
[3] Y.K.-M Peng, et al., Plasma Phys. Control. Fusion **47** (2005) B263.
[4] J.E. Menard, et al., Nucl. Fusion **51** (2011) 103014.
[5] F. Najmabadi, et al., Fusion Engineering and Design **65** (2003) 143.
[6] H.R. Wilson, et al., Nucl. Fusion **44** (2004) 917.
[7] S.A. Sabbagh, et al., Nucl. Fusion **46** (2006) 635.
[8] J.W. Berkery, et al., Phys. Rev. Lett. **104** (2010) 035003.
[9] S.A. Sabbagh, et al., Nucl. Fusion **50** (2010) 025020.
[10] S.A. Sabbagh, et al., Phys. Rev. Lett. **97** (2006) 045004.
[11] S.A. Sabbagh, et al., "Resistive Wall Mode Stabilization and Plasma Rotation Damping Considerations for Maintaining High Beta Plasma Discharges in NSTX", *23rd IAEA Fusion Energy Conference*, Daejeon, Republic of Korea, 11-16 October 2010, paper EXS/5-5.
[12] J.-K. Park, et al., Phys. Rev. Lett. **99** (2007) 195003.
[13] S. P. Gerhardt, J. E. Menard, J.-K. Park, et al., Nucl. Fusion **49** (2009) 032003.
[14] R. Hazeltine, et al., "Research Needs for Magnetic Fusion Sciences – Report of the Research Needs Workshop (ReNeW), June 8-12, 2009, USDOE Office of Fusion Energy Sciences."
[15] R. Fitzpatrick and T. C. Hender, Phys. Fluids B 3 (1991) 644.
[16] T. C. Hender, R. Fitzpatrick, A. W. Morris, et al., Nucl. Fusion **32** (1992) 2091.
[17] R. J. La Haye, R. Fitzpatrick, and T. C. Hender, et al., Phys. Fluids **B** 4 (1992) 2098.
[18] J.-K. Park, et al., Phys. Rev. Lett. **102** (2009) 065002.
[19] T.E. Evans et al., Phys. Rev. Lett. **92** (2004) 235003.
[20] J.M. Canik et al., Phys. Rev. Lett. **104** (2010) 045001.
[21] O. Sauter, et al., Phys. Plasmas **4** (1997) 1654.
[22] C. C. Hegna, Phys. Plasmas **6** (1999) 3980.
[23] J.E. Menard, et al., Nucl. Fusion **50** (2010) 045008.
[24] J.-K. Park, et al., Phys. Plasmas. **16** (2009) 056115.
[25] J.E. Menard, et al., ITER Task Agreement #C19TD22FU, "The study of the error fields using Ideal Perturbed Equilibrium Code (IPEC)" (2010).
[26] S.P. Gerhardt, et al., Plasma Phys. Contr. F. **52** (2010) 104003.
[27] J.-K. Park, et al., Nucl. Fusion **52** (2012) 023004.
[28] R. J. Buttery, A. H. Boozer, Y. Q. Liu, J.-K. Park, et. al., Phys. Plasmas **19** (2012) 056111.
[29] A. J. Cole, C. C. Hegna, J. D. Callen, Phys. Rev. Lett. **99** (2007) 065001.
[30] R. Fitzpatrick, Nucl. Fusion **7** (1993) 1049.
[31] R. Fitzpatrick, Phys. Plasmas **8** (2001) 2760.
[32] A. J. Cole and R. Fitzpatrick, Phys. Plasmas **13** (2006) 032503.
[33] R. Fitzpatrick, Phys. Plasmas **17** (2010) 112502.
[34] R. Fitzpatrick, Plasma Phys. Control. Fusion **54** (2012) 094002.
[35] R. J. La Haye, Phys. Plasmas **13** (2006) 055501.
[36] K.C. Shaing, Phys. Plasmas **10** (2003) 1443.

[37] K.C. Shaing, Phys. Plasmas **13** (2006) 052505.
[38] K.C. Shaing, Phys. Plasmas **14** (2007) 049903.
[39] K.C. Shaing, P. Cahyna, M. Becoulet, et al., Phys. Plasmas **15** (2008) 082506.
[40] K.C. Shaing, S.A. Sabbagh, and M. Peng, Phys. Plasmas **14** (2007) 024501.
[41] K.C. Shaing, S.A. Sabbagh, M.S. Chu, et al., Phys. Plasmas **15** (2008) 082505.
[42] K.C. Shaing, Plasma Phys. Control. Fusion **52** (2010) 072001.
[43] K.C. Shaing, S.A. Sabbagh, and M.S. Chu, Plasma Phys. Control. Fusion **51** (2009) 035004.
[44] K.C. Shaing, S.A. Sabbagh, and M.S. Chu, Plasma Phys. Control. Fusion **51** (2009) 055003.
[45] K.C. Shaing, M.S. Chu, and S.A. Sabbagh, Plasma Phys. Control. Fusion **51** (2009) 075015.
[46] K.C. Shaing, J. Seol, Y.W. Sun, et al., Nucl. Fusion **50** (2010) 125008.
[47] K.C. Shaing, S.A. Sabbagh, and M.S. Chu, Nucl. Fusion **50** (2010) 025022.
[48] K C. Shaing, M.S. Chu, and S.A. Sabbagh, Plasma Phys. Control. Fusion **52** (2010) 025005.
[49] K.C. Shaing, M.S. Chu, and S.A. Sabbagh, Nucl. Fusion **50** (2010) 125012.
[50] K.C. Shaing, T.H. Tsai, M.S. Chu, et al., Nucl. Fusion **51** (2011) 073043.
[51] K.C. Shaing, M.S. Chu, C.T. Hsu, et al., Plasma Phys. Control. Fusion **54** (2012) 124033.
[52] S. Satake, J.-K. Park, et al., Phys. Rev. Lett. **107** (2011) 055001.
[53] K. Kim, J.-K. Park, A. H. Boozer, G. Kramer, Phys. Plasmas **19** (2012) 082503.
[54] K. Kim, J.-K. Park, A. H. Boozer, accepted for publication in Phys. Rev. Lett. (2013).
[55] S.A. Sabbagh, et al., Nucl. Fusion **44** (2004) 560.
[56] W. Zhu, S.A. Sabbagh, R. Bell, et al., Phys. Rev. Lett. **96** (2006) 225002.
[57] A. M. Garofalo et al., Phys. Plasmas **16** (2009) 056119.
[58] A. J. Cole et al., Phys. Rev. Lett. **106** (2011) 225002.
[59] S.A. Sabbagh, Y.S. Park, Y.M. Jeon, et al., *"Initial KSTAR Stability and Rotation Alteration Results for High Normalized Beta Plasmas Near or Exceeding the Ideal MHD No-wall Stability Limit"*, 23rd KSTAR conference, Buyeo, South Korea (2013).
[60] J.-K. Park, Y. M. Jeon, the 23rd KSTAR conference, Buyeo, South Korea (2013).
[61] V.A. Soukhanovskii, et al., Nucl. Fusion **51** (2011) 012001.
[62] S.P. Gerhardt, et al., Nucl. Fusion **51** (2011) 073031.
[63] J.W. Berkery, et al., Phys. Rev. Lett. **106** (2011) 075004.
[64] H. Reimerdes, et al., Phys. Rev. Lett. **93** (2004) 135002.
[65] J.W. Berkery, et al., Proc. 24th Int. Conf. on Fusion Energy (San Diego, USA, 2012) (Vienna: IAEA) paper EX/P8-07.
[66] J.W. Berkery, et al., Phys. Plasmas **17** (2010) 082504.
[67] B. Hu, et al., Phys. Plasmas **12** (2005) 057301.
[68] H. Reimerdes, et al., Phys. Rev. Lett. **106** (2011) 215002.
[69] S.A. Sabbagh, et al., Nucl. Fusion **44** (2004) 560.
[70] S.A. Sabbagh, et al., submitted to Phys. Rev. Lett.
[71] T.H.S. Abdelaziz and M. Valasek, Proc 16th IFAC World Congress, Prague (2005).
[72] O. Katsuro-Hopkins, et al., Nucl. Fusion **47** (2007) 1157.
[73] J.M. Bialek et al., Phys. Plasmas **8**, 2170 (2001).
[74] A.H. Boozer, Phys. Plasmas **6**, 3180 (1999).
[75] R. J. Buttery, T. C. Hender, D. F. Howell, et al., Nucl. Fusion **41** (2001) 985.
[76] A. H. Glasser, J. M. Greene, and J. L. Johnson, Phys. Fluids **18** (1975) 875.

[77] H. R. Wilson, J. W. Connor, R. J. Hastie, and C. C. Hegna, Phys. Plasmas **3** (1996) 248.
[78] S.A. Sabbagh, A.C. Sontag, J.M Bialek, et al., Nucl. Fusion **46** (2006) 635.
[79] J.-K. Park, et al., Nucl. Fusion **51** (2011) 023003.
[80] K.C. Shaing, S.P. Hirschman, and J.D. Callen, Phys. Fluids **29** (1986) 521.
[81] K.C. Shaing, *Phys. Rev. Lett.*, **87** (2001) 245003.
[82] K.C. Shaing, T.H. Tsai, M.S. Chu, et al., Nucl. Fusion **51** (2011) 073043.
[83] S.A. Sabbagh, J.M. Bialek, R.E. Bell, et al., Nucl. Fusion **44** (2004) 560.
[84] S.A. Sabbagh, J.W. Berkery, R.E. Bell, et al., Nucl. Fusion **50** (2010) 025020.
[85] S.A. Sabbagh, *et al.*, "Resistive Wall Mode Stabilization and Plasma Rotation Damping Considerations for Maintaining High Beta Plasma Discharges in NSTX", *23rd IAEA Fusion Energy Conference*, Daejeon, Republic of Korea, 11-16 October 2010, paper EXS/5-5.
[86] W. Zhu, S.A. Sabbagh, R. Bell, et al., Phys. Rev. Lett. **96** (2006) 225002.
[87] A. J. Cole, J.D, Callen, W.M. Solomon, et al., Phys. Rev. Lett. **106** (2011) 225002.
[88] J.-K. Park, Phys. Plasmas **18** (2011) 110702
[89] S.A. Sabbagh, J.W. Berkery, R.E. Bell, *et al.*, Nucl. Fusion **50** (2010) 025020.
[90] M.-D. Hua, et al., Plasma Phys. Control. Fusion **52** (2010) 035009.
[91] A.M. Garofalo, et al., Phys. Rev. Lett. **101** (2008) 195005.
[92] Y. Sun, et al., Plasma Phys. Control. Fusion **52** (2010) 105007.
[93] Y. Sun, Y. Liang, K.C. Shaing, et al., Nucl. Fusion **51** (2011) 053015.
[94] H. Reimerdes, et al., Nucl. Fusion **45** (2005) 368.
[95] S.P. Gerhardt, et al., "Disruptions, Disruptivity, and Safer Operating Windows in the High-β Spherical Torus NSTX", submitted to Nuclear Fusion (2012).
[96] D.G. Whyte, et al., J. Nucl. Mater. **363-365** (2007) 1160
[97] G. Pautasso, et al., Plasma Phys. Contr. F. **51** (2009) 124056.
[98] E.M. Hollmann, et al., Phys. Plasmas **17** (2010) 056117.
[99] D.G. Whyte, et al., Fusion Sci. Technol. **48** (2005) 954.
[100] C. Reux, et al., Nucl. Fusion **50** (2010) 095006.
[101] P. Lang et al., Phys. Rev. Lett. **79** (1997) 1487.
[102] R. Maingi et al., Plasma Phys. Contr. F. **46** (2004) A305.
[103] V. Kotov, et al., "Numerical study of the ITER divertor plasma with the B2-EIRENE code package," Bericht des Forschungszentrums Julich, Jul-4257, November (2007)
[104] S.L. Allen, Rev. Sci. Instrum. **68** (1997) 1261.
[105] A.S. Kukushkin, et al., Nucl. Fusion, **47** (2007) 698.
[106] D.L. Rudakov, et al., Nucl. Fusion, **45** (2005) 1589.
[107] D.P. Stotler and C.F.F. Karney, Contrib. Plasm. Phys. **34** (1994) 392.
[108] D.P. Stotler, et al., J. Nucl. Mater., **363-365** (2007) 686.
[109] V.A. Izzo, et al., Phys. Plasmas, **15** (2008) 056109.
[110] T.D. Rognlien, et al., Contrib. Plasm. Phys. **34** (1994) 362.
[111] T.D. Rognlien, et al., J. Nucl. Mater. **266-269** (1999) 654.
[112] D.P. Stotler, et al., Contrib. Plasm. Phys. **50** (2010) 368.
[113] T.C. Hender, et al., Nucl. Fusion **47** (2007) S128.
[114] T.K. Gray, et al., J. Nucl. Mater. **415** (2011) S360.
[115] V. Riccardo, et al., Nucl. Fusion **45** (2005) 1427.

[116] E. Hollmann, private communication.
[117] A.H. Boozer, Phys. Plasmas **19** (2012) 058101.
[118] D.A. Humphreys and A. G. Kellman, Phys. Plasmas **6** (1999) 2742.
[119] L.E. Zakharov, Phys. Plasmas **15** (2008) 062507.
[120] L.E. Zakharov, et al., Phys. Plasmas **19** (2012) 055703.
[121] S.P. Gerhardt, et al., Rev. Sci. Instrum. **82** (2011) 103202.
[122] S.P. Gerhardt, et al., Nucl. Fusion **52** (2012) 063005.
[123] S.P. Gerhardt, et al., Nucl. Fusion **53** (2013) 023005.
[124] L.E. Zakharov, et al., Phys. Plasmas **19** (2012) 055703.
[125] G. Counsell, et al., Plasma. Phys. Contr. F. **49** (2007) 435.
[126] J. Breslau, et al., "MHD Calculation of halo currents and vessel forces in NSTX VDEs", paper PP8.00017, APS-DPP, Providence, RI (2012).
[127] S.P. Gerhardt, et al., Nuclear Fusion **52** (2012) 083020.
[128] T.E. Evans et al., Phys. Rev. Lett. **92** (2004) 235003.
[129] Y. Liang et al., Phys. Rev. Lett. **98** (2007) 265004.
[130] W. Suttrop et al., Phys. Rev. Lett. **106** (2011) 225004.
[131] Y.M. Jeon, J.-K. Park et al, Phys. Rev. Lett. **109** (2012) 035004.
[132] A. Kirk, J. Harrison, Y. Liu et al., Phys. Rev. Lett. **108** (2012) 255003.
[133] L.L. Lao, et al., Fusion Sci. Tech. **48** (2005) 968.
[134] S.A. Sabbagh, et al., Nucl. Fusion **41** (2001) 1601.
[135] F. Levinton, et al., Rev. Sci. Inst. **70** (1999) 810.
[136] E.L. Foley, et al., Rev. Sci. Inst. **79** (2008) 10F521.
[137] R. Grimm, J. Greene, and J. Johnson, "Methods in Computational Physics, Vol. 16," (Academic Press, New York, 1976) Chap. Computation of the Magnetohydrodynamic Spectrum in Axisymmetric Toroidal Confinement Systems, pp. 253-280.
[138] H. Reimerdes, et al., Phys. Rev. Lett. **106** (2011) 215002.
[139] J.W. Berkery, et al., Phys. Plasmas **18** (2011) 072501.
[140] K. Kim, et al., "Study of neoclassical toroidal viscosity in tokamaks with a δf particle code and resonant nature of magnetic braking," Proc. 24th Int. Conf. on Fusion Energy (San Diego, USA, 2012) (Vienna: IAEA) paper TH/P2-27.
[141] Y.Q. Liu, et al., Phys. Plasmas **15** (2008) 112503.
[142] Y.Q. Liu, et al., Plasma Phys. Control. Fusion **52** (2010) 104002.
[143] J.E. Menard, et al. "The role of rotation and kinetic damping in high-beta ST plasma stability", Proc. 39th EPS Conf. 2012, P1.061
[144] Z.R. Wang, et al., Phys. Plasmas **19** (2012) 072518.
[145] N.M. Ferraro, et al., Phys. Plasmas **17** (2010) 102508.
[146] N.M. Ferraro, et al., Phys. Plasmas **19** (2012) 056105.
[147] D.P. Stotler and B. LaBombard, J. Nucl. Mater. **337-339** (2005) 510.
[148] D. Heifetz, et al., J. Comp. Phys. **46** (1982) 309.
[149] S. Satake, R. Kanno, and H. Sugama, Plasma and Fusion Research **3** (2008) S1062.
[150] S. Satake, H. Sugama, R. Kanno, and J.-K. Park, Plasma Phys. Control. Fusion **53** (2011) 054128.
[151] S. Satake, J.-K. Park, H. Sugama, and R. Kanno, Phys. Rev. Lett. **107** (2011) 055001.